TAMPEREEN TEKNILLINEN YLIOPISTO
TAMPERE UNIVERSITY OF TECHNOLOGY

Tiina Keipi

Technology Development and Techno-Economic Analysis of Hydrogen Production by Thermal Decomposition of Methane

Julkaisu 1519 • Publication 1519

Tampere 2017

Tampereen teknillinen yliopisto. Julkaisu 1519
Tampere University of Technology. Publication 1519

Tiina Keipi

Technology Development and Techno-Economic Analysis of Hydrogen Production by Thermal Decomposition of Methane

Thesis for the degree of Doctor of Science in Technology to be presented with due permission for public examination and criticism in Festia Building, Auditorium Pieni Sali 1, at Tampere University of Technology, on the 8th of December 2017, at 12 noon.

Tampereen teknillinen yliopisto - Tampere University of Technology
Tampere 2017

Doctoral candidate: Tiina Keipi
Laboratory of Chemistry and Bioengineering
Faculty of Natural Sciences
Tampere University of Technology
Finland

Supervisor: Professor Jukka Konttinen
Laboratory of Chemistry and Bioengineering
Faculty of Natural Sciences
Tampere University of Technology
Finland

Instructor: University Lecturer Henrik Tolvanen
Laboratory of Chemistry and Bioengineering
Faculty of Natural Sciences
Tampere University of Technology
Finland

Pre-examiners: Professor Alberto Abánades
Departamento de Ingeniería de la Energía
Technical University of Madrid
Spain

Associate Professor Mika Järvinen
Department of Mechanical Engineering
School of Engineering
Aalto University
Finland

Opponent: Professor Klas Engvall
School of Chemical Science and Engineering
Department of Chemical Engineering
KTH Royal Institute of Technology
Sweden

ISBN 978-952-15-4057-8 (printed)
ISBN 978-952-15-4069-1 (PDF)
ISSN 1459-2045

ABSTRACT

The transition to the hydrogen economy has been proposed as a sustainable solution for the simultaneous depletion of fossil fuels and the increase in global energy demand since the 1970s. However, the current fossil fuel-based hydrogen production causes significant CO_2 emissions. On the other hand, extensive hydrogen production by water electrolysis powered by renewable electricity requires a remarkable increase in the renewable electricity generation capacity. Therefore, alternative solutions are needed in order to promote the hydrogen economy, develop hydrogen infrastructure, and smoothen the transition to the wide-scale renewable-based hydrogen production in the future.

In this work, thermal decomposition of methane (TDM) was studied as a transition period solution towards the hydrogen economy. In TDM, methane is converted to hydrogen and solid carbon thereby avoiding the direct CO_2 emissions. A laboratory-scale test reactor was designed and constructed in this work in order to experimentally study the TDM reaction. The experimental results were combined with mathematical modeling to find a suitable TDM reaction mechanism for reactor design studies. A global reaction mechanism with reaction parameters optimized in this study was found applicable for this purpose.

The TDM product carbon utilization possibilities were evaluated by conducting a market survey. According to the experimental TDM studies in the literature, the product carbon from non-catalytic TDM at temperatures above 1450 K is carbon black. Carbon black is mainly utilized in rubber industry and its market value vary from 500 EUR per tonne to 2,000 EUR per tonne depending on the quality. As a part of the technology development, a design path was outlined to assist the selection of the reaction, reactor, and process parameters for a TDM application. The path was followed in this work when potential industrial-scale technology concepts for hydrogen production by TDM were designed. The economic feasibility of these processes was evaluated and comparison was conducted with two other hydrogen production technologies, i.e., steam methane reforming (SMR) and water electrolysis.

According to the economic analysis, a break-even value for the TDM product carbon was found as 310 EUR per tonne of carbon in the current market situation and 280 EUR per tonne of carbon in a potential market situation in 2030 above which the hydrogen production by TDM would be economically feasible in comparison with SMR. The CO_2 emissions from the hydrogen production by TDM were considerably lower than in SMR. Electrolysis could provide an economical option for the production of CO_2-free hydrogen when it is powered by inexpensive renewable electricity, but its availability is expected to remain limited in the near future. By contrast, the feedstock availability through the existing natural gas network provides a possibility for demand-driven hydrogen production by TDM. Thus, the most suitable application for TDM was identified in this work as small or medium industrial scale on-site hydrogen production, which minimizes hydrogen transportation costs. The TDM technology implementation could be further advanced by creating a sufficiently large market for the product carbon and tightening the CO_2 emission regulation.

TIIVISTELMÄ

Vety-yhteiskuntaan siirtymistä on jo 1970-luvulta lähtien ehdotettu ratkaisuksi fossiilisten energiavarantojen ehtymiseen ja samanaikaiseen maailmanlaajuiseen energiankulutuksen kasvuun. Nykyinen fossiilisiin polttoaineisiin perustuva vedyntuotanto on kuitenkin merkittävä hiilidioksidipäästöjen aiheuttaja. Toisaalta vedyn laajamittainen tuotanto veden elektrolyysillä käyttäen uusiutuvaa sähköä vaatisi uusiutuvan sähkön tuotantokapasiteetin merkittävää lisäämistä. Vety-yhteiskunnan edistämiseksi tarvitaan vaihtoehtoisia ratkaisuja, joiden avulla voidaan kehittää vetyinfrastruktuuria ja näin helpottaa siirtymistä laajamittaiseen elektrolyysiin perustuvaan vedyntuotantoon.

Tässä työssä tutkittiin metaanin termisen hajottamisen (thermal decomposition of methane, TDM) soveltuvuutta siirtymäajan teknologiaksi vedyn tuotantoon. TDM-menetelmässä metaani hajotetaan korkeassa lämpötilassa vedyksi ja kiinteäksi hiileksi eikä menetelmässä synny suoria CO_2-päästöjä. Tässä työssä rakennettiin testilaitteisto TDM-reaktion kokeelliseen tutkimukseen. Kokeelliset tulokset yhdistettiin matemaattiseen mallinnukseen tarkoituksena löytää TDM-reaktiota kuvaava reaktiomekanismi käytettäväksi reaktorisuunnittelussa. Sopivimmaksi osoittautui globaali reaktiomekanismi, jonka reaktioparametrit olivat optimoitu käyttäen tämän työn kokeellisia mittaustuloksia.

TDM-menetelmän tuotehiilen käyttömahdollisuuksia arvioitiin markkinaselvityksen avulla. Kirjallisuudessa esitettyjen kokeellisten tutkimusten mukaan reaktiolämpötilan ollessa yli 1450 K ei-katalyyttinen TDM-reaktio tuottaa hiilimustaa, jonka pääasiallinen käyttökohde on kumiteollisuus ja jonka markkinahinta on laadusta riippuen 500 €–2000 € per tonni. Yhtenä osana teknologian kehitystyötä selvitettiin reaktio-, reaktori- ja prosessiparametrien valinnan merkitystä TDM-prosessissa. Tuloksia käytettiin hyväksi, kun tässä työssä suunniteltiin mahdollisia teollisen mittakaavan teknologiakonsepteja TDM-menetelmään perustuvaan vedyntuotantoon. Näiden prosessien kustannukset arvioitiin ja niitä verrattiin höyryreformointiin ja veden elektrolyysiin.

Taloudellisen analyysin perusteella rajahinnaksi TDM-menetelmällä tuotetulle hiilelle muodostui 310 € per tonni nykyisessä markkinatilanteessa ja 280 € per tonni vuoden 2030 mahdollisessa markkinatilanteessa. Näitä suuremmilla tuotehiilen arvoilla TDM-menetelmä todettiin kilpailukykyiseksi höyryreformointiin verrattuna. TDM-menetelmään perustuvan vedyntuotannon CO_2-päästöt ovat huomattavasti alhaisemmat kuin höyryreformoinnissa. Veden elektrolyysillä olisi mahdollista tuottaa vetyä edullisesti ja ilman CO_2-päästöjä käyttäen halpaa uusiutuvaa sähköä mutta tällaisen sähkön saatavuuden odotetaan säilyvän rajoitettuna lähitulevaisuudessa. Sitä vastoin TDM-menetelmässä tarvittavan maakaasun saatavuus nykyisen maakaasuverkon kautta on hyvä, mikä mahdollistaa kulutustarpeen mukaisen vedyntuotannon. Kokonaisuudessaan TDM-menetelmä soveltuu parhaiten pieni- tai keskikokoiseen teollisen mittakaavan vedyn tuotantoon, joka tapahtuu hajautetusti lähellä käyttökohdetta, jolloin vedyn kuljetuskustannukset saadaan minimoitua. TDM-menetelmän käyttöönottoa edistäisi riittävän suuren markkinan kehittäminen sen tuotehiilelle sekä päästörajojen tiukentaminen.

PREFACE

This work was carried out in Tampere University of Technology in the Department of Chemistry and Bioengineering (2014–2016) and the Laboratory of Chemistry and Bioengineering (2017). The financial support received from Fortum, Gasum, Neste (former Neste Oil), Helen (former Helsingin Energia), Carbon Capture and Storage Program (CCSP) research program coordinated by CLIC Innovation Ltd with funding from the Finnish Funding Agency for Technology and Innovation (Tekes), the Tampere University of Technology Graduate School, Gasum Gas Fund, Walter Ahlström foundation, and Fortum Foundation is gratefully acknowledged.

I would like to thank my first supervisor, Prof. Risto Raiko (2014–2015), for giving me this research topic, participating in the test reactor development, and guiding me through my first years as a researcher. Equally, I want to thank my second supervisor, Prof. Jukka Konttinen (2015–2017), for supporting and encouraging me in my research. Moreover, I want to express my gratitude to my instructor Dr. Henrik Tolvanen for his endless guidance and supervision. Additionally, each person from the funding partners and collaborators, who participated in my work and provided the excellent points of view on this research, deserve thanks for their work. Especially, I want to express my gratitude towards Dr. Mari Tuomaala from Gasum and Risto Sormunen from Fortum who contributed to this work from beginning to end.

I deeply appreciate the guidance of Prof. Terese Løvås and Dr. Tian Li during my visit in the Department of Energy and Process Engineering at Norwegian University of Science and Technology. Our collaboration was highly valuable for my thesis and the time I spend in Trondheim was educational in many ways. I also want to thank my colleagues and friends in Trondheim for making my time there special.

I want to thank my co-authors Ville Hankalin and Jaakko Nummelin from ÅF-Consult as well as Dr. Katariina Tolvanen for their contribution and advice regarding my work. Markus Fager-Pintilä and Jaana Rajamäki are acknowledged for the research they conducted in our laboratory prior this work. Moreover, laboratory engineers Jarmo Ruusila, Timo Lindqvist, and Juha Savolainen are thanked for helping me with the experimental setup and Dr. Mari Honkanen for conducting the microscopic analysis of the carbon samples. All my coworkers at TUT deserve thanks for their support during these years. Especially Dr. Aino Vettenranta and Anna Pääkkönen have provided me with valuable advice and encouragement.

Finally, I want to thank my family and friends for their support. Lastly, thank you Marko, my loved one, for reminding me every day what is important in life.

Tampere, November 27, 2017

Tiina Keipi

LIST OF PUBLICATIONS

This thesis is based on the following four original publications which are referred to in the text as Publications I–IV. The publications are reproduced with kind permissions from the publisher. Additionally, some unpublished material is presented and discussed.

I T. Keipi, V. Hankalin, J. Nummelin, R. Raiko, Techno-economic analysis of four concepts for thermal decomposition of methane: Reduction of CO_2 emissions in natural gas combustion, Energy Conversion and Management 110 (2016) 1–12.

II T. Keipi, K. E. S. Tolvanen, H. Tolvanen, J. Konttinen, Thermo-catalytic decomposition of methane: The effect of reaction parameters on process design and the utilization possibilities of the produced carbon, Energy Conversion and Management 126 (2016) 923–934.

III T. Keipi, T. Li, T. Løvås, H. Tolvanen, J. Konttinen, Methane thermal decomposition in regenerative heat exchanger reactor: Experimental and modeling study, Energy 135 (2017) 823–832.

IV T. Keipi, H. Tolvanen, J. Konttinen, Economic analysis of hydrogen production by methane thermal decomposition: Comparison to competing technologies. Submitted to Energy Conversion and Management in August 2017

AUTHOR'S CONTRIBUTION

I The author conducted the process design and techno-economic analysis together with MSc Hankalin and MSc Nummelin. The author had the main responsibility on the manuscript writing. All co-authors commented the manuscript.

II The author planned the research with Dr. H. Tolvanen and conducted the calculations and the majority of the literature survey. Dr. K. Tolvanen conducted the literature review of the carbon utilization possibilities. The author wrote the manuscript, which was commented by all co-authors.

III The author designed and constructed the experimental setup with the help of Dr. Tolvanen. The author conducted all the measurements and was responsible for analyzing the experimental data. The author carried out the reaction and reactor modeling under guidance of Dr. Tolvanen, Dr. Li, and Prof. Løvås. The author wrote the manuscript, which was commented by all co-authors.

IV The author planned the research with Dr. Tolvanen and conducted the process design and the techno-economic analysis and processed the results. The author wrote the manuscript, which was commented by all co-authors.

The work was conducted under the supervision of Prof. Raiko (Publication I) and Prof. Konttinen (Publications II–IV).

LIST OF SYMBOLS AND ABBREVIATIONS

Latin symbols

A	frequency factor	(various)
A_c	cross-sectional area of the bed	m^2
c	concentration	mol cm^{-3}
c_p	specific heat capacity at constant pressure	J kg^{-1} K^{-1}
C	component investment cost	EUR
d_p	diameter of the bed particles	m
e	scale factor	-
E_a	activation energy	J mol^{-1}
$\triangle H_r^0$	reaction standard enthalpy	J mol^{-1}
h_c	convective heat transfer coefficient	W m^{-2} K^{-1}
i	interest rate	-
k	rate constant	(various)
K_c	equilibrium constant	-
L_c	characteristic length	m
$\dot{m}$	mass flow rate	kg s^{-1}
m	rate constant for backward reaction	-
M_i	molecular mass of component i	kg mol^{-1}
n	rate constant for forward reaction	-
n_i	molar amount of component i	mol
N	investment period	a
P	pressure	Pa
r_i	reaction rate	mol m^{-3} s^{-1}
R	reactor tube radius	m
R_u	universal gas constant	J mol^{-1} K^{-1}
S	capacity	(various)
T	temperature	K
t	time	s
V_c	characteristic velocity	m s^{-1}
x	coordinate in axial direction of the reactor tube	m
Y_i	mass fraction of gas species i	-

Greek symbols

ε_v	void fraction	-
μ	dynamic viscosity	N s m^{-2}
ρ	density	kg m^{-3}

Subscripts

b	bulk
backward	reaction direction backward
C	carbon
CH_4	methane
forward	reaction direction forward
H_2	hydrogen
s	solid

Abbreviations

CAPEX	capital expenditure
CCS	carbon capture and storage
CCU	carbon capture and utilization
CRF	capital recovery factor
EDS	energy-dispersive X-ray spectrometry
FTIR	Fourier transform infrared spectroscopy
GHG	green house gas
IEA	International Energy Agency
LS	large scale
MDEA	methyldiethanolamine
MEA	monoethanolamine
MWCNT	multiwalled carbon nanotubes
n/a	not applicable
O&M	operation and maintenance
OPEX	operational expenditure
PEM	polymer electrolyte membrane
PSA	pressure swing adsorption
RHER	regenerative heat exchanger reactor
SC	small scale
SEM	scanning electron microscopy
SMR	steam methane reforming
SNG	synthetic natural gas
TDM	thermal decomposition of methane
TDMG	TDM with product carbon gasification
TEM	transmission electron microscopy
WGS	water-gas shift

Contents

Chapter 1

Introduction

Hydrogen, the most ubiquitous element in the universe, is currently mainly utilized in industrial processes rather than in energy production. Globally, 7.2 EJ of hydrogen was utilized in 2013 [1], an amount which equals 1.3% of the world primary energy consumption [2]. The main industrial applications for hydrogen are ammonia production, which accounts for 54% of the overall hydrogen consumption, and oil refineries (35% of the hydrogen consumption) whereas other applications in chemical industry, food industry, and manufacturing are responsible for using the rest of the hydrogen [3]. Hydrogen itself does not contain carbon, and thus, hydrogen utilization as such does not generate CO_2 emissions that contribute to the climate change. However, the hydrogen production is a significant source of CO_2 emissions. Currently, hydrogen originates mainly from fossil sources since 48% of hydrogen is produced from natural gas by steam methane reforming, 30% derive from petroleum refining, 18% is produced by coal gasification whereas water electrolysis accounts for the remaining 4% [3]. Due to the fossil origin, hydrogen production causes 500 Mt of CO_2 emissions yearly, which accounts for almost 2% of the energy-related CO_2 emissions [4]. Water electrolysis enables hydrogen production without CO_2 emissions but widening the hydrogen production by electrolysis would require a significant increase in the renewable electricity generation capacity.

Hydrogen utilization as an energy carrier in the society has been seen as a tempting alternative to the fossil-based economy for decades. The concept of hydrogen economy was first presented by Bockris at the early 1970s [5]. Bockris proposed a system where hydrogen production occurs by electrolysis, hydrogen is piped to the consumers (industry, households, and transportation sector) who convert the hydrogen to electricity by fuel cells. The main driver for the hydrogen economy already back then was to respond to the increasing energy consumption in the future and to reduce pollution originating from the energy production [5]. However, the transition towards hydrogen economy requires both availability of hydrogen produced with low CO_2 emissions and the development of hydrogen transportation, distribution, and utilization infrastructure.

Several projects that promote hydrogen utilization in the societies have arisen very recently. One of these projects is on-going in the UK where a majority of

the citizens (80%) use natural gas for everyday heating and cooking [6]. The UK has a target to decarbonise its natural gas grid by turning to hydrogen. Hydrogen will be produced from natural gas by steam reforming, currently the most mature hydrogen production technology, and the CO_2 emissions will be captured and stored to minimize the environmental impact of the process. Intraday and inter-seasonal hydrogen storage will occur in salt caverns, which is a widely utilized technology for natural gas [6]. The conversion of the gas grid from natural gas to hydrogen will begin in the city of Leeds, and hydrogen can be fed to the grid earliest in 2025 [6]. Moreover, Norway is exploring the possibility to produce hydrogen from renewable energy or fossil resources with a coupling to decarbonisation [7,8]. The aim is to export the produced hydrogen from Norway to Central Europe.

As was already mentioned, natural gas is currently the primary feedstock for hydrogen production. The International Energy Agency (IEA) predicts that natural gas is the only fossil fuel whose consumption will increase during the coming decades and estimates an 50% increase in natural gas consumption from the current value by 2040 [9]. The increase in natural gas consumption is enabled by the development of advanced natural gas production methods that has doubled the natural gas resources during the recent years [10]. The known natural gas reserves can suffice the current gas production for the next 60 years [9]. Additionally, the resources are geographically widely dispersed and many countries have an access to these resources. Therefore, the natural gas reserves and the existing gas infrastructure could be utilized to promote the hydrogen economy by increasing the hydrogen production from natural gas.

Applying thermal decomposition of methane (TDM) to natural gas or any other methane source provides a potential solution for producing hydrogen with low CO_2 emissions. In this method, methane is thermally converted to hydrogen and solid carbon. The only source of CO_2 emissions in TDM is the heat generation for the process. TDM was commercially utilized almost 100 years ago for producing carbon black for rubber industry, but was replaced later with a more efficient oil-furnace process based on the use of aromatic oils as feedstock. The scientific research of TDM has been conducted since then and several pilot plants for TDM have been commissioned. The discovery of carbon nanotubes increased the research interests towards TDM from 1990 onwards. Most recently, the concerns about the CO_2 emissions originating from the current fossil-fuel based economy have raised interest towards TDM again, since it could provide a solution for more environmentally-friendly energy production. Thus, TDM has been presented as a transition period solution towards the hydrogen economy. Starting the hydrogen infrastructure development and hydrogen utilization as soon as possible would smoothen the transition to the hydrogen economy later when renewable electricity generation capacity is sufficiently large to enable hydrogen production by water electrolysis.

1.1 Research objectives

The objective of this work was to provide tools assisting the TDM reactor and process design as well as to reveal the techno-economic conditions where TDM could become a viable technology for hydrogen production. The developed tools assist the TDM reactor design and dimensioning as well as the selection of the process parameters for a hydrogen production process based on TDM. The tools were utilized when conducting the TDM process design and techno-economic analysis in this work. As a result, the market conditions where TDM could become an economically feasible hydrogen production technology were identified. More specifically, the aims of this thesis were:

- To present and analyze alternative process concepts for applying TDM in commercial scale (Publication I).
- To analyze the effect of reaction and reactor parameters on the TDM process design and on the product carbon value (Publication II).
- To study the TDM reaction experimentally and find a suitable reaction mechanism and rate expression for describing the non-catalytic TDM reaction at the temperatures up to 1500 K. (Publication III)
- To analyze the cost of realizing TDM in a commercial scale and compare the economic feasibility of hydrogen production by TDM with other competitive technologies (Publication IV).

The thesis has the following structure: Following the introduction, Chapter 2 presents the background of the hydrogen economy development, introduces the selected hydrogen production technologies (TDM, steam methane reforming, and water electrolysis), and summarizes the state of the art in the research of TDM. The TDM reaction and reactor modeling is presented in Chapter 3. Chapter 4 summarizes the experimental methods applied in this work to study the TDM reaction and analyze the TDM product carbon. Chapter 5 provides the principles to the economic analysis conducted in this work. The results are presented and discussed in Chapter 6. Finally, Chapter 7 summarizes the most important results of this work and Chapter 8 proposes future research topics in this field.

Chapter 2

Background

2.1 Towards hydrogen economy

The world is heavily dependent on fossil resources as 80% of the primary energy supply has a fossil origin [4]. Moreover, two thirds of the anthropogenic green house gases (GHG) originate from the energy sector [4]. Therefore, new solutions are required in order to ensure the availability of affordable energy and simultaneously decrease the environmental impact of the energy production and consumption. A transfer from the fossil economy to the hydrogen economy could respond to the growing energy demand without GHG emissions. In the hydrogen economy, renewable and emission free electricity originating e.g. from wind or solar power is utilized for hydrogen production. Utilizing renewable energy for hydrogen production provides a storing option for the fluctuating renewable power so that it is easier to match the energy demand. Moreover, hydrogen transportation enables transferring energy from the area of surplus renewable energy to the area of high energy demand. [11]

Hydrogen can be stored in large-scale in underground geological formations, e.g. in salt caverns that are currently utilized for natural gas storage. Selecting the place for hydrogen storage requires that the geological formations, topography, land availability, environmental impact, and legal issues are considered [12]. The Chevron Phillips Clemens Terminal in Texas has experience in underground hydrogen storage since 1980's [13]. Furthermore, Air Liquide commissioned very recently the world's largest hydrogen storage facility [14]. This underground cavern located in Texas is able to store hydrogen amount which equals the monthly production of a large-scale steam reformer unit. Due to the small molecule size, hydrogen leaks easier than natural gas. Thus, the permeability of the cavern walls as well as the properties of all the pipelines and sealings must be taken into account more carefully than in the case of natural gas [12].

The current wind and solar energy production accounts for less than 2% of the global primary energy supply [2]. However, the introduction of hydrogen economy would require a much wider renewable electricity production capacity. Therefore, utilizing the fossil resources for hydrogen production provides an

opportunity for stepwise transition towards hydrogen economy. Developing the hydrogen infrastructure by using fossil fuels would smoothen the transfer to the hydrogen economy powered by renewable electricity in the future [11]. The currently applied feedstock materials for hydrogen production are coal, natural gas, petroleum fractions in oil refining, biomass, and water. Decarbonisation of the hydrogen originating from a fossil source is an option to reduce the GHG emissions. However, this would require applying carbon capture and storage (CCS) but the technology suffers from the high costs and the lack of the CO_2 transportation and storage infrastructure. This restrains the wider utilization of fossil fuel-based hydrogen production technologies. [15]

Applying TDM to natural gas provides a possibility to produce hydrogen with lower CO_2 emissions than other fossil-based technologies. Instead of CO_2, TDM produces solid carbon and is therefore not dependent on the progress of conventional CCS technology or CO_2 transportation and storage infrastructure. Development of the infrastructure for hydrogen transportation, distribution, and consumption is a time-consuming process. However, the production of low-CO_2 hydrogen by utilizing the vast fossil natural gas reserves could promote the hydrogen infrastructure development and later simplify the hydrogen economy expansion.

2.2 Hydrogen production technologies

This chapter presents three hydrogen production methods that were chosen for analysis in this work. The steam methane reforming (SMR) was chosen for analysis since it is the currently most applied technology for industrial hydrogen production. By contrast, water electrolysis powered by renewable electricity is projected to become the dominant method for generating hydrogen in the future hydrogen economy [11]. Production of hydrogen with a renewable origin is possible if a vast amount of renewable and emission free electricity is available. The third method is the hydrogen production decarbonisation by applying TDM to natural gas. Since this technology would utilize the existing natural gas grid, it could provide a transition period solution for widening the hydrogen production and promoting the hydrogen economy.

2.2.1 Steam methane reforming

The first industrial steam reformers date back to the 1950s and later SMR has become the most applied technology for hydrogen and synthesis gas production [16]. A simplified process chart for natural gas reforming is shown in Fig. 2.1. The technical and economic aspects of SMR are discussed in Publication IV in detail.

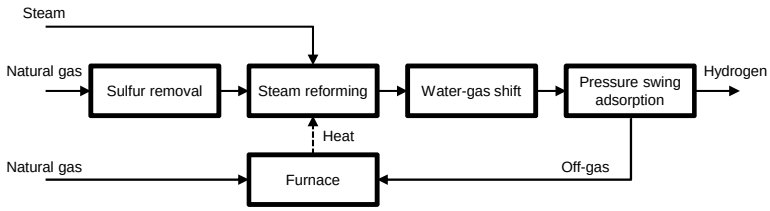

Fig. 2.1: Steam methane reforming process. [17]

First step in SMR is the pre-treatment where sulfur is removed from the natural gas to avoid catalyst poisoning later in the process. The heavier hydrocarbons in natural gas are converted to methane in a catalytic pre-reformer reactor prior the main reformer. The most applied reformer reactor type in industrial hydrogen production is a tubular steam reformer [18]. In this reactor type, natural gas flows in the reforming tubes through a nickel catalyst bed at reactor temperature between 770 K and 1170 K and pressure above 20 bar. The reforming tubes are placed inside a furnace, where the heat needed in the reformer is produced by a combustion of a mixture of the off-gas that originates from the hydrogen separation process and an additional natural gas stream. The principal chemical reaction in methane reforming is shown in Eq. 2.1, but several other reactions occur in the reactor as well [17].

$$\mathrm{CH_4 + H_2O \rightarrow 3H_2 + CO} \qquad \triangle H_\mathrm{r}^0 = +206\,\mathrm{kJ\,mol^{-1}} \tag{2.1}$$

The gas from the reformer is handled in a water-gas shift (WGS) reactor where CO reacts with water over a catalyst in order to produce more hydrogen [17]:

$$\mathrm{CO + H_2O \rightarrow CO_2 + H_2} \qquad \triangle H_\mathrm{r}^0 = -41\,\mathrm{kJ\,mol^{-1}} \tag{2.2}$$

Commercial SMR plants are available both in a small scale with hydrogen production capacity from 10 $\mathrm{Nm^3\ h^{-1}}$ to 1,000 $\mathrm{Nm^3\ h^{-1}}$ [19] and in a large scale with hydrogen production capacity up to 100,000 $\mathrm{Nm^3\ h^{-1}}$ [1].

The minimum purity for merchant hydrogen defined by The Compressed Gas Association is 99.8% [17], and therefore, a hydrogen purification step is required in SMR. The currently most applied hydrogen separation technology is pressure swing adsorption (PSA), which enables production of hydrogen with an extremely high purity, 99%–99.999% [20]. Hydrogen separation by PSA is based on changing pressure levels in the PSA reactor. The impurities in the gas mixture are selectively adsorbed to a solid material at high pressure after which the pressure is decreased to desorb the impurities from the reactor. The solid adsorbents are reused in this cyclic process. [20]. The advantages of PSA are the high purity of hydrogen and very low operation costs in comparison to other hydrogen separation technologies [21]. However, PSA is reasonable to use only on medium and large-scale applications [20] and commercial PSA units are available at hydrogen production capacity range from 100 $\mathrm{Nm^3\ h^{-1}}$ to 390,000 $\mathrm{Nm^3\ h^{-1}}$ [22].

Another possible method for large-scale hydrogen purification is cryogenic distillation [20]. This technology is based on gas separation at extremely low temperature, where gas components selectively condense to form a liquid phase [20]. The main disadvantage of cryogenic distillation is the high energy consumption, and therefore, it is suitable for large scale applications only [20]. Furthermore, the maximum hydrogen purity level of approximately 99% can be achieved with cryogenic distillation [20]. Nevertheless, cryogenic distillation enables storing the separated hydrogen as liquid which increases the energy density of hydrogen and simplifies its transportation.

The environmental impact of SMR could be reduced with CCS technology where CO_2 is sequestrated from the process and injected into a geological formation. The IEA has stated that CCS will have a critical role in reducing global CO_2 emissions [23]. The large point sources of CO_2 emissions, generally defined as yearly emissions larger than 0.1 Mt-CO_2, are mainly power plants using fossil fuels as well as some industrial processes such as cement production, iron and steel production, oil refining, and natural gas processing. The currently leading CCS technology for SMR plants is capturing CO_2 from the syngas after the WGS reactor by using methyldiethanolamine (MDEA) solvent [24]. The first stage in chemical absorption is where the sorbent reacts with CO_2 in the gas stream and it is followed by a regeneration stage, where the same reaction occurs in the opposite direction releasing the CO_2. The most common solvents in chemical absorption are amines (e.g. monoethanolamine (MEA), and MDEA). Chemical absorption is the most suitable technology for capturing CO_2 at low partial pressure as is the case in SMR syngas. [25]

CCS provides a possibility to decarbonise the hydrogen production by SMR and reduce the environmental impact of the process. According to [26], there are five hydrogen production plants around the world that have coupled CO_2 capture with the steam reforming process. An alternative to the long-term storage of CO_2 is turning it into chemicals and fuels, a process called carbon capture and utilization (CCU). CCU is seen as an economically favorable option since it converts waste (CO_2) into marketable products. The main issue hindering the hydrogen production decarbonisation is the lack of wide CO_2 transport and storage infrastructure [26]. Furthermore, the demand for decarbonised hydrogen is insufficient and the hydrogen transportation and utilization infrastructure is inadequate.

2.2.2 Water electrolysis

Hydrogen production by electrolysis is based on water splitting into hydrogen and oxygen by using electricity. The main components of an electrolyzer are an anode, a cathode and a separator between these two as well as a liquid or solid electrolyte. The currently most developed electrolyzers are alkaline electrolyzers and polymer electrolyte membrane (PEM) electrolyzers. Using water as feedstock enables the production of very high-purity hydrogen for fuel cells or for industrial processes with high quality requirements [3]. However, further development is required to scale-up the electrolyzers since alkaline electrolyzers are currently available

only for small industrial needs (up to 1000 Nm^3 h^{-1}) and PEM electrolyzers for applications below 100 Nm^3 h^{-1} [27].

Alkaline electrolysis is the most mature electrolyzer technology and its costs are relatively low in comparison with the other electrolysis technologies, since those can be manufactured from abundant and inexpensive materials [27]. Moreover, alkaline electrolyzers have a high reliability and durability, and moreover, those provide an opportunity to operate at elevated pressures. Nevertheless, the ability of the alkaline electrolyzer to tolerate fluctuating power sources such as renewable energy needs to be improved [27]. The electricity consumption of the currently available commercial alkaline electrolyzers varies between 50 kWh kg^{-1} and 60 kWh kg^{-1} [28]. Additionally, hydrogen purity that can be achieved with these systems vary within the range of 99.3%–99.9998% [28].

PEM electrolyzers are commercially available as well, but the cost of those is approximately twice the cost of alkaline electrolyzers [28]. However, PEM electrolyzers are compact and safe to operate as well as able to handle fluctuating power loads [27]. The commercial PEM electrolyzers have an electricity consumption that varies from 54 kWh kg^{-1} to 65 kWh kg^{-1} and the produced hydrogen purity is in the range of 99.9%–99.9998% [28]. The economics of hydrogen production by water electrolysis is studied in Publication IV.

Despite the fact that electrolyzers have been commercially available for decades, further development is required in order to produce larger and more efficient electrolyzers. Another issue preventing the utilization of electrolysis for large-scale hydrogen production is the limited availability of renewable electricity. According to the estimates given by the IEA [9], renewable electricity generation will increase rapidly during the following decades. The IEA main scenario predicts that renewable energy accounts around 60% of the power generation capacity in 2040. The technology development decreases the costs; solar photovoltaics are expected to face a cost cut of 40%–70% and wind power a cost cut of 10–25% by 2040 [9]. Implementing electrolyzers to produce hydrogen by water electrolysis at a large scale requires the technical development of both in the field of electrolyzers and renewable energy generation, as well as extensive market penetration of renewable power generation technologies. Therefore, it is estimated that the hydrogen production by electrolysis can meet the demands of the wide-scale hydrogen economy not earlier than in the second half of the 21st century [29, 30].

2.2.3 Thermal decomposition of methane

The TDM reaction can be applied to produce hydrogen at high reaction temperature from a methane source such as natural gas. The reaction produces elemental carbon as a by-product. The global reaction equation for TDM is [31]:

$$\mathrm{CH_4(g)} \rightarrow \mathrm{C(s)} + 2\mathrm{H_2(g)} \qquad \triangle H_\mathrm{r}^0 = 75\,\mathrm{kJ\,mol^{-1}} \tag{2.3}$$

The main advantage of TDM over other hydrogen production technologies is that instead of CO_2, which is a harmful component to the climate, it produces solid carbon that is easier to store and can be a marketable product. However, in order to reach reasonable reaction times for industrial applications, the thermal

non-catalytic TDM requires a reaction temperature above 1300 K, which can be achieved by using high-temperature heat or electricity. Thus, the overall CO_2 emissions from the process depend on the energy source applied to produce this heat.

The energy balance of TDM is thoroughly studied in Publication II. An energy balance for the theoretical TDM reaction with no losses in a case where the reaction temperature is 1500 K and methane conversion is 0.9 is shown in Fig. 2.2. In this work, the denotation for methane conversion varies from 0, when the TDM reaction does not exist, to 1, when all the methane reacts in TDM. Sensible enthalpy refers to the heat required to heat up the feedstock prior the TDM reaction and toe the heat bound to the products due to the high reaction temperature. The reaction enthalpy (numeric value presented in Eg. 2.3) is required in order to conduct the TDM reaction. The methane fuel energy accounts for the balance of the input energy. Due to the methane conversion below 1 assumed here, 8% of the output energy is in a form of methane fuel energy. In this case, the larger share of the output energy is bound as hydrogen fuel energy. The energy penalty of TDM method is the energy bound to the product carbon which remains unutilized as the carbon is not burned. Therefore, in order to make TDM economically profitable, the marketing value of the produced hydrogen and solid carbon must exceed the value of the energy bound to the carbon as well as the reaction enthalpy. Part of the heat needed in the process could be provided by utilizing waste heat from some other process.

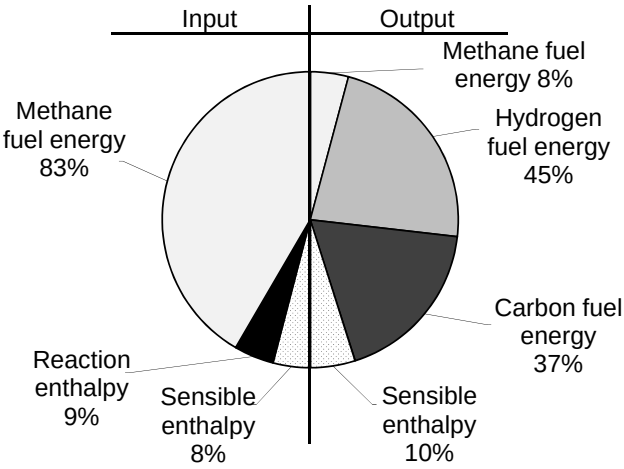

Fig. 2.2: Theoretical, i.e. no losses taken into account, energy balance for TDM at the reaction temperature of 1500 K and with the methane conversion of 0.9.

The history of commercial TDM applications dates back to the 1920s. Back then, TDM was applied to produce thermal black for tire manufacturing due to the growing car industry with a process called thermal black process. Typically, the thermal black process consists of two refractory-lined cylindrical furnaces that

are operated in a cyclic manner. The gaseous product from the process, which contains approximately 90% of hydrogen, is burned in one of the furnaces to heat it up. Simultaneously, natural gas is fed to the other furnace, which was heated earlier to the temperature of approximately 1600 K. The product gas conveys the thermal black to the bag filters from where it is collected and finalized by bagging or pelletizing. However, the more efficient oil-furnace process, in which heavy, highly aromatic oil is used as feedstock, was invented in 1943 and it rapidly became the dominant method for producing carbon black for rubber industry. In the oil-furnace process, part of the feedstock is combusted in order to provide the heat needed to pyrolyze the remaining oil. Nowadays, the oil-furnace process dominates the carbon black production. [32]

In the 1960s, a pilot plant for continuous hydrogen production by TDM was operated by Universal Oil Products [33]. The technology was based on methane decomposition over a nickel catalyst in a moving bed reactor at the temperature of 1090 K–1370 K. Hydrogen was the primary product of the process and the product carbon was simply combusted to produce heat, which caused CO_2 emissions. Several decades later, GasPlas operated a commercial plant to produce both hydrogen and carbon black by TDM in Canada from 1998 to 2001 [34]. In this Kvaerner Carbon Black and Hydrogen Process, the hydrocarbon feedstock was decomposed to carbon black and hydrogen by using plasma burners [35]. The plant was decommissioned due to technical problems that occurred in the plasma technology [36].

The scientific research of the TDM reaction began in the 1960s [37–41]. The discovery of carbon nanotubes at the beginning of the 1990s [42, 43] resulted in wide research interest towards the production of carbon nanotubes by catalytic methane decomposition that has lasted until present [44–52]. Among the metal catalysts, Ni, Fe, and Co have been found as the most suitable for methane decomposition. The methane decomposition reaction has been detected already at the temperature of 470 K in a presence of a nickel catalyst [53]. However, reaction temperatures between 750 K and 1050 K are more applicable when using metal catalysts. Metal catalysts give a higher reaction rate and higher methane conversion at lower temperatures than carbon catalysts [54]. By contrast, the main disadvantages of metal catalysts are that the carbon formation in methane decomposition may break up the catalyst or sequester the catalyst from the reaction. Furthermore, separating the catalyst particles from the solid carbon may be troubled and the impurities originating from the catalyst may diminish the application possibilities of the product carbon.

At the late 1990's, Muradov [31] presented the concept of on-site production of hydrogen and methane blends from natural gas by TDM. This resulted in an extensive research of carbonaceous catalysts [55–57] as well as non-catalytic TDM [58–61] at the beginning of 21st century. The advantages of carbonaceous catalysts are the low cost in comparison with metal catalysts, the possibility to utilize the product carbon without separating the catalysts from it and that the product carbon could be a suitable catalyst for the reaction after activation [55, 62–64]. Furthermore, a tempting option proposed frequently [64–66] is that the product carbon could autocatalyze the reaction, but the experiments

have shown only short periods of autocatalytic effects at the beginning of the reaction [62,67]. Most widely studied carbonaceous catalysts for methane decomposition are activated carbon and carbon black due to their preferable activity and stability. The most suitable temperature range for carbonaceous catalysts in methane decomposition is between 1050 K and 1300 K.

An important issue to take into account when considering the possibilities to produce hydrogen by TDM is the product carbon utilization. In this work, the application possibilities of the TDM product carbon were evaluated by surveying the current production volumes and market prices of different carbon products. The results are presented in Publication II. Moreover, an extensive literature survey of experimental TDM studies was carried out in order to clarify the dependence of the TDM product carbon type on the reaction conditions (Fig. 2.3). In comparison with a similar survey published in 2005 [33], more experimental TDM research has been conducted and wider temperature ranges have been applied since then. Furthermore, the TDM product carbon morphology and properties have been studied more frequently recently. The TDM reaction with a metal catalyst has a tendency to produce filamentous carbon such as carbon nanotubes. By contrast, carbon catalysts can produce both amorphous and crystalline carbon. At temperatures above 1450 K, where the reaction equilibrium does not restrict the TDM reaction, the non-catalytic TDM has been observed to produce carbon black (Publication II).

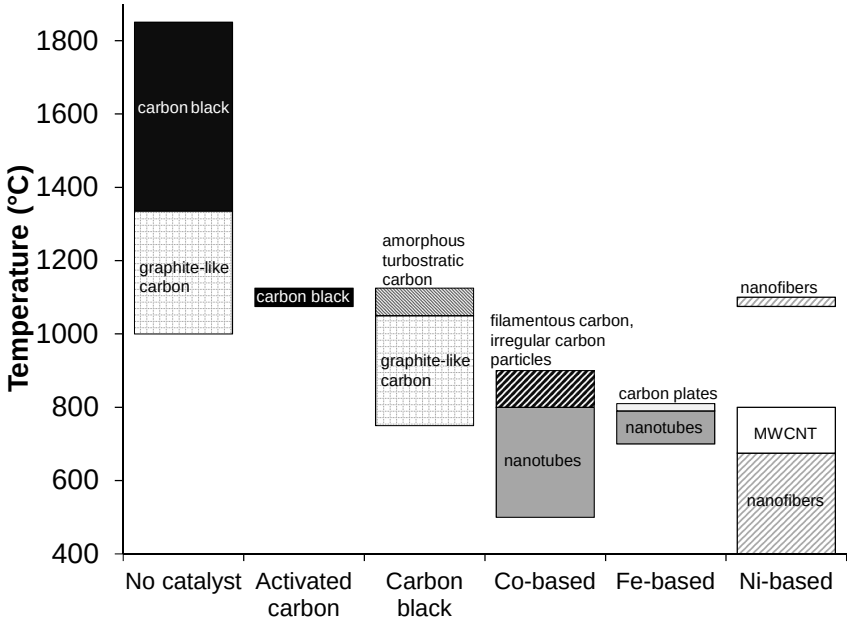

Fig. 2.3: The TDM product carbon type dependence on the reaction temperature in non-catalytic reaction and with five different reaction catalysts. MWCNT=Multiwalled carbon nanotubes (Publication II)

The value of the different TDM carbon types was estimated based on a market analysis presented in Publication II and updated here. The results are summarized in Table 2.1. The single and double walled nanotubes have the highest value among the possible TDM product carbon types. The price of multiwalled carbon nanotubes (MWCNT) is dependent on the carbon purity and tube diameter. The quality of industrial grade MWCNTs is lower than research grade products, which means the higher content of amorphous carbon and production residues in the industrial grade product. The industrial grade MWCNTs typically have purity of 90% and are suitable for conductive plastics and polymers, paints, and epoxies. [68] The prices of carbon black, activated carbon or metallurgical coke are less than that for nanotubes.

Table 2.1: Prices of various carbon products. MWCNT=Multiwalled carbon nanotubes

	Details	Price	Ref.
Single/double walled nanotubes		21,000–260,000 EUR kg^{-1}	[68]
MWCNT	Research grade quality	500–21,000 EUR kg^{-1}	[68]
MWCNT	Industrial grade, tube diameter 10 nm	340–390 EUR kg^{-1}	[68]
MWCNT	Industrial grade, tube diameter 20 nm...40 nm	170–340 EUR kg^{-1}	[68]
Carbon black		0.5–2 EUR kg^{-1}	[69–71]
Activated carbon		1.5 EUR kg^{-1}	[72]
Metallurgical coke		0.12–0.32 EUR kg^{-1}	[73]

The dependency of the TDM product carbon type on the TDM reaction temperature is summarized in Fig. 2.4. Moreover, the possible applications of each carbon type are listed. The price range for carbon nanotubes is wide and some of the applications are currently at a research stage. This work focuses on non-catalytic TDM at temperatures above 1200 K, where the TDM product carbon is expected to be carbon black. Therefore, the following introduces the principles of the carbon black formation and properties.

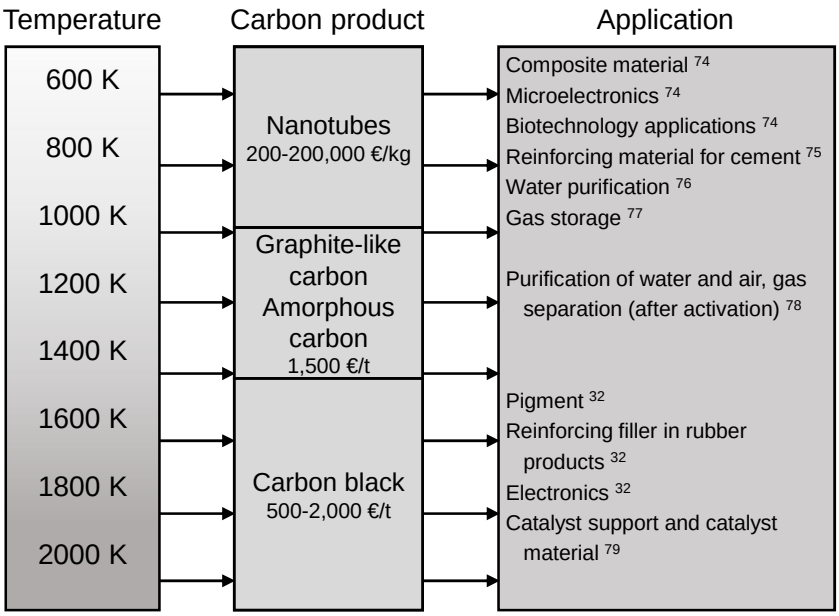

Fig. 2.4: The dependency of the product carbon type on the TDM reaction temperature and application possibilities for the carbon. [32, 74–79]

The Encyclopedia of Chemical Technology [32] defines carbon black as a generic name for products which mainly consist of elemental carbon and have an extremely fine particle size. Furthermore, thermal black is defined as a type of carbon black that has larger particle size and is produced by the thermal decomposition of gaseous hydrocarbons, for example, methane. The main application for carbon black is a filler in rubber compounds, where it improves the physical properties of the material [80]. The non-rubber applications such as paints and inks account for 10% of the carbon black consumption [80].

Generally, the formation of carbon black is divided into the following phases: the formation of carbon black precursors from the hydrocarbon molecules at the gas phase, nucleation of the precursors, aggregate formation, surface growth on particles or aggregates, agglomeration due to the collision of the aggregates, and finally the reactions of the carbon black surface with the gas phase [32]. The main part of the carbon black mass is produced by surface growth rather than through the formation of new carbon black particles [81]. The surface growth, which occurs after the formation of aggregates, causes the aggregates to be the smallest existing entity in carbon black [81]. Thus, aggregates can be separated into particles only by fracturing.

Since the main application for carbon black is rubber products, its properties are generally regarded from that perspective. When the utilization possibilities of the carbon black are considered, particle size is one of the most important parameters [32]. The particle size greatly affects the specific surface area of carbon black, and therefore determines the area where the carbon black can further inter-

face with other compounds. According to [32], increasing the temperature during carbon black formation increases the surface area of carbon black. The specific surface area can be determined from the particle size measurements by using a transmission electron microscope (TEM) or directly with the following standardized methods: nitrogen adsorption, iodine adsorption, and the adsorption of cetyltrimethylammonium bromide [32]. Furthermore, the smaller particle size of carbon black indicates better reinforcing properties and abrasion resistance [82].

When considering the everyday use, the carbon black structure, which generally refers to the morphology of the aggregates, is also an important parameter [32]. The aggregate size and shape, and the distribution of these factors affect the ability of carbon black to perform as a reinforcing agent or as a pigment [32]. In addition to the particle size and structure, the surface activity is also an important parameter affecting the utilization of carbon black [32].

In comparison with the currently dominating carbon black production technology, oil-furnace process, the benefit of TDM is that direct CO_2 emissions are not produced in TDM and the purity of the produced hydrogen is high. Thus, the by-product carbon from hydrogen production by TDM could replace the carbon black currently produced from aromatic oils. However, the current demand for carbon black in rubber industry is limited, which sets a limit to the TDM application possibilities. According to a rough estimate presented in Publication II, replacing 6% of the current global annual hydrogen production by TDM would simultaneously produce all the carbon black currently required in the industry. Increasing the TDM utilization from this extent would require developing new applications for the product carbon. The following large-scale applications for the TDM product carbon are highlighted in Publication II: building or construction material, replacing metallurgical coke in steel production, direct fuel cells for electricity generation, and soil amendment.

The primary technological challenges in TDM are related to the high reactor temperature and to the solid carbon formation. As always, using high reaction temperatures, which in case of TDM may be over 2000 K, requires applying specialized materials that may cause considerable costs. Additionally, the product carbon deposition in the reactor may cause a reactor clogging and prevent continuous operation. The carbon deposition has been detected to become harder as the reaction temperature increases [83]. The heat required in TDM may be produced by an additional combustion of fossil fuels, which causes direct CO_2 emissions, or using electricity, in which case the primary source and the production efficiency of this electricity defines the emissions of the produced hydrogen [84]. Applying a catalyst decreases the reactor temperature requirement but causes another problem: catalyst deactivation due to the carbon formation on the catalyst surface. Metal catalysts can be regenerated to restore the catalyst activity. However, regeneration causes additional CO_2 emissions, which would make TDM less appealing hydrogen production method. Using the product carbon from TDM as a reaction catalyst has been widely presented as an inexpensive and environmentally favorable option when the overall life-cycle of the process has been evaluated [65]. Nevertheless, in experimental tests, a steady decrease of

the catalytic activity of the product carbon has been detected due to the changes on the carbon surface [67].

The reactor technologies applied for experimental studies of TDM were surveyed in this work and the results are presented in Publication II. Catalytic TDM has been studied mainly in fluidized bed reactors or in fixed bed reactors. In contrast, non-catalytic TDM experiments have been carried out with flow reactors and liquid metal reactors. In most cases, the laboratory setups have been heated by an electrical oven, but additionally, microwaves, plasma, and concentrated solar energy have been tested. Despite the reactor type, the carbon removal from the reactor is a challenge that may prevent the continuous operation [84].

Several economic analyses of hydrogen production by TDM have been conducted. Muradov and Veziroğlu [30] found the minimum selling price for the solid carbon from TDM to be 350 USD t_C^{-1} in order that TDM could compete economically with SMR. Later, Triphob et al. [85] presented an economic analysis for applying TDM to produce hydrogen for fuel cells. In that study, the main advantage of hydrogen production by TDM was that it produces less CO_2 emissions than SMR, and in addition, the costly CCS step in the process would be avoided. Triphob et al. assumed the TDM carbon value of approximately 1,100 USD t_C^{-1}. Recently, Parkinson et al. [86] conducted a techno-economic analysis of hydrogen production by TDM in molten metal reactors. In this concept, methane is bubbled through a molten metal bed whose temperature is above 1300 K and the occurring TDM reaction produces hydrogen. When assuming a moderate product carbon value (200 USD t_C^{-1}) and that the molten metal bed has no catalytic effects and is heated by an electric arc, TDM was able to compete with SMR only when a CO_2 tax of 78 USD $t_{CO_2}^{-1}$ was added. The authors of that paper proposed to invest in research in order to find a suitable catalyst for the molten metal reactor that enables the operation at temperatures below 1300 K since it would decrease the energy demand of the process.

The total CO_2 emissions of hydrogen production by TDM have been proven to be less than those from the conventional hydrogen production by the steam reforming of natural gas [87]. In a very recent study, Weger et al. [88] proposed TDM as a technology that would enable environmentally clean transition from the current economy based on fossil fuels to the hydrogen economy. According to the analysis, employing TDM to produce hydrogen enables a significant reduction of GHG emissions, up to 27%, in comparison with the current situation. Achieving this high emission reduction requires that the methane leakages in the process are under control and the produced hydrogen is efficiently utilized in fuel cells.

2.3 Technical comparison of hydrogen production processes

The selected hydrogen production technologies were evaluated by analyzing the opportunities in each technology and the main barriers preventing the execution of those. The key properties of each hydrogen production technology are summarized in Table 2.2.

Table 2.2: Key properties of the selected hydrogen production technologies.

	SMR	Alkaline electrolysis	TDM
Technology maturity	Mature technology [1]	Mature technology [1]	Research/ piloting stage
Optimal capacity	Large scale, 150–300 MW_{H_2} [1]	Small scale, up to 3 MW_{H_2} [3]	Small to medium industrial scale (Publication IV)
Investment cost	340–510 EUR $kW_{H_2}{}^{-1}$ [1]	760–1,100 EUR $kW_{H_2}{}^{-1}$ [28]	1,100–1,400 EUR $kW_{H_2}{}^{-1}$ (Publication IV)

SMR is a mature technology and the currently existing plants ensure that the technology will be in use at least in the near future. Furthermore, there is an existing natural gas infrastructure from the reserves through pipes to the SMR plants. An option for mitigating the CO_2 emissions from the SMR plant is applying CCS, but the CCS infrastructure development will be on-going for decades. The IEA estimates that by 2050 CCS would be fully developed and widely utilized both in power production and in industrial applications [23]. The IEA lists the most important actions needed to fulfill CCS as follows: to identify new viable storage sites, to demonstrate large-scale CCS projects that test the compatibility of the individual technologies as well as to increase the understanding and acceptance of the CCS technology among the public and stakeholders. SMR is economically feasible technology in large-scale centralized hydrogen production. The transportation of hydrogen from the production site to the consumers requires the development of the transportation and distribution infrastructure.

There are various challenges related to water electrolysis. More development in electrolyzer technology is still required in order to decrease the costs. Moreover, the availability of inexpensive renewable electricity is a necessity for electrolysis applications, and therefore, a vast amount of renewable power generation capacity needs to be installed. Due to the fluctuating nature of the renewable electricity generation, transportation and storage of either electricity or hydrogen is required. Distributed hydrogen production by electrolysis would require transporting the renewable electricity from its production site. By contrast, centralized hydrogen production would be coupled to wide hydrogen transportation and distribution infrastructure. Electricity is suitable for short-term (<100 h) storage whereas hydrogen is more efficient in long-term storage [89]. Therefore, it is possible that hydrogen and electricity may coexist as energy carriers in the future energy system [89].

As is the case with SMR, TDM would benefit from the existing natural gas infrastructure. Furthermore, as TDM is applicable in distributed hydrogen production, the demand for hydrogen transportation is minor in comparison with centralized production. Thus, hydrogen handling can be minimized and instead the natural gas can be transported and stored as such. There are various possibilities to handle the elemental solid carbon from TDM. Storing the solid carbon is much easier and safer than storing gaseous CO_2 [30]. Various industrial ap-

plication possibilities for the TDM product carbon were listed in the previous section. By contrast, CCU provides an opportunity to utilize the CO_2 from SMR to generate marketable products. However, hydrogen generation causes only a fraction of all CO_2 emissions and many other CO_2 sources will exist in the future. The CCS technology development results in a situation where plenty of CO_2 for CCU applications would be available from various industrial and power generation sources. An essential benefit of hydrogen production by TDM is that it is dependent neither on the development of CCS technology and infrastructure nor the installation rate of the renewable power capacity.

Chapter 3

Reaction and reactor modeling

In this work, the TDM reaction and reactor modeling was carried out by applying two reaction mechanisms: a global reaction mechanism and a 37-step elemental reaction mechanism. The reaction parameters for the global reaction mechanism were optimized based on experiments conducted at TUT with a non-catalytic TDM test reactor. The suitability of the global TDM mechanism with the optimized parameters to describe the TDM reaction was verified utilizing experimental data in the literature. Additionally, the global TDM mechanism was compared with the 37-step TDM reaction mechanism presented in the literature. The experiments and modeling work is described in detail in Publication III. The TDM reaction modeling was essential for the reactor design and dimensioning that was additionally conducted in this work.

3.1 Regenerative heat exchanger reactor

The technological challenges that prevents applying TDM in an industrial scale have been discussed by Abánades et al. [84] who demanded developing "a continuous, reliable, sustainable, and economic process" for TDM. They highlighted the requirement for a solution that enables the TDM product carbon removal from the process either mechanically, chemically or by process control. To meet the needs of such setup, this work presents a new reactor type, a regenerative heat exchanger reactor (RHER). In this work, the RHER reactor technology was evaluated in a technical and economic sense as presented in Publication I. Four commercial scale process concepts for TDM were designed and compared with each other. The TDM reactor technologies in the concepts under research were: (Concept 1) the methane burner with a partial methane combustion which was a modification of the current oil-furnace process for carbon black production, (Concept 2) the high-temperature reactor powered by electricity or plasma, (Concept 3) the catalytic fluidized bed reactor and (Concept 4) the RHER reactor.

The principle of RHER, first presented in Publication I, is shown in Fig. 3.1. In RHER, a gaseous hydrocarbon is fed to the reactor from the bottom and the solid bed material flows in the countercurrent direction. Heating elements are utilized to achieve a suitable reactor temperature that enables the TDM reaction in the reactor. Alternatively, the required heat could be produced by partial combustion inside the reactor. However, in order to avoid CO_2 and CO components in the product gas, this option was not studied further in this work. The solid carbon deposits on the bed material surface and it is removed from the reactor by bed material circulation. Additionally, the bed material flow enables heat transfer from the product gas to the bed material at the end of the reactor and vice versa at the beginning of the reactor. Thus, the countercurrent flow of the gas and the bed material enables efficient heat transfer in the reactor and evens the temperature profile in the reactor. Moreover, from the scientific point of view, the solid bed material in the RHER provides a stable heat profile for the experimental studies of reaction kinetics.

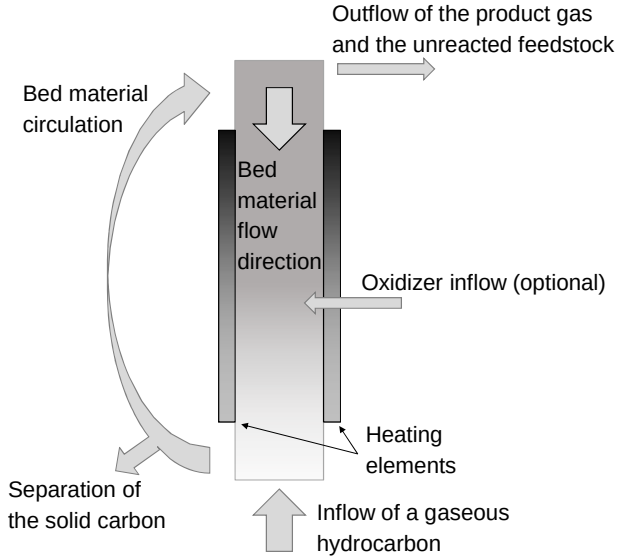

Fig. 3.1: The principle of the regenerative heat exchanger reactor, RHER. [90]

After separating the solid carbon from the bed material, the bed material would be circulated back to the reactor by lifting it pneumatically or mechanically. The bed material circulation system must maintain gas tight in order to prevent air flowing into the reactor. Additionally, it is speculated that the carbon removal from the bed material would occur by mechanical shaking and that the separation would become easier the more carbon has been deposited on the bed material surface. However, the bed material circulation and carbon separation have not been experimentally tested and proved in this work.

3.2 TDM reaction kinetics

In this work, the TDM reaction was described using a global reaction mechanism, which is the simplest way to study a chemical reaction. The global reaction equation for TDM is shown in Eq. 2.2.3. The reaction rate was assumed to consist of two terms, which described the forward and backward reactions:

$$\frac{\mathrm{d}n_{\mathrm{CH_4}}}{\mathrm{d}t} = k_{\mathrm{forward}} \cdot {c_{\mathrm{CH_4}}}^{n} - k_{\mathrm{backward}} \cdot {c_{\mathrm{H_2}}}^{m}, \tag{3.1}$$

where $n_{\mathrm{CH_4}}$ is the amount of methane (mol), t is time (s), $c_{\mathrm{CH_4}}$ and $c_{\mathrm{H_2}}$ are the concentrations of methane and hydrogen (mol cm^{-3}), k_{forward} and k_{backward} are the rate constants, and n and m are the respective reaction orders (-) for forward and backward reactions [91]. For simplicity, the backward reaction rate was assumed to be dependent on the hydrogen concentration only. The backward reaction is much slower in comparison with the forward reaction at the reactor environment used in this work. Therefore, it was assumed that an excess amount of carbon would be available for the backward reaction to occur and the carbon amount would not limit the backward reaction rate. This simplified model (Eq. 3.1) could be complemented by taking into account the effect of the product carbon surface area on the backward reaction rate. However, this would require more detailed data on the solid carbon surface area development in the reaction environment.

In the case of both forward and backward reactions, the rate constants were assumed to follow the Arrhenius equation:

$$k = A \cdot \exp\left[-E_{\mathrm{a}}/(R_{\mathrm{u}}T)\right], \tag{3.2}$$

where A is the frequency factor, E_{a} is the activation energy (J mol^{-1}), R_{u} is the universal gas constant (8.314 J mol^{-1}K^{-1}), and T is the temperature (K) [91]. The rate constants and frequency factors use units of cm^3, J, mol, and s.

In this work, the reaction parameters in Eqs. 3.1–3.2 were optimized by utilizing the experimental data achieved with the laboratory-scale test reactor. Totally four reaction parameters were determined by the optimization procedure: the frequency factor and the activation energy for the forward reaction ($A_{forward}$ and $E_{\mathrm{a},forward}$, respectively) and the reaction orders for both forward and backward reactions (n and m, respectively). The remaining reaction parameters for the backward reaction ($A_{backward}$ and $E_{\mathrm{a},backward}$) were solved utilizing the relationship between the rate constants, defined as the equilibrium constant [91]:

$$K_c = \frac{k_{\mathrm{forward}}}{k_{\mathrm{backward}}}. \tag{3.3}$$

The values for the equilibrium constant K_c (-) were taken from the literature [92] and modified into the following exponential form:

$$K_c = 941{,}272.1 \cdot \exp\left[-96{,}425.0/(R_{\mathrm{u}}T)\right]. \tag{3.4}$$

The numerical values for the frequency factor and the activation energy of the backward reaction were solved by combining Eqs. 3.3 and 3.4.

Another TDM reaction mechanism evaluated in this work was a 37-step reaction mechanism that was originally developed by Olsvik and Billaud [93] at the 1990's and later improved by Ozalp [94]. Among the kinetic models for the TDM reaction presented in the literature [61, 93–97], the 37-step reaction mechanism was selected as it was presented with full information regarding the reaction mechanism and kinetic parameters [94] Originally, the reaction mechanism consisted of 36 homogenous gas phase reactions and it was derived from the experiments of non-catalytic TDM carried out in a plug flow reactor at the reactor temperature up to 1273 K and with low methane conversion values (<0.01) [93]. Later, the mechanism was further studied and an irreversible reaction describing the solid carbon formation was added to the mechanism [94]. The 37-step reaction mechanism follows the reaction path:

methane → ethane → ethylene → acetylene → solid carbon & hydrogen.

Ozalp et al. [94] successfully applied the 37-step mechanism to describe the solid carbon formation by TDM at reaction temperatures above 2000 K. However, in the same study, the 37-step mechanism was not able to predict the experimentally observed solid carbon formation at temperatures below 2000 K. Therefore, in this work, the 37-step mechanism was further adjusted in order to improve its ability to predict the solid carbon formation by TDM at temperatures below 2000 K. The analysis, the development work, and the results are presented in detail in Publication III.

3.3 Packed bed reactor model

A packed bed reactor model combined with the global TDM reaction mechanism was applied to study the TDM reaction occurring in the experimental setup. Additionally, the packed bed reactor model was utilized for designing and dimensioning of the RHER reactor in the TDM process studies.

Principally, the packed bed reactor consists of solid particles and a gas flow through the bed. The proportion of the empty space in the packed bed, i.e. the void fraction, was experimentally defined to equal that in the experimental setup by counting beads in a certain volume and estimating the void fraction mathematically. The pressure drop ($\mathrm{d}P$) along a differential reactor length ($\mathrm{d}x$) was written as [98]:

$$\frac{\mathrm{d}P}{\mathrm{d}x} = \frac{150\mu\, V_\mathrm{c}}{{L_\mathrm{c}}^2} + \frac{1.75\rho\, V_\mathrm{c}^2}{L_\mathrm{c}}, \tag{3.5}$$

where μ is the dynamic viscosity (N s m^{-2}), and ρ is density (kg m^{-3}). Furthermore, V_c is the characteristic velocity (m s^{-1}) and L_c is characteristic length (m) that are defined as follows:

$$V_\mathrm{c} = \frac{\dot{m}}{\rho \varepsilon_\mathrm{v} A_\mathrm{c}} \tag{3.6}$$

and

$$L_{\mathrm{c}} = d_{\mathrm{p}} \left(\frac{\varepsilon_{\mathrm{v}}}{1 - \varepsilon_{\mathrm{v}}} \right), \tag{3.7}$$

where $\dot{m}$ is the gas mass flow rate (kg s^{-1}), A_{c} is the cross-sectional area of the bed (m^2), d_{p} is the diameter of the spherical bed particles (m), and ε_{v} is the void fraction (-) [98].

The heat transfer in the test reactor was studied separately, but was not attached to the packed bed reactor model, since it would have slowed down the reaction parameter optimization. The temperature measurement setup during the experiments was such that the measurement points presented a mixture of the solid bed material temperature and gas temperature, but the gas and solid temperatures were not measured separately. Therefore, it was assumed that the temperatures of the gas and solid material were equal. In order to verify this assumption, separate numerical analysis was conducted that took into account the heat transfer in the reactor. In the analysis, the test reactor was modeled as a packed bed reactor, the bed temperature was defined equal with the measured reactor temperature profile and the gas temperature was calculated based on heat transfer between the gas and bed. The change in gas temperature ($\mathrm{d}T_{\mathrm{b}}$) along a differential reactor length ($\mathrm{d}x$) was calculated as follows:

$$\frac{\mathrm{d}T_{\mathrm{b}}}{\mathrm{d}x} = \frac{2\pi R h_{\mathrm{c}}}{\dot{m} c_p} (T_{\mathrm{s}} - T_{\mathrm{b}}) \tag{3.8}$$

where R is the total radius of the reactor tube (m), h_{c} is the convective heat transfer coefficient between the bed and gas (W m^2K^{-1}), $\dot{m}$ is the gas mass flow rate (kg s^{-1}), c_p is the specific heat capacity of the gas at constant pressure (J kg^{-1} K^{-1}), and T_{s} is the bed temperature (K) [98].

According to the numerical analysis, the gas and bed temperatures deviate most at the beginning and at the end of the reactor tube which are not heated and where the temperature therefore changes steeply. At the beginning of the reactor tube, the gas temperature was at maximum 15 K lower than the bed temperature and at the end of the reactor tube, the gas temperature was at maximum 15 K higher than the bed temperature with the gas flows in question. However, the temperatures were highly similar in the middle of the reactor, where the temperature was the highest. Regarding the TDM reaction modeling, the part where the temperature is above 1000 K is the most remarkable area and the assumption that the bed and gas temperature are equal is valid. According to a sensitivity analysis, the gas volumetric flow needs to be tenfold and the heat transfer area between the gas and beads should be one third of that what was calculated in order to achieve a significant deviation between the gas and bed temperatures.

Additionally, the gas temperature in the radial direction in the reactor was assumed uniform. This assumption was considered valid since the gas velocity was low and the heat capacity of the bed was high in comparison with the gas as the heat transfer analysis presented above demonstrates. Thus, with the gas volumetric flows used in the experiments, it was reasonable to assume that the

gas temperature in the test reactor was uniform in the radial direction and that it equals the bed temperature measured during the experiments.

3.4 Constant pressure reactor model

In order to verify the reaction parameters that were optimized using the packed bed reactor model, a homogenous 0-dimensional constant pressure reactor model in LOGESoft [99] was applied to study the TDM reaction. In this model, the methane decomposition was calculated based on the pre-defined reaction mechanism and reactor temperature. The reactor temperature profiles from the experiments were converted to time-dependent profiles during the reaction parameter optimization in order to enable implementing those into the constant pressure reactor model. Moreover, the constant pressure reactor model enabled studying the 37-step TDM reaction mechanism that would have been too complicated to implement into the packed bed model in MATLAB.

In the constant pressure reactor model, the reactor was a closed system whose mass (m (kg)) followed the mass conservation equation:

$$\frac{\partial m}{\partial t} = 0, \tag{3.9}$$

where t is time (s). Additionally, the mass fraction of each species i in the gas mixture (Y_i (-)) was calculated for the closed system as

$$\frac{\partial Y_i}{\partial t} = \frac{r_i M_i}{\rho}, \tag{3.10}$$

where r_i is the reaction rate (mol m^{-3} s^{-1}) and M_i is the molecular mass (kg mol^{-1}) of the ith species in the gas mixture, and ρ is the density (kg m^{-3}) [100]. The thermodynamic properties of gases were calculated by utilizing the NASA polynomials [99]. The constant pressure reactor model was found appropriate for reactor simulations, since a pressure drop of 0.3% at maximum occurred along the total reactor length according to calculations conducted during the reaction parameter optimization.

According to a comparative analysis, the methane conversion results were not dependent on the reactor model selection, but both the packed bed reactor model and the constant pressure reactor models provided highly similar methane conversion values when using the global TDM reaction mechanism with optimized parameters. This verifies the reliability of the packed bed reactor model used for reactor parameter optimization. Furthermore, the applicability of the global mechanism with the optimized reaction parameters to predict the TDM reaction was evaluated by using experimental results presented in the literature. Additionally, comparison was conducted between the global TDM reaction mechanism and the 37-step TDM reaction mechanism.

3.5 The reaction parameter optimization for TDM

The reaction parameter optimization was conducted by applying a particularly written MATLAB-based function where the TDM reaction occurs in the packed bed reactor. The function combined the global TDM reaction mechanism, the gas flows, and the packed bed reactor model in order to simulate the test reactor. The function defined the gas properties along the reactor length based on the measured reactor temperature profile, determined the pressure drop in the reactor (Eqs. 3.5-3.7), and calculated the methane conversion based on the reaction rate (Eqs. 3.1-3.4).

Totally 48 separate measurement cases were used for the optimization. In each case, the function calculated the methane conversion at the end of the reactor and compared that with the experimental value. Each experimental case was equally weighted meaning that each of the 48 experimental cases had an equal effect on the reaction parameter optimization. The function 'fminsearch' in MATLAB was utilized in order to optimize the reaction parameters by minimizing the square error between the modeled methane conversion value and the corresponding experimental one. Figure 6.5 in Section 6.1 presents four example cases each of which contains the gas temperature profile as a function of gas residence time in the reactor as well as the experimental and modeled methane conversion values.

Chapter 4

Experimental

4.1 Laboratory-scale test reactor

A laboratory-scale test reactor for TDM experiments was designed and partially constructed by the author at TUT. The reactor setup is presented in detail in Publication III. The test reactor design was based on previous knowledge gained from the design, construction, and testing of a small-scale test reactor at TUT laboratory [101]. The test reactor was utilized to study the carbon deposition on the bed material particles. Furthermore, due to the large heat capacity of the bed material in comparison with the gas, the experimental data from the test reactor was used for the TDM reaction kinetics studies. The temperature profile in the reactor as well as the composition of the feed gas and product gas were measured for reactor modeling purposes. Additionally, the quality of some carbon samples was analyzed.

The test reactor has been presented in detail in Publication III, but the key aspects are summarized here. A picture and schematics of the test reactor are shown in Fig. 4.1. The alloy reactor tube (Kanthal APM) with substantial wall thickness (5 mm) was chosen. Flanges at both ends of the reactor tube enabled opening and closing the reactor. The flanges were sealed with copper seals in order to keep the reactor gas tight during the operation. The reactor temperature profile was continuously determined using K-type thermocouples at eight measurement points and recording the data in 2-second intervals.

The middle part of the reactor was heated with electrical heating modules (Fibrothal RAC 200/500) in circular shape and these elements were covered with an additional insulation layer to minimize the thermal losses from the reactor. Three heating elements (heating power of 19.7 kW per piece) were separately adjusted with a combination of a thyristor unit (Eurotherm 7100A) and temperature controllers (Eurotherm 3204).

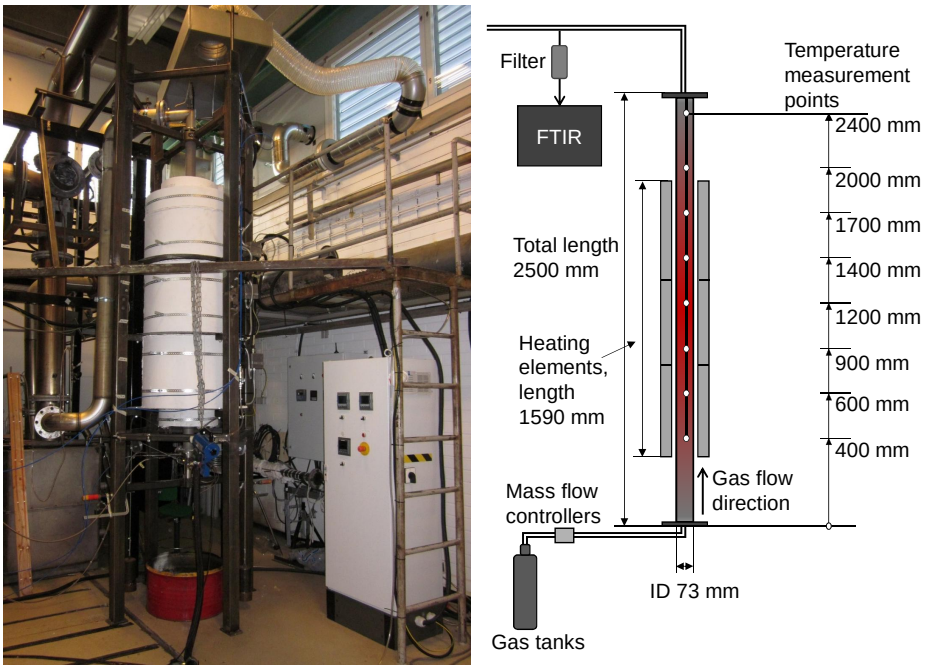

Fig. 4.1: Picture and schematics of the laboratory-scale test reactor. (Publication III)

The reactor tube was filled with spherical inert ceramic beads (diameter 10 mm) that stabilized the reactor temperature profile and provided a surface for carbon accumulation in the reactor. The gas mixture fed to the reactor contained methane (purity 99.995%) and nitrogen (purity 99.95%) and the gas flow rates were controlled with mass flow controllers in the range up to 15 dm^3 min^{-1}. The measurement uncertainty provided by the mass flow controller manufacturer was 0.5%.

Before each measurement, the reactor was heated up and the reactor was kept inert with a nitrogen flow of 6 dm^3 min^{-1}. When a stable reactor temperature profile was achieved, the methane/nitrogen gas mixture was fed to the reactor. After exiting the reactor tube, part of the product gas was extracted from the main stream, flowed through a filter in order to remove the remaining carbon particles, and conveyed to the in-line gas composition analysis.

Totally, 48 separate cases were measured which had a unique combination of reactor temperature profile as well as composition of feed gas and product gas as shown in Table 4.1.

Table 4.1: The inlet gas composition, temperature profiles, and corresponding methane conversion values for each experimental case. (Publication III)

	Gas input (dm^3 min^{-1})		Temperature (°C) as a function of reactor height (m)								Methane conv. (-)
Case	CH_4	N_2	0.4	0.6	0.9	1.2	1.4	1.7	2	2.4	
1	0.1	6	226	390	593	738	744	801	666	90	0.000
2	0.1	6	783	942	941	949	925	940	710	84	0.006
3	1	8	660	800	798	977	956	1050	837	93	0.052
4	1	8	663	800	797	979	955	1050	837	94	0.055
5	1	6	684	828	935	995	967	998	811	102	0.058
6	1	8	796	920	982	1024	995	1026	825	103	0.068
7	0.15	6	905	1020	1050	1025	1006	1020	768	67	0.069
8	0.5	5	635	800	827	972	973	1049	813	89	0.076
9	0.5	5	656	800	806	976	966	1053	816	89	0.081
10	1	6	660	800	801	976	959	1050	824	90	0.084
11	1	6	664	800	798	978	957	1050	831	92	0.085
12	1	8	942	1024	1016	1023	989	1025	829	107	0.092
13	0.5	5	801	918	983	1025	995	1025	810	100	0.097
14	1	6	725	863	968	1025	995	1025	819	102	0.103
15	1	6	801	921	985	1026	995	1025	816	100	0.108
16	1	5	669	800	797	980	957	1050	825	92	0.110
17	0.3	6	899	1025	1025	1026	1013	1027	766	59	0.115
18	0.05	5	618	801	841	969	983	1050	801	86	0.124
19	0.5	5	945	1025	1020	1024	988	1025	813	105	0.151
20	1	8	270	560	904	1045	1053	1069	850	109	0.164
21	1	6	943	1025	1018	1024	988	1025	821	106	0.166
22	0.05	5	805	920	985	1025	994	1025	808	102	0.182
23	1	8	245	534	903	1045	1058	1070	852	107	0.188
24	0.05	5	942	1025	1023	1025	987	1026	810	107	0.191
25	0.05	5	227	527	916	1044	1066	1070	834	101	0.195
26	0.05	5	257	550	908	1045	1057	1070	837	106	0.222
27	0.05	5	649	801	814	973	968	1050	812	89	0.270
28	0.5	5	262	552	908	1045	1056	1070	838	105	0.277
29	0.5	5	233	529	909	1045	1063	1070	838	102	0.305
30	1	6	266	557	905	1045	1056	1070	847	107	0.322
31	1	6	239	531	905	1046	1060	1070	846	105	0.329
32	0.1	6	945	1081	1089	1093	1061	1082	837	92	0.458
33	0.1	6	970	1099	1108	1111	1078	1100	859	93	0.603
34	1	15	1138	1165	1159	1165	1128	1165	938	83	0.726
35	1	10	1137	1165	1163	1165	1133	1165	891	77	0.744
36	0.1	8	1032	1146	1155	1159	1124	1150	910	95	0.783
37	1	10	1142	1165	1161	1165	1130	1165	917	80	0.788
38	1	5	1130	1161	1163	1160	1126	1161	839	92	0.795
39	0.7	6	1176	1163	1163	1168	1138	1165	883	110	0.812
40	0.1	6	1036	1150	1159	1162	1128	1155	888	95	0.815
41	1	5	1140	1165	1164	1165	1133	1165	884	77	0.824
42	0.15	6	1123	1165	1165	1165	1138	1165	865	75	0.825
43	0.5	6	1071	1163	1163	1168	1139	1165	880	108	0.831
44	1	5	1136	1170	1167	1170	1145	1169	864	68	0.832
45	0.3	6	1064	1164	1165	1168	1142	1166	874	107	0.842
46	0.15	6	1062	1164	1168	1170	1146	1169	864	107	0.854
47	0.05	6	1124	1171	1169	1170	1148	1170	858	67	0.878
48	0.05	6	1134	1166	1165	1166	1135	1165	872	76	0.906

The gas residence time in the reactor varied between 6 s and 21 s. The methane conversion in the experiments was calculated based on the values received by the outlet gas analysis.

4.2 Gas analysis

A part of the product gas from the reactor was analyzed with Fourier transform infrared spectroscope (FTIR) analyzer. FTIR was chosen for gas analysis since it enables simultaneous qualitative and quantitative gas composition analysis. In FTIR, the gas sample is exposed to infrared radiation and the resulting spectrum is analyzed. As the infrared spectrum is unique to each gas component, the gas composition can be analyzed based on the measured spectrum. Fourier transformation is applied to mathematically transform the measured frequency spectrum to gas composition data. [102]

The gas analysis consisted of a 10-second sampling period and a 20-second analysis period continuously following each other. Since FTIR cannot measure biatomic homonuclear molecules, such as hydrogen, a separate gas composition analyzes with gas chromatography were conducted at the early stage of this project [101]. These analyzes confirmed the presence of hydrogen in the TDM product gas and verified the method applied in this work for calculating the methane conversion and hydrogen amount in the product gas.

4.3 Product carbon characterization

The morphology of the selected product carbon particles was analyzed by electron microscopy. The experimental arrangement in the TDM test reactor was such that it was not possible to take a carbon sample from the reactor without cooling down the system, opening the flanges, and removing the bed material from the reactor. Therefore, only several experimental cases were run for an exceptionally long period of time to produce the amount of carbon required in the analyses. The time period for the carbon production was up to three hours. These tests were conducted only in order to produce carbon for analysis purposes. The intent was not to study the maximum time period the reactor could be operated before the product carbon would block the reactor and prevent the gas flowing through it.

During the experiments, the product carbon deposited on the surface of the ceramic beads. The carbon samples were collected so that the reactor tube was opened, all the ceramic beads were removed from the reactor, and several beads were selected for the analysis purposes.

4.3.1 Scanning electron microscopy

Scanning electron microscopy (SEM) is widely utilized to examine the microscopic surface structure of materials. In SEM, an electron beam scans over the sample surface and the emitted electrons are collected with detectors. The resulting

SEM images provide a three-dimensional appearance of the topography of the sample's surface. [103] In this work, the selected product carbon samples were analyzed with a scanning electron microscope (SEM, Zeiss, ULTRAplus). For the SEM analyses, the ceramic beads were attached to the aluminum stub with carbon glue and the carbon deposited on the bead's surface was analyzed.

4.3.2 Transmission electron microscopy

In transmission electron microscope (TEM), an electron beam is accelerated by high voltage and transmitted through the sample that has the thickness of less than 200 nm. The TEM image formation is based on the interaction between the electrons and the sample. The resolution in TEM may be as high as in order of 0.1 nm. TEM provides two-dimensional images of the inner structure of the sample and reveals the morphology and crystallization of the examined material. The TEM system is frequently equipped with an energy-dispersive X-ray spectrometer (EDS) that enables examining the elemental composition of the sample. EDS measures the X-ray distribution that is emitted from the sample atoms and the chemical elements in the sample are identified by sorting the signal by energy those contain. [104]

The transmission electron microscope (TEM, Jeol, JEM-2010) used for carbon analysis in this work was equipped with an energy dispersive spectrometer (EDS, Thermo Scientific, Noran Vantage with Si(Li) detector). For TEM analyses, samples were taken by scratching a piece of carbon from the bead's surface. The samples were prepared by crushing the product carbon slightly between laboratory glass slides, mixing the powder with ethanol, and applying a drop of powder dispersion onto the copper grid with a holey carbon film.

4.4 Experimental arrangement evaluation

The two major sources of uncertainty during the measurements were the volumetric gas flow measurement with the mass flow controllers and the gas composition analysis with FTIR. The measurement uncertainty defined by the device manufacturer was 0.5% for the mass flow controllers and an absolute value of 0.2% points for FTIR. These two measurement uncertainties were combined to calculate the overall uncertainties, which are marked as error bars in the results presented in Fig. 2 in Publication III.

In the gas composition analysis by FTIR, the measurement uncertainty was denoted as an absolute value of 0.2% points. Therefore, when the methane proportion in the inlet gas (a mixture of nitrogen and methane) was low, the measurement uncertainty was high in relative terms. In several cases this resulted in a situation where the uncertainty of the methane conversion was especially high, up to 160% of the experimentally defined value. Therefore, the measurement accuracy could be improved by eliminating the cases with exceptionally high measurement uncertainty. Substitutive experiments could be conducted by applying narrower gas concentration measurement ranges in FTIR or using higher methane content in the inlet gas. Some of the experiments were conducted with

an extremely low methane concentration in the inlet gas in order to widen the range of experimental conditions. For safety reasons, in all experiments methane was diluted with nitrogen.

The experimental data consisted of a great number of individual measurements each conducted in a case-specific environment. Therefore, comparing the experimental cases with each other was possible only by using the mathematical model. It was not possible to revise the experimental data before modeling for example by excluding any inconsistent measurement point. This modification would contain a risk that the excluded measurement point would better describe the studied phenomenon than the remaining points, but this risk was avoided in this work.

Chapter 5

Process design and economic analysis

In this work, an economic analysis of three hydrogen production technologies i.e. TDM, SMR, and water electrolysis was conducted. Production capacity in the processes was selected as 1,000 Nm^3 h^{-1} of hydrogen, which is applicable to fulfill the hydrogen requirement of a small industrial application e.g. in food industry, electronics industry, glass production or metal processing [3]. In the hydrogen economy, this hydrogen production capacity would meet the demand of a commercial fueling station that is capable of serving up to 500 cars per day [105]. The diving range of a hydrogen fueled car has been announced to be up to 500 km [106]. The hydrogen production capacity of 1,000 Nm^3 h^{-1} is at the upper capacity limit of the currently commercially available alkaline electrolyzers [27]. Moreover, two hydrogen production capacities were assumed for SMR: 1,000 Nm^3 h^{-1} and 100,000 Nm^3 h^{-1}. The hydrogen production capacity of 100,000 Nm^3 h^{-1} equals the consumption of a large industrial process e.g. oil refining, ammonia synthesis or methanol synthesis [3]. Alternatively, the capacity would be suitable for centralized hydrogen production in the hydrogen economy [107]. The large hydrogen production capacity was chosen for SMR since the economic viability of this technology increases with the unit size. Additionally, an option to reduce the CO_2 emissions from SMR by CCS was taken into account by coupling CO_2 capture to the large-scale SMR process. The economic feasibility of CCS technology is the highest when applied to large point source emissions.

5.1 TDM processes

Two TDM process schemes (named as TDM and TDMG) were designed and evaluated in this work. The starting point of the process design was the concept design conducted at the early stage of this work (presented in Publication I). Both processes applied RHER reactor technology for conducting the TDM reaction.

A simplified version of the flow chart for the TDM process is shown in Fig. 5.1 whereas the detailed process scheme is presented in Publication IV. In the TDM

process, the heat needed in the RHER reactor is produced by burning additional natural gas. The TDM product carbon is removed from RHER by bed material circulation, separated, pelletized, and packed to be marketed. Furthermore, the carbon particles in the TDM product gas are filtered out and hydrogen is separated by using membranes. The remaining gas from the hydrogen separation by membranes is recirculated to the RHER reactor. Heat is internally transferred from the hot flows to the cold flows in order to minimize the external heat requirement. Moreover, cooling is added to the process to avoid material damages caused by too high temperatures.

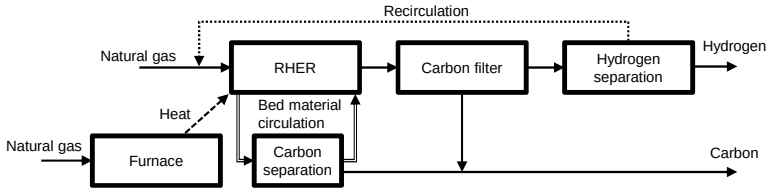

Fig. 5.1: Flow chart of the TDM process applied in the economic analysis. (Publication IV)

Membranes provide a suitable technology for hydrogen purification in small-scale applications. The driving force for gas separation in membranes is the pressure gradient over the membrane thickness [20]. The gas mixture is fed to the high-pressure side and hydrogen migrates across the membrane to the low-pressure side [20]. The scalability of membranes enables using those both in industrial and portable applications [20]. Usually, the membrane processes are easy to control by operating the temperature and pressure at least when the feed gas composition does not vary significantly over time [17].

Another TDM application is the TDMG process, where the majority of the TDM product carbon is gasified in order to maximize the hydrogen production. A simplified flow chart is shown in Fig. 5.2 and a detailed scheme in Publication IV. The TDM product carbon gasification occurring in the TDMG process can be an economically feasible option if the product carbon has a low value or if separating the carbon from the bed material turns out difficult or expensive. In the TDMG process, the bed material in the RHER reactor is circulated to a separate gasifier where the solid carbon is gasified with steam and the resulting product gas is handled in a WGS reactor. Finally, hydrogen in the product gas is separated by PSA and the off-gas is combusted along with additional natural gas to produce the heat required both in the RHER reactor and in gasification. In a case that the CO_2 content of the off-gas is high and CO_2 transportation infrastructure is available nearby the plant, the off-gas could be piped directly to a CO_2 storage. The RHER product gas treatment including the carbon filtering from the gas and hydrogen separation by membranes are similar to that in the TDM process. Furthermore, heat transfer units are utilized in the TDMG process to minimize

the external heat requirement, and thus the CO_2 emissions that originate from the heat production, and to provide cooling when necessary.

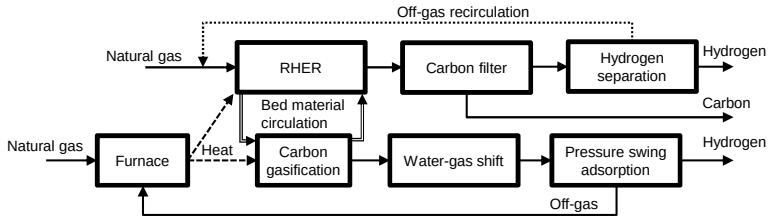

Fig. 5.2: Flow chart of the TDMG process (TDM coupled with product carbon gasification) applied in the economic analysis. (Publication IV)

The TDM product carbon gasification was not experimentally studied in this work. However, the gasification gas composition was calculated by using the experimental data from petroleum coke gasification as a reference [108]. The petroleum coke gasification was chosen for comparison due to its high carbon content (93%). This corresponds to the carbon content of the TDM product carbon samples analyzed in this work.

5.2 Process calculations

As a whole, six hydrogen production processes were evaluated in this work: (i) small-scale TDM, (ii) small-scale TDMG, (iii) small-scale electrolysis, (iv) small-scale SMR, (v) large-scale SMR, and (vi) large-scale SMR with a CCS coupling. A large-scale TDM technology was not studied here because it is hypothesized that the RHER reactor for TDM is not scalable, but that it would require utilization of several parallel reactors. Using parallel reactors would obviously result in higher cost in comparison to the SMR technology, where large size brings high economic benefits. Mass balance calculations were conducted for each hydrogen production process by following the defined process flow charts and calculation boundaries presented in Publication IV. The starting point of the analysis was the pre-defined hydrogen production capacity. The feedstock demand and the emissions were calculated to correspond the hydrogen requirement. The amount of reaction products from each process step was calculated based on the pre-defined reaction conditions and reaction equations. The initial process values and calculation assumptions with source references are comprehensively presented in Publication IV. However, the key aspects of the analyses are summarized here.

In the TDM and TDMG processes, the TDM reaction in the RHER reactor was simulated by utilizing the global TDM reaction mechanism with the optimized parameters that were introduced in this work. The reactor dimensions were calculated based on the feedstock volumetric flows and on the gas residence time in the reactor that was required in order to achieve the pre-defined methane

conversion. In the TDMG process, the gasification gas was fed into the WGS reactor, where the conversion was selected so that CO content below 3% was achieved after WGS and the gas composition was therefore suitable to be fed into the PSA unit [17]. The TDM reactor both in TDM and TDMG process was assumed as cylindrical reactor tube. The reactor diameter was selected as 1.5 m and the length of each reactor was calculated based on the required gas residence time in the reactor. As a result, the reactor length was 12.4 m in the TDM process and 4.4 m in the TDMG process.

In electrolysis, the electricity requirement was calculated using the specific energy consumption defined for alkaline electrolyzers. Additionally, the oxygen produced in the electrolysis corresponded to the hydrogen production. In SMR, the product gas composition after reformer and WGS was calculated by taking into account the major reaction equations (Eqs. 2.1–2.2). Additionally, these gas compositions were confirmed to equal typical gas compositions in SMR presented in [17]. The most important technical values in each process as well as the mass balance analysis results are shown in Table 5.1. The other fuel gases in Table 5.1 refer to the furnace flue gas components other than CO_2, i.e. nitrogen, water, and oxygen.

Table 5.1: The mass balance results of the hydrogen production processes. SS=small scale, LS=large scale, n/a=not applicable (Publication IV)

	TDM-SS	TDMG-SS	Electrol.-SS	SMR-SS	SMR-LS	SMR-LS+CCS	
Technical values							
Reactor temp.	1500	1500	n/a	1123	1123	1123	K
H_2 production	1,000	1,000	1,000	1,000	100,000	100,000	$Nm^3\ h^{-1}$
H_2 purity	0.9995	0.9995	0.9980	0.9995	0.9995	0.9995	-
Mass balance, input							
CH_4, feedstock	0.10	0.06	n/a	0.07	6.9	6.9	$kg\ s^{-1}$
CH_4, fuel	0.02	0.01	n/a	0.02	2.0	2.4	$kg\ s^{-1}$
Air	0.30	0.35	n/a	0.73	73	81	$kg\ s^{-1}$
Water	n/a	0.09	0.22	0.12	12	12	$kg\ s^{-1}$
TOTAL	0.41	0.52	0.22	0.94	94	102	$kg\ s^{-1}$
Mass balance, output							
H_2	0.02	0.02	0.02	0.02	2.5	2.5	$kg\ s^{-1}$
Product carbon	0.07	0.01	n/a	n/a	n/a	n/a	$kg\ s^{-1}$
O_2	n/a	n/a	0.20	n/a	n/a	n/a	$kg\ s^{-1}$
CO_2, emitted	0.04	0.17	n/a	0.24	24	11	$kg\ s^{-1}$
CO_2, captured	n/a	n/a	n/a	n/a	n/a	14	$kg\ s^{-1}$
Other flue gases	0.27	0.32	n/a	0.67	67	74	$kg\ s^{-1}$
TOTAL	0.41	0.52	0.22	0.94	94	102	$kg\ s^{-1}$

The external energy requirement in each process was calculated by taking into account the demand for feedstock pre-heating, the reaction enthalpies, and the defined conversion values at each process step. The process couplings for the internal heat transfer and the PSA off-gas combustion in TDMG and SMR reduced the external energy demand. The external heat requirement values and the mass balance analysis results were utilized to define the operational costs in each process.

5.3 Economic analysis

The economic analysis of the selected hydrogen production processes was based on the technical analysis and cost data adopted from the literature. The capital expenditure (CAPEX) evaluation for SMR and electrolysis was based on investment cost estimations for whole processes presented in the literature. Different investment costs were assumed for the small-scale SMR and for the large-scale SMR [1]. Accordingly, the electrolysis investment costs were assumed to be higher in the current situation than in the future [28]. A cost range for the CO_2 capture, pressurization, transportation, and storage in the large-scale SMR was adopted from the literature [109, 110]. The data regarding the investment costs of SMR and electrolysis is presented in Table 1 in Publication IV.

In contrast, the CAPEX evaluation of the TDM and TDMG processes was based on cost estimations for individual process components. The CAPEX of a certain component (C_2) with capacity S_2 was estimated by using the equation:

$$C_2 = C_1 \left(\frac{S_2}{S_1} \right)^e \tag{5.1}$$

where C_1 is the CAPEX of a reference component with capacity S_1 and e is a scale factor that typically has values from 0.4 to 0.9 [111]. The accuracy of the equation is ±50% and it allows preliminary CAPEX estimations. In order to avoid underestimating the process costs, a contingency equaling 30% of the equipment costs was added to the total investment cost of TDM and TDMG processes. The CAPEX costs and the capacities of the reference components as well as the scale factors utilized for the TDM and TDMG CAPEX estimations are presented in Publication IV.

The overall CAPEX in each process was divided into annual CAPEX costs by using the equation:

$$\text{Annual CAPEX} = \text{CRF} \cdot \text{Total capital cost} \tag{5.2}$$

where CRF (capital recovery factor) was defined as [112]

$$\text{CRF} = \frac{i(1+i)^N}{(1+i)^N - 1} \tag{5.3}$$

where i is the interest rate (-), N is the investment period in years. An interest rate of 10% and a 10-year investment period was chosen in this work.

The operational expenditure (OPEX) was a sum of feedstock, power, and CO_2 emission allowance costs as well as other operation and maintenance (O&M) costs. The O&M costs were proportional to the CAPEX of a certain process component or the whole process as presented in Publication IV. The Total annual costs for each process were calculated as:

$$\text{Total annual costs} = \text{Annual CAPEX} + \text{Annual OPEX} - \text{Annual income} \quad (5.4)$$

where Annual income consisted of the market value of the products other than hydrogen, i.e., the TDM product carbon and oxygen from electrolysis. The total specific hydrogen production cost (EUR MWh^{-1}) was achieved by dividing the Total annual cost with the yearly hydrogen production capacity.

The hydrogen production costs were studied in the current market situation and in possible market environments in 2030. First, the OPEX and CAPEX in each hydrogen production process were calculated in the current market situation and the results are shown in Table 5.2. Natural gas cost was assumed as 20 EUR MWh^{-1} [113] and electricity cost as 30 EUR MWh^{-1} [114]. Additionally, the CO_2 emission allowance cost was defined as 10 EUR $t_{CO_2}^{-1}$, which is slightly higher than the current market price (6 EUR $t_{CO_2}^{-1}$ [115]), but the value was used to highlight the significance of the emissions. In contrast, a pessimistic value for the TDM product carbon (0 EUR t_C^{-1}) and oxygen from the electrolysis (0 EUR $t_{O_2}^{-1}$) were selected to avoid overestimating the process incomes. However, a sensitivity analysis was conducted with oxygen values up to 70 EUR $t_{O_2}^{-1}$ (based on evaluations in [116, 117]) and product carbon values up to 300 EUR t_C^{-1}. Additionally, the costs of electricity and natural gas were varied as a part of this sensitivity analysis.

Table 5.2: The annual OPEX and the total CAPEX for the hydrogen production processes in the current market situation. SS=small scale, LS=large scale (Publication IV)

	TDM-SS	TDMG-SS	Electrol.-SS	SMR-SS	SMR-LS	SMR-LS+CCS	
OPEX							
Methane	780	547	-	618	61,753	64,546	kEUR a^{-1}
CO_2 emis. allow.	8	42	-	61	6,099	2,778	kEUR a^{-1}
Electricity	-	6	982	11	1,064	1,064	kEUR a^{-1}
Other O&M	27	24	15	87	1,089	1,089	kEUR a^{-1}
TOTAL OPEX	815	620	997	776	70,004	97,662	kEUR a^{-1}
CAPEX							
Equipment	3,233	2,361	2,974	10,705	133,815	162,000	kEUR
Contingency (30%)	970	708	-	-	-	-	kEUR
TOTAL CAPEX	4,203	3,069	2,974	10,705	133,815	162,000	kEUR
Total H_2 prod. cost	72.0	53.8	71.1	117.0	44.1	57.4	kEUR MWh^{-1}

Potential market environments in 2030 were analyzed by applying various operational costs. The following cost values were used as a basis of the analysis: the CO_2 emission allowance cost as 50 EUR $t_{CO_2}{}^{-1}$, natural gas cost as 40 EUR MWh^{-1}, and electricity cost as 50 EUR MWh^{-1}. The cost estimation for natural gas was based on the market analyses of the U.S. Energy Information Administration [118] and European Commission [119]. The CO_2 emission allowance and electricity cost estimations were based on expert opinions. Due to the intermittent nature of renewable power generation, a limited amount of renewable electricity with an extremely low cost (10 EUR MWh^{-1}–30 EUR MWh^{-1}) was assumed to be available for electrolysis. Finally, a sensitivity analysis for electricity and natural gas cost as well as TDM product carbon and oxygen value was carried out.

Chapter 6

Results and discussion

The structure of the research work conducted and presented in this thesis is shown in Fig. 6.1. The work is divided into five consecutive steps where the results from each step have been utilized in the sequential step. The existing data in this work consists of the data presented in the literature and of the previous research of this topic conducted at TUT. Prior to this work, Fager-Pintilä [120] and Rajamäki [101] conducted TDM experiments with a small-scale test reactor at TUT. The experimental work they carried out helped when designing the test reactor build in this work. Additionally, the experimental studies presented in the literature (compiled in Publication II) were utilized when planning the experiments and selecting a suitable reaction mechanism for modeling purposes.

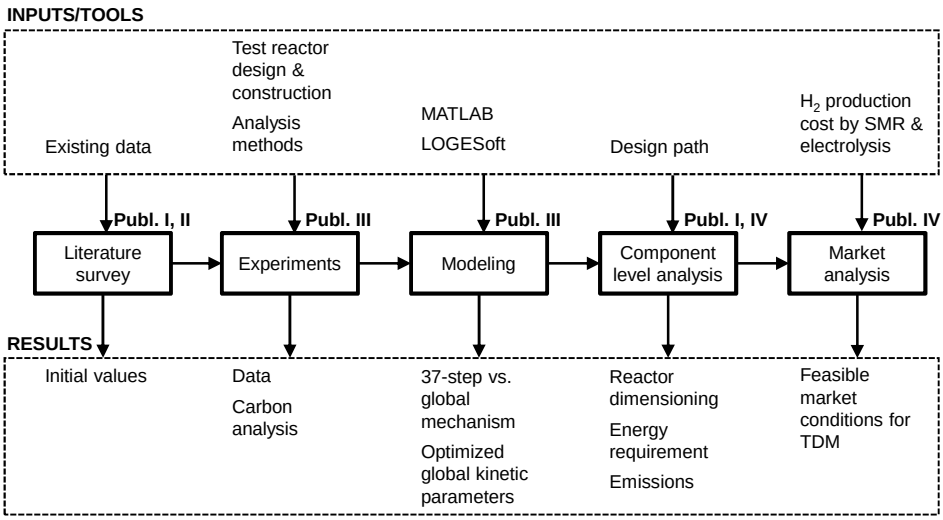

Fig. 6.1: The structure of the work. The numeric notation indicates the publication where the analysis and results are presented.

The experimental data produced in this work was combined with mathematical modeling to find a suitable reaction mechanism for describing the TDM reaction (Publication III). Based on an extensive literature survey, a design path (shown in Fig. 6.2) was created in order to assist the selection of the reaction, reactor, and process parameters for a TDM application (Publication II). The reactor design was conducted by following the design path and by applying the experimental and modeling results achieved in this work. The reactor cost evaluation was conducted by utilizing the cost estimations presented in Publication I.

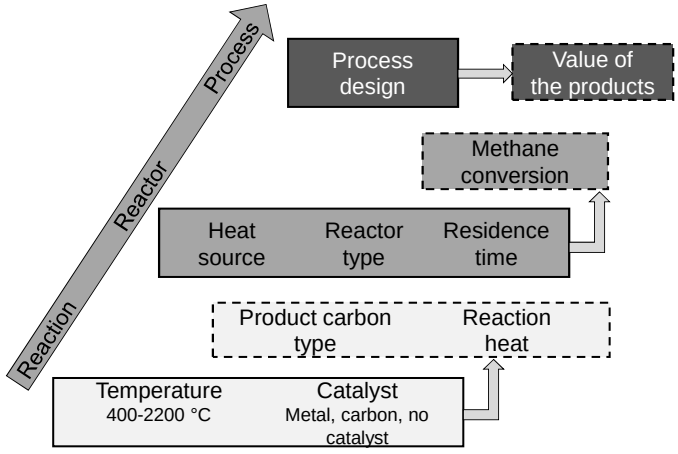

Fig. 6.2: The procedure for selecting the reaction, reactor, and process parameters for a TDM application. (Publication II)

Next, process design was conducted by applying the results of the component analysis. The last part of the work was a market analysis where the overall costs of the designed hydrogen production processes were evaluated. Thus, the market analysis exploits all the data and knowledge gained during the work. As a result, the market conditions were TDM could be an economically feasible hydrogen production technology in comparison with SMR and water electrolysis were identified.

6.1 Experimental and modeling

The experiments with the test reactor provided both data for the TDM reaction modeling studies and carbon samples for qualitative analysis. The elemental composition of the carbon samples was studied with EDS. According to the results, the carbon content in all studied samples was 94-wt% at minimum. The impurities in the samples were calcium, which most likely originated from the ceramic bed material in the test reactor, as well as copper, tin, and silicon, which derived from the sample holder, the grid, and the detector in the TEM analyzer.

The carbon analyses were conducted by studying whole beads of the bed material on which the carbon had been accumulated. An example of the analyzed

carbon samples is presented in Figs. 6.3 and 6.4. This carbon sample originates from an experiment denoted as Case 16 whose test conditions are shown below in Fig. 6.5 and presented more detailed in Publication III. The SEM images in Fig. 6.3 present the surface structure of the product carbon sample. The image with the lowest magnification shows that a carbon layer has been deposited on the bed material surface and that the thickness of this layer varies. The images with a higher magnification were taken from the area where the carbon layer thickness was the highest. The carbon accumulations consist of spherical carbon particles with a diameter well below 1 μm. The spherical particles have formed aggregates and those have further agglomerated. The tendency to form aggregates rather than individual particles indicates a higher structure and better quality of the carbon black [121].

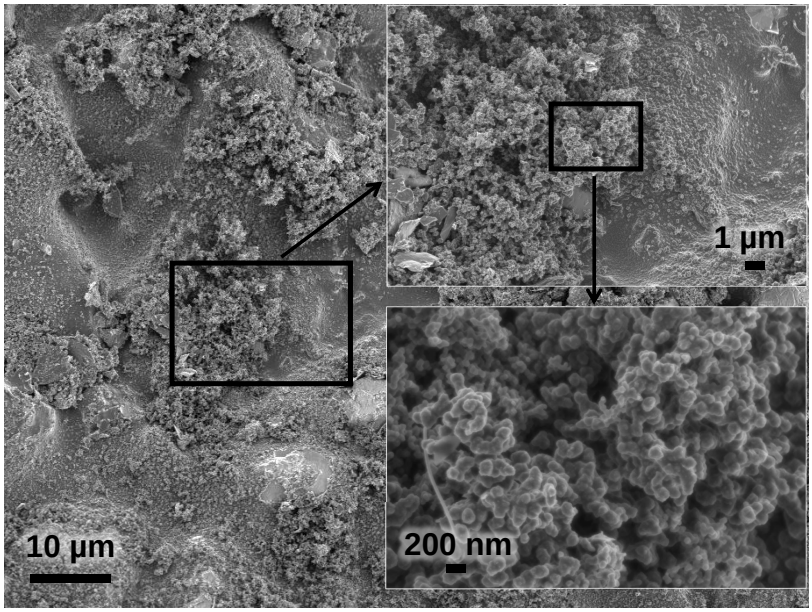

Fig. 6.3: SEM image of the TDM carbon sample with selected magnifications. The carbon sample originates from an experiment denoted as Case 16 in Table 4.1.

TEM images revealing the inner structure of the carbon accumulate in the same sample are shown in Fig. 6.4. The image with the highest magnification reveals a structure that is hypothesized to originate from the carbon particle growth that has occurred by the formation of successive carbon layers as described in Section 2.2.3.

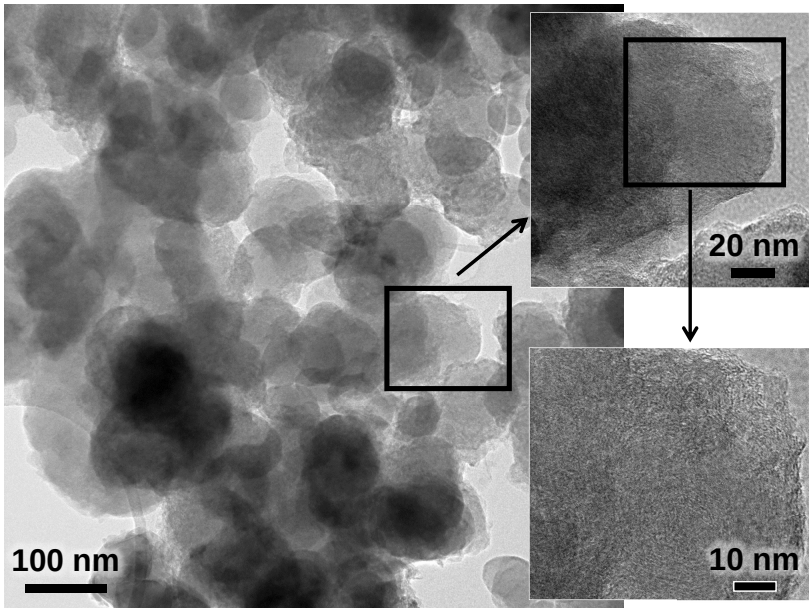

Fig. 6.4: TEM image of the TDM carbon sample with selected magnifications. The carbon sample originates from an experiment denoted as Case 16 in Table 4.1.

As in this work, Abánades et al. [83] studied the structure of the TDM product carbon from their experiments and detected spherical carbon particles. For example, in their study, a TDM experiment at the temperature of 1723 K produced carbon with a particle diameter between 100 nm and 300 nm. In comparison, approximately the same particle size was achieved in this work, as shown in Fig. 6.3. However, in this work, the test reactor nominal temperature during this specific experimental case was a somewhat lower, 1323 K. In another experimental study, TDM was powered by concentrated solar power at the reactor wall temperature of 2073 K and the product was carbon black with a notably smaller particle size, 20 nm–40 nm [60].

As a part of the previous experimental research of TDM at TUT, the TDM product carbon structure at the atomic level was analyzed [101]. The X-ray diffraction analyses referred to that the product carbon had a crystalline structure. In a crystal structure, the atoms are arranged in a regular manner, whereas the opposite is true for an amorphous structure, where the atoms have no organized locations [104]. Graphite is a highly crystalline structure whereas carbon black consists of graphite platelets, but contrary to graphite, the platelets are not precisely positioned with respect to successive layers. Thus, carbon black has a graphitic crystalline structure which is intermediate between the crystalline structure that is found in graphite and the disordered structure of non-graphitic carbons. [32]

As described in Section 2.2.3, the particle size is important but not the only factor defining the carbon black properties. The small particle size is preferred since it indicates good rubber properties and results in large surface area,

which indicates good interfacing with other components in rubber. However, the amount of carbon produced was not sufficiently large to reliably measure the specific surface area of the carbon samples.

The reaction parameters for the global TDM reaction mechanism (Eqs. 3.1 and 3.2) were optimized based on the experiments of thermal non-catalytic TDM at the reactor temperatures up to 1500 K. The results are shown in Table 6.1.

Table 6.1: The optimized reaction parameters for the global TDM reaction. n/a=not applicable (Publication III)

	forward	unit	backward	unit
A	$8.5708 \cdot 10^{12}$	$mol^{(1-n)}$ $(cm^3)^n$ s^{-1}	$1.1190 \cdot 10^7$	$mol^{(1-m)}$ $(cm^3)^m$ s^{-1}
E_a	337,120	J mol^{-1}	243,160	J mol^{-1}
n	1.123	-	n/a	n/a
m	n/a	n/a	0.9296	-

In the literature, the first studies of methane decomposition kinetics have focused on the initial stage of the reaction and the first order reaction has been found suitable for describing the TDM reaction [40, 122–125]. The reaction parameters presented in the literature have been derived from the experiments conducted at various environments at the temperatures of 995 K–1965 K and at the pressures of 0.017 bar–12 bar. In these reaction conditions, the activation energy values have ranged from 332,000 J mol^{-1} to 450,000 J mol^{-1}. [40, 122–125] Later, the global reaction mechanism ($CH_4 \rightarrow 2H_2 + C$) was studied in [61, 126]. In these studies, the activation energy defined by Steinberg [126] was very low, 131,000 J mol^{-1}. This activation energy is lower than in the previous studies and lower than would have been expected in the environment where low temperatures (973 K–1173 K) and high pressures (28.6 bar–56.8 bar) were applied. A hypothesis provided by Plevan et al. [127] was that the TDM product carbon could have catalyzed the reaction, and thus, increased the reaction rate resulting in low activation energy. Most recently Rodat et al. [61] found an activation energy of 370,000 J mol^{-1} based on experiments at high temperature (1500 K–2300 K) and low pressure (0.04 bar). In conclusion, a great variety of activation energies for TDM were found in the literature. However, due to variations in the experimental reaction environment in these studies, reaction parameters that could predict all the experiments cannot be derived [127]. The reaction mechanism in this work is close to first order kinetics and the activation energy is within the range of values presented in the literature. The frequency factors shall be compared only when the reaction mechanism is exactly equal. Therefore, the reaction parameters introduced in this study are applicable only when exactly the same reaction mechanism is utilized and the reaction environment is similar to that in this work.

As an example, the experimental and modeling results for four studied cases are presented in Fig. 6.5. The reaction environments of all studied cases are presented in Table 4.1. The reactor temperature was measured during the ex-

periments and fitted to time-dependent profile during the reactor modeling. The methane conversion curves have been calculated using the global TDM reaction mechanism with optimized reaction parameters. Case 43 and Case 34 provide the examples of cases where the reactor nominal temperature was high whereas Case 17 and Case 16 represent the experiments conducted at lower reactor maximum temperature. Due to the reaction parameter optimization procedure, which minimized the absolute difference between the experimental and modeled methane conversion, rather than the relative difference, the modeling values followed better the experiments in the cases where the reactor temperature, and consequently, the methane conversion was high.

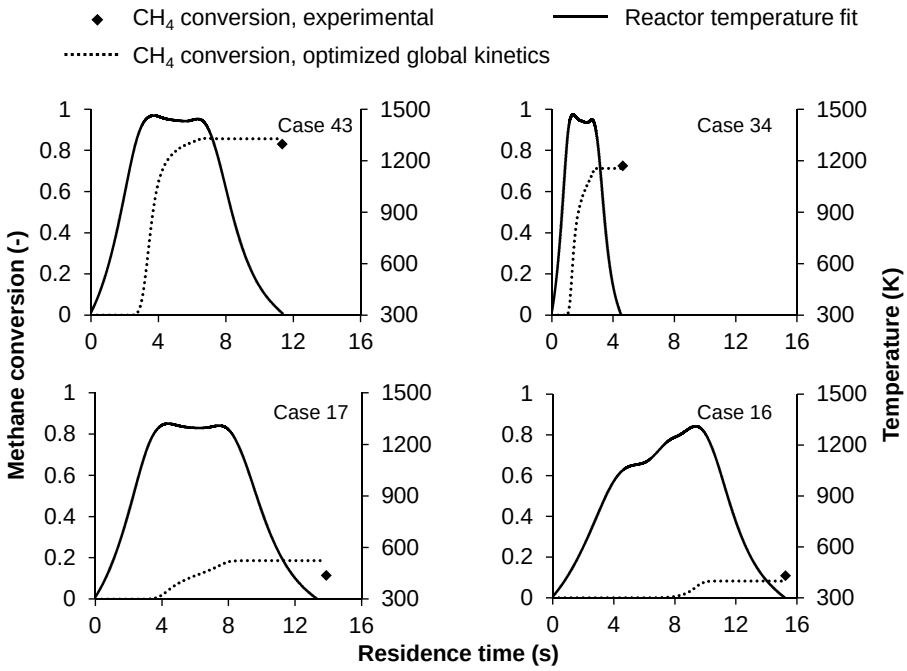

Fig. 6.5: Graphical presentation of four experimental cases. Reactor temperature fit as a function of gas residence time as well as methane conversion in experiments and calculated with the optimized global kinetics. The full case-specific data is presented in Table 4.1. (Publication III)

The global reaction mechanism with the optimized reaction parameters was found suitable for predicting the TDM experiments in this work. Additional comparison was conducted by using the experimental data of Plevan et al. [127], which has been achieved in a flow-through reactor at reactor nominal temperatures of 1023 K–1173 K. The global mechanism was able to predict this experimental data and especially good agreement was achieved at the two cases with lower temperature as shown in Fig. 6.6. Additionally, a comparison was conducted between the global mechanism and the 37-step reaction mechanism adopted from

the literature. The global TDM mechanism with the optimized reaction parameters provided better agreement with the experiments in Fig. 6.6 than the 37-step reaction mechanism. Similarly, the 37-step reaction mechanism predicted too low methane conversion values when it was applied to simulate the experiments carried out in this work (results are presented in Publication III).

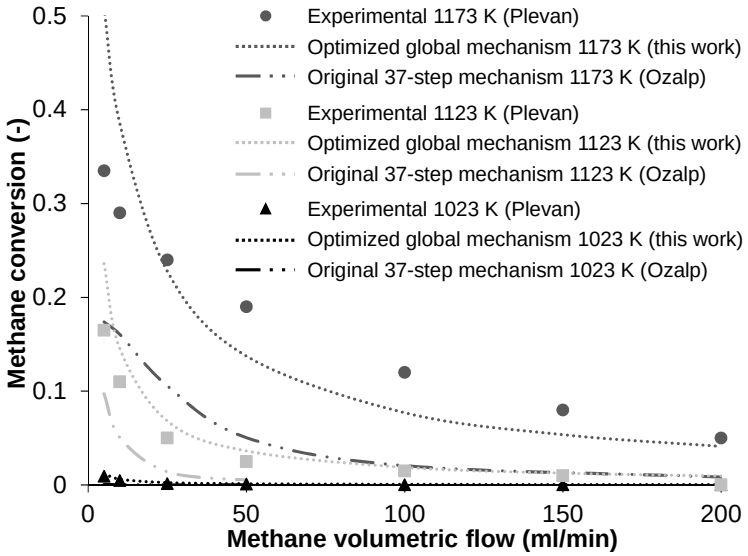

Fig. 6.6: The methane conversion values achieved with the global TDM mechanism with reaction parameters optimized in this study (dotted lines) and with the 37-step mechanism of Ozalp et al. [94] (dash-dot lines) compared with experimental results of Plevan et al. [127] (marker symbols). (Publication III)

The 37-step mechanism was originally developed based on experiments where the temperature was measured using a single measurement point and deriving the whole reactor temperature profile from this value [93]. In other words, the 37-step reaction mechanism was developed at the constant temperature of 1243 K which was 30 K below the measured reactor maximum temperature. The hypothesis in this work is that the lack of the exact environment definition during the experiments causes the inability of the 37-step mechanism to predict the experimental results presented both in this work and in the literature.

Furthermore, the solid carbon formation by the 37-step mechanism was studied in this work by utilizing reaction flow and sensitivity analyses (shown in Publication III). Based on these analyses, a slight adjustment of the 37-step reaction mechanism was proposed. The adjustment of the reaction parameters for the reaction describing the solid carbon formation was found to improve the ability of the 37-step reaction mechanism to predict the experimental results in [128] as discussed in Publication III.

Overall, the global mechanism with the optimized reaction parameters was found suitable for describing TDM reaction in the reaction environment of RHER.

RHER provides a non-catalytic environment where the residence time in the reactor varies from several seconds up to 20 s and the reactor temperature is up to 1500 K. Therefore, the global mechanism was chosen to predict the TDM reaction in the further component and market level analyses.

6.2 Market analysis

The CAPEX and OPEX of the six evaluated hydrogen production processes are shown in Fig. 6.7. The graph presents the costs in the current market situation and with pessimistic market values for the TDM product carbon and oxygen from electrolysis as defined previously in Section 5.3. According to the results in Fig. 6.7, SMR is economically feasible technology for large-scale applications, and in this case, the natural gas cost is the major parameter defining the hydrogen production costs. On the contrary, SMR is significantly more expensive technology in a small scale than electrolysis or TDM. Electricity is the major cost component in the electrolysis OPEX. As far as the hydrogen production costs are concerned, TDM is not economically competitive with SMR in the current market situation if the TDM product carbon has no commercial value as it is assumed in Fig. 6.7. The assumption that the product carbon has no market value could hold for example in a situation where TDM is utilized as a CCS method and the product carbon is stored for long-term to eliminate the CO_2 emissions.

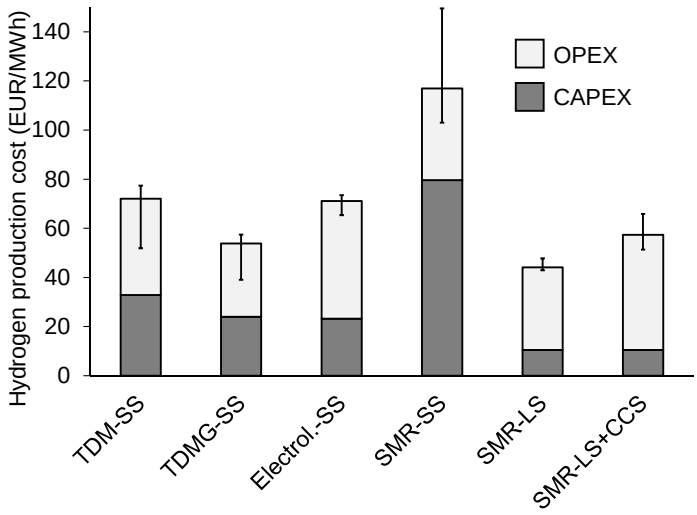

Fig. 6.7: The CAPEX and OPEX of the hydrogen production technologies in the current market situation with the following operational cost values: natural gas cost 20 EUR MWh^{-1}, electricity cost 30 EUR MWh^{-1}, CO_2 allowance cost 10 EUR $t_{CO_2}^{-1}$, TDM product carbon value 0 EUR t_C^{-1} and oxygen value 0 EUR $t_{O_2}^{-1}$. The error bars were calculated by considering the uncertainty in the CAPEX estimations. SS=small scale, LS=large scale (Publication IV)

The hydrogen production costs in each process were calculated in the current market situation by taking into account operational cost ranges that were considered appropriate. The hydrogen production cost by TDM when the product carbon value is 0 EUR t_C^{-1} is presented as a dash dotted line in Fig. 6.8. The cost difference between TDM and SMR (long dash line) decreases when the CO_2 allowance cost increases. However, even as high a value as 100 EUR $t_{CO_2}^{-1}$, does not make TDM economically competitive in comparison with SMR, if the TDM product carbon has no market value. Taking into account the TDM product carbon value between 100 EUR t_C^{-1} and 300 EUR t_C^{-1}, reduces the hydrogen production cost notably. As an example, the hydrogen production cost by TDM is less than by SMR when the CO_2 allowance cost of 10 EUR $t_{CO_2}^{-1}$ and the TDM product carbon value exceeds 310 EUR t_C^{-1}. Alternatively, the hydrogen production costs by TDM with the product carbon value of 100 EUR t_C^{-1}–300 EUR $t_C^{-1}$are within the same range as the cost by SMR coupled with CCS. The cost range for SMR coupled with CCS (line pattern) takes into account the variations in the CCS costs presented in the literature. Similarly, the hydrogen production cost by TDMG (dash line in Fig. 6.8), where the TDM product carbon is gasified, is within the same cost range than the cost by SMR coupled with CCS. Furthermore, Fig. 6.8 presents how the hydrogen production cost by electrolysis varies between 71 EUR MWh^{-1} and 118 EUR MWh^{-1} when the electricity cost ranges from 30 EUR MWh^{-1} to 60 EUR MWh^{-1}. Thus, electrolysis is a more expensive option for hydrogen production than TDM. Last, small-scale SMR provides the highest hydrogen production costs among the studied processes in the current market situation.

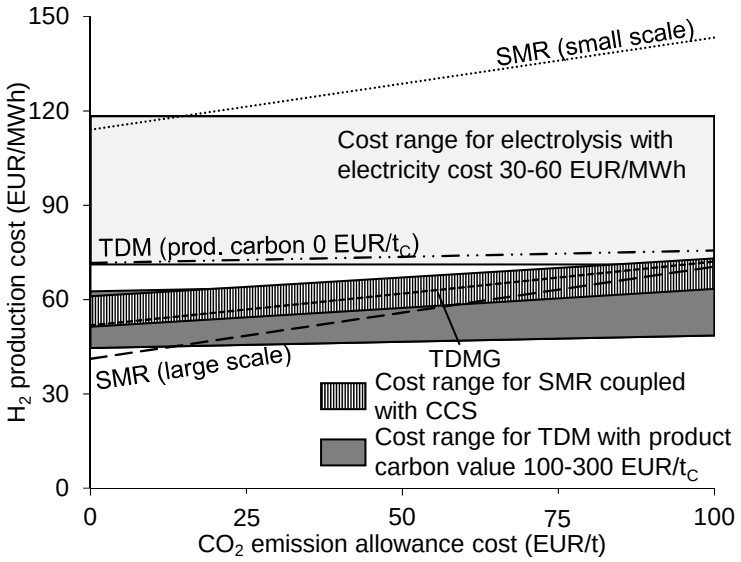

Fig. 6.8: Hydrogen production costs with different technologies in the current market situation with varying CO_2 allowance cost. The selected OPEX values: electricity cost 30 EUR MWh^{-1}, natural gas cost 20 EUR MWh^{-1}, oxygen value 0 EUR $t_{O_2}^{-1}$, and full load hours 7000 h a^{-1}. Additionally, ranges for hydrogen production costs are presented by taking into account the following cost factors: electricity cost 30–60 EUR MWh^{-1} in electrolysis, TDM product carbon value 100–300 EUR t_C^{-1}, and CCS costs presented in the literature for SMR. (Publication IV)

A case representing the hydrogen production costs with different technologies in potential future market environments in 2030 is depicted in Fig. 6.9. Here, the hydrogen production costs are presented as a function of natural gas cost. The hydrogen production cost by TDM is presented with a product carbon value of 0 EUR t_C^{-1} (dash dotted line) and with a product carbon value ranging from 100 EUR t_C^{-1} to 300 EUR t_C^{-1} (grey area). A break even price for the TDM product carbon was found as 280 EUR t_C^{-1} above which TDM is economically more feasible hydrogen production process than SMR when the natural gas cost is assumed as 40 EUR MWh^{-1}. Natural gas is used as feedstock both in SMR and in TDM, and therefore, increasing the natural gas cost does not bring cost benefits to TDM. The cost range for SMR coupled with CCS (line pattern) was calculated by taking into account the variations in the CCS costs presented in the literature. An alternative feedstock to the fossil natural gas could be synthetic natural gas (SNG) or biomethane. The SNG production costs have predicted to vary from 40 EUR MWh^{-1}–390 EUR MWh^{-1} in the current market situation to 72 EUR MWh^{-1}–218 EUR MWh^{-1} in the 2050 market situation depending on the cost and availability of renewable electricity, oxygen value, and process heat utilization [129]. The biomethane production cost is estimated as 70 EUR MWh^{-1} [129]. Due to the high production costs of SNG and biomethane, those are not

economically competitive feedstock alternatives to natural gas unless the CO_2 neutrality of these feedstocks would provide a competitive advantage.

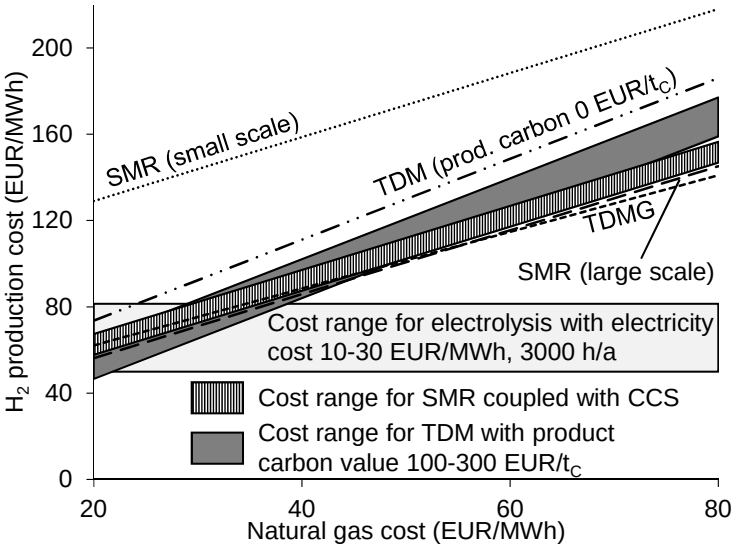

Fig. 6.9: Hydrogen production costs with different technologies in potential market environments in 2030. The selected OPEX values: electricity cost 50 EUR MWh^{-1}, CO_2 allowance cost: 50 EUR $t_{CO_2}^{-1}$, oxygen value 0 EUR $t_{O_2}^{-1}$, and full load hours 7000 h a^{-1}. Additionally, ranges for hydrogen production costs are presented by taking into account the following cost factors: electricity cost of 10–30 EUR MWh^{-1} in electrolysis with availability of 3000 h a^{-1}, TDM product carbon value of 100–300 EUR t_C^{-1} , and CCS costs presented in the literature for SMR. (Publication IV)

Electrolysis provides hydrogen with a low operational cost when inexpensive electricity is available as is shown in Fig. 6.9. Renewable electricity is expected to have a low cost, but the generation is fluctuating and this results in low availability. The IEA has predicted low availability (3000 h a^{-1}) for very low cost renewable electricity [1] and this was taken into account in this work. Thus, electrolysis is not a suitable technology in demand-driven applications unless a hydrogen storage is implemented. In contrast to electrolysis, the feedstock availability does not restrict the operation time of a TDM process, and therefore, it enables demand-driven hydrogen production.

Another graph illustrating possible future (2030) market environments is shown in Fig. 6.10. The graph highlights the effect of oxygen value on the hydrogen production costs by electrolysis. Increasing the oxygen value up to 70 EUR $t_{O_2}^{-1}$, decreases the electrolytic hydrogen cost by 17 EUR $MWh_{H_2}^{-1}$. The hydrogen production cost by TDM would be less than by electrolysis with the product carbon value of 300 EUR t_C^{-1} when assuming the electricity cost above 55 EUR MWh^{-1} and a high oxygen value.

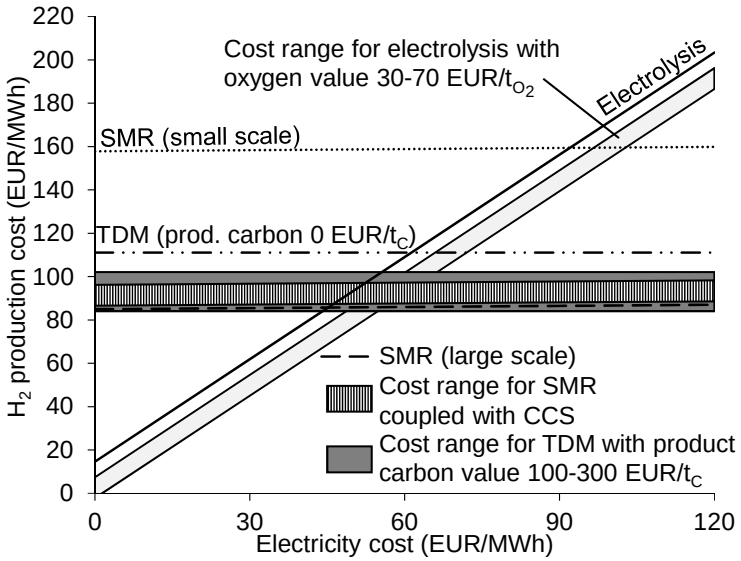

Fig. 6.10: Hydrogen production costs with different technologies in potential market environments in 2030. The selected OPEX values: natural gas cost 40 EUR MWh^{-1}, CO_2 allowance cost 50 EUR $t_{CO_2}^{-1}$, and full load hours 7000 h a^{-1}. Additionally, ranges for hydrogen production costs are presented by taking into account the following cost factors: TDM product carbon value of 100–300 EUR t_C^{-1} and oxygen value of 0–70 EUR $t_{O_2}^{-1}$ in electrolysis. (Publication IV)

Centralized large-scale hydrogen production requires hydrogen transportation and distribution infrastructure but its costs were not taken into account in Figs. 6.8–6.10. A transportation distance over 100 km have been estimated to cause an additional cost of 45 EUR MWh^{-1} of hydrogen and distance below 50 km an additional cost of 22 EUR MWh^{-1} of hydrogen [130]. Furthermore, hydrogen storage cost has been evaluated to equal 23 EUR MWh^{-1} of hydrogen based on the natural gas storage costs in cavern storage [11]. When the hydrogen transportation and storage costs are taken into account, the distributed hydrogen production by TDM may turn into a less costly option than centralized hydrogen production by SMR. Moreover, many countries have an existing natural gas network, which would enable transporting natural gas to distribution points, where hydrogen could be produced on-site by TDM.

In addition to the economic analysis, the specific CO_2 emissions of hydrogen production were calculated for each technology. According to the results, the specific CO_2 emissions of produced hydrogen in TDM are significantly lower than in SMR, even though CCS is coupled to SMR (Table 6.2). The CO_2 emissions in SMR could be further reduced by capturing CO_2 not only from the syngas, but also from the furnace flue gas [131]. However, this would cause additional costs. Producing hydrogen with zero CO_2 emissions requires that renewable electricity is utilized in electrolysis. According to the economic analysis, the

hydrogen production costs by TDMG are within the same range as the costs in the production by SMR coupled with CCS. However, the CO_2 emissions in TDMG process are significant. In order to reduce these emissions, TDMG should be coupled with CCS. However, applying CCS to a small CO_2 emissions source is currently not economically feasible, and in order to improve the economics, the process should be scaled up.

Table 6.2: The specific CO_2 emissions of hydrogen production by different technologies. Electrolysis is assumed to be powered by CO_2-free electricity. (Publication IV)

Process	Emissions, $kg_{CO_2}\ MWh_{H_2}^{-1}$
TDM	40
TDMG	203
SMR	293
SMR with CCS	133
Electrolysis	0

The most potential application for TDM is small-scale on-site hydrogen production for distributed hydrogen demand. As a main benefit, TDM could provide remarkable CO_2 emission reductions in hydrogen production. However, this would require relevant applications for the TDM product carbon where a sufficient price for the carbon can be assumed (approximately 300 EUR t_C^{-1}). According to a rough estimation presented in Publication II, the current carbon black demand would be met by producing 6% of the global hydrogen demand by TDM. This simplified estimation reveals the fact that the extent of the carbon utilization possibilities restricts the TDM application prospects.

An alternative large-scale application for the TDM product carbon discussed in Publication II was replacing metallurgical coke, that is currently produced from fossil coal. The global demand for metallurgical coke is 50-times that of carbon black, and therefore, this could extend the TDM application possibilities greatly. The price of metallurgical coke during the recent years has varied between 120 EUR t_C^{-1} and 320 EUR t_C^{-1} [73]. For example, when assuming an average carbon value of 220 EUR t_C^{-1}, TDM would be less expensive than SMR when the CO_2 cost would be 42 EUR $t_{CO_2}^{-1}$. Replacing metallurgical coke with the TDM product carbon would result in additional CO_2 emission reductions since the coke production from fossil coal would be avoided.

The break-even prices for the TDM carbon previously presented in the literature are in line with the results of this work. Competitiveness with SMR in hydrogen production has been reached with the TDM carbon value of 350 USD t_C^{-1} [30]. In another study, a combination of TDM product carbon value of 200 USD t_C^{-1} and a carbon tax of 78 USD $t_{CO_2}^{-1}$ was found sufficient to make TDM economically feasible in hydrogen production compared with SMR [86].

6.3 Technology feasibility analysis

Further economic calculations were conducted in order to summarize all the results achieved in this work. The resulting illustration in Fig. 6.11 presents the connection between the production capacities and hydrogen production costs in each technology. The cost ranges were calculated for three technologies (TDM, SMR, and water electrolysis) with suggested plant sizes and other technology selections. The results are dependent on these assumptions and selections, and therefore, Fig. 6.11 presents values that are highly case-specific. The parameters that have the greatest effect on the costs in each technology were identified and those parameters were altered within relevant ranges. The parameter ranges were selected by taking into account the technical limitations and considering the probability of different market conditions. The chart does not take into consideration the hydrogen transportation costs.

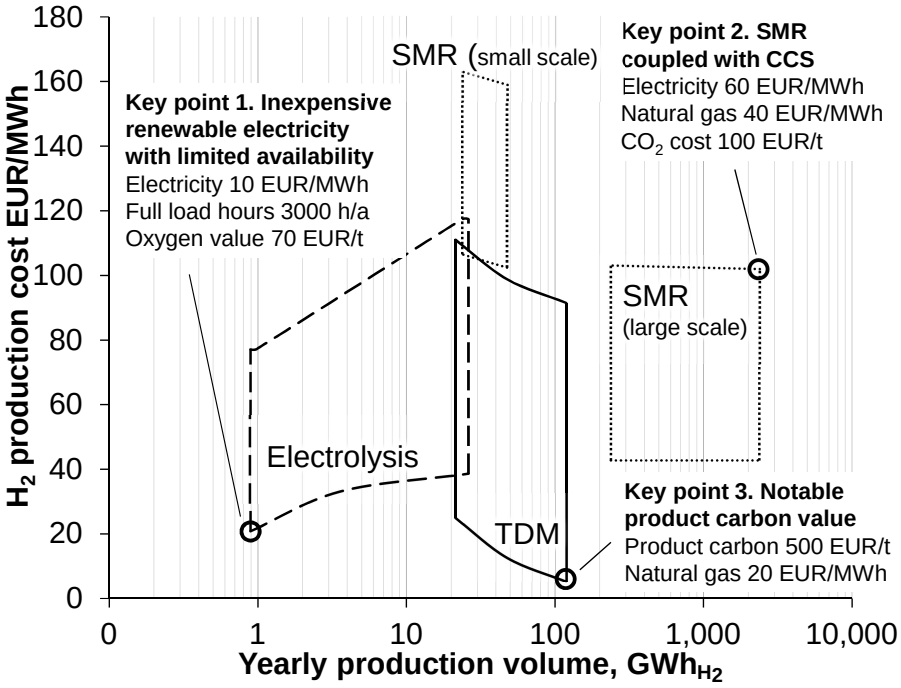

Fig. 6.11: Vision of the production costs and applicable volumes in hydrogen production by TDM, SMR, and electrolysis with suggested technical values. The key points explain the economic conditions where the lowest (TDM and electrolysis) and highest (large-scale SMR) hydrogen production costs are achieved. Variable ranges: natural gas cost 20–40 EUR MWh^{-1}; CO_2 allowance cost 10–100 EUR $t_{CO_2}^{-1}$; full load hours 8000 h a^{-1} (SMR and TDM) and 3000–8000 h a^{-1} (electrolysis); electricity cost 30–60 EUR MWh^{-1} (SMR and TDM) and 10–60 EUR MWh^{-1} (electrolysis); oxygen value 0–70 EUR $t_{O_2}^{-1}$; methane conversion in TDM 0.7; TDM product carbon value 0–500 EUR t_C^{-1}

The current cost of hydrogen production by SMR was found as 42 EUR MWh^{-1}, which equals the cost presented in [132], and it is hard to the other technologies to compete with that in the current market situation. The natural gas cost is the major parameter affecting the hydrogen production costs by SMR, whereas the CO_2 emission allowance cost has a minor effect. When the CO_2 emission allowance cost increases, coupling CCS to SMR becomes economically feasible. As a result, the hydrogen production cost by SMR is up to 102 EUR MWh^{-1} when assuming a CCS coupling and high natural gas cost (Key point 2 in Fig. 6.11). The electrolyzer technology is currently available only in a small scale and more development is required in order to reduce the costs of this technology. Inexpensive renewable electricity enables producing hydrogen at low cost by electrolysis (Key point 1 in Fig. 6.11). However, the availability of this electricity is expected to be limited in the coming decades. The cost uncertainty in TDM is high and it is mainly originating from the uncertainty in the product carbon value. An extremely low hydrogen production cost by TDM is achieved when a product carbon value of 500 EUR t_C^{-1} is assumed (Key point 3 in Fig. 6.11).

Chapter 7

Summary and conclusions

The objective of this work was to develop TDM technology by providing tools assisting the TDM reactor and process design as well as to evaluate the technical and economic possibilities to produce hydrogen by TDM. The technology development in this work began with the experimental research of the TDM reaction which was combined with mathematical modeling. The TDM reactor modeling was an essential part of the process design of the potential commercial scale TDM applications. Moreover, the economic feasibility of hydrogen production by these TDM processes was evaluated and a cost comparison was carried out between the TDM processes and two other hydrogen production technologies, i.e., SMR and water electrolysis.

The experimental setup was particularly designed for this work. The test reactor enabled producing a great amount of individual measurements where the reaction environment during the experiments was accurately defined. The exact reaction environment definition is a necessity for the reaction kinetics studies. For example, assuming too high a temperature in kinetics modeling, results in too high activation energy, and consequently, the reaction rate will be too low. A global TDM reaction mechanism with the reaction parameters optimized in this work was found suitable for describing non-catalytic TDM at the temperatures below 1500 K. The global TDM reaction mechanism was applied for the design of a novel reactor concept for TDM presented in this work, the RHER reactor.

A design path assisting the selection of the reaction, reactor, and process parameters for a commercial scale TDM application was outlined in this work. The design path was followed when process design of potential commercial scale TDM applications was carried out. The process cost analysis was based on the cost of similar process components found in the process industry. In the economic analysis, the product carbon was identified as the key competitive advantage of TDM. Additionally, the minimum value for the TDM product carbon was found as 310 EUR t_C^{-1} in the current market situation and 280 EUR t_C^{-1} in a potential market situation of 2030 above which the hydrogen production by TDM becomes economically more feasible than by SMR. These values are below the current market value of carbon black used in rubber industry. However, the carbon black demand is limited, and thus, it may provide an application

only for a limited amount of TDM product carbon. Alternatively, replacing metallurgical coke in steel production could provide a large-scale application for the TDM product carbon. In order to reduce the uncertainty related to the carbon utilization possibilities and value, an alternative process coupling where the TDM product carbon was gasified in order to produce more hydrogen was introduced in this work. This process was found economically viable at the TDM product carbon values below 230 EUR t_C^{-1}, but the drawback of the process are the CO_2 emissions originating from the product carbon gasification.

In this work, TDM was found as a suitable technology for small or medium industrial scale hydrogen production that occurs on-site. In comparison to centralized production, distributed hydrogen production minimizes the need for hydrogen transportation. Furthermore, the CO_2 emissions in hydrogen production by TDM are low and the technology would benefit from the existing natural gas network. The good feedstock availability would enable demand-driven hydrogen production by TDM whereas hydrogen production by electrolysis is dependent on the renewable electricity generation. Thus, TDM could be utilized to promote the hydrogen economy and to develop the hydrogen infrastructure while the renewable electricity capacity increases to a level that is required for extensive hydrogen production by electrolysis.

To summarize, the main contributions of this thesis are:

- Presenting optimized reaction parameters for a global reaction mechanism describing non-catalytic TDM at temperatures up to 1500 K to be utilized in the TDM reactor design.
- Designing and analyzing process concepts for commercial scale TDM applications and presenting the process cost evaluations.
- Outlining a design path assisting the selection of the reaction, reactor, and process parameters for a commercial scale TDM application.
- Determining the market conditions where TDM would be an economically viable method for hydrogen production in comparison with SMR and water electrolysis.
- Identifying the carbon product as a key competitive advantage of TDM and calculating an economic feasibility limit for the TDM carbon value as 280-310 EUR per tonne.
- Showing that the most suitable application for TDM is in small or medium industrial scale on-site hydrogen production where the current natural gas network would be exploited and the demand for hydrogen transportation would be minimized.

Chapter 8

Future work

In the beginning of the 20th century, the TDM technology was applied in a commercial scale in rubber industry, but was replaced by a more efficient oil-furnace process. Later, the environmental concerns related to the current fossil-based economy have resulted in renewed interest towards the technology. Due to the extensive scientific research conducted during the preceding decades, the TDM phenomena and the TDM reaction fundamentals are carefully identified. More recently, possible technology concepts have been outlined and the technology has even been piloted. In order to contribute to the previous knowledge in this field, reactor technology development and feasibility analysis was carried out in this work. The next stage in the technology commercialization process would be technology demonstration in a relevant environment.

The major issues that could advance the TDM technology implementation include creating a sufficiently large market for the product carbon and tightening the CO_2 emission regulations. Commercial applications for the product carbon would increase the interest towards TDM. Furthermore, the TDM product carbon value appeared to cause the largest uncertainty when the TDM process costs or application possibilities were evaluated. The TDM technology demonstration would provide knowledge about the quality and homogeneity of the TDM product carbon from a continuous process, which is needed in order to identify the actual carbon applications. Tighter emission regulations would increase the interest towards new technologies and decrease the gap in economic feasibility in hydrogen production between TDM and the current production by SMR.

Regarding the RHER reactor technology development, the bed material circulation in the reactor and the carbon separation from the bed material were considered in this work on a speculative level. Therefore, these issues remain to be experimentally verified. These issues are the most important factors affecting the scalability of the RHER reactor that are not fully understood. Similarly, the TDM product carbon gasification shall be experimentally studied. Furthermore, using the TDM product carbon as a supercapacitor material arose in this work as a high-value application for a limited amount of carbon. Supercapacitor is an electronic component suitable for short-term electricity storage. Thus, the elec-

trical properties of the TDM product carbon shall be studied in order to evaluate its suitability for this application.

Bibliography

[1] International Energy Agency (IEA), Technology Roadmap - Hydrogen and Fuel Cells, Tech. rep. (2015).
URL https://www.iea.org/publications/freepublications/publication/TechnologyRoadmapHydrogenandFuelCells.pdf

[2] International Energy Agency (IEA), Key world energy statistics 2016, Tech. rep. (2016).
URL http://www.iea.org/publications/freepublications/publication/KeyWorld2016.pdf

[3] J. Töpler, J. Lehmann (Eds.), Hydrogen and Fuel Cell: Technologies and Market Perspectives, Springer-Verlag, 2014.

[4] International Energy Agency (IEA), CO_2 emissions from fuel combustion, Tech. rep. (2016).
URL http://www.iea.org/bookshop/729-CO2_Emissions_from_Fuel_Combustion

[5] J. O. Bockris, A hydrogen economy, Science 176 (1972) 1323. doi:http://dx.doi.org/10.1126/science.176.4041.1323.

[6] H21 Leeds City Gate report, Tech. rep., Northern Gas Networks (2016).
URL http://www.northerngasnetworks.co.uk/archives/document/h21-leeds-city-gate

[7] SINTEF, HYPER Research Project, Accessed: 08/2017 (2017).
URL https://www.sintef.no/en/projects/hyper/

[8] Statoil, Statoil 2030 climate roadmap, Accessed: 08/2017 (2017).
URL https://www.statoil.com/en/news/2030-climate-roadmap.html

[9] International Energy Agency (IEA), World Energy Outlook 2016, Tech. rep. (2016).
URL http://www.worldenergyoutlook.org/publications/weo-2016/

[10] International Energy Agency (IEA), World Energy Outlook 2011: Are we entering a golden age of gas?, Tech. rep. (2011).
URL http://www.worldenergyoutlook.org/goldenageofgas

[11] L. Jörissen, Fuel Cells in the Waste-to-Energy Chain: Distributed Generation Through Non-Conventional Fuels and Fuel Cells, Springer-Verlag, 2012, Ch. Prospects of Hydrogen as a Future Energy Carrier.

[12] A. Ozarslan, Large-scale hydrogen energy storage in salt caverns, International Journal of Hydrogen Energy 37 (2012) 14265–14277. doi:https://doi.org/10.1016/j.ijhydene.2012.07.111.

[13] AIS Software, Storing Hydrogen Underground, Accessed: 10/2017 (2017).
URL https://www.aissoftware.com/storing-hydrogen-underground/

[14] Hydrocarbon Processing, Air Liquide commissions world's largest hydrogen storage facility, Accessed: 10/2017 (2017).
URL http://www.hydrocarbonprocessing.com/news/2017/01/air-liquide-commissions-world-s-largest-hydrogen-storage-facility

[15] Marcello De Falco, Angelo Basile (Eds.), Enriched Methane: The First Step Towards the Hydrogen Economy, Springer International Publishing, 2016.

[16] J. Rostrup-Nielsen, L. J. Christiansen, Concepts in Syngas Manufacture, Imperial College Press, 2011.

[17] E. K. Liu, C. Song, V. Subramani, Hydrogen and Syngas Production and Purification Technologies, John Wiley & Sons, Inc., 2010.

[18] J. R. Rostrup-Nielsen, T. Rostrup-Nielsen, Large-scale hydrogen production, in: The 6th World Congress of Chemical Engineering, Melbourne Australia 2001, 2001.

[19] HyGear, HY.GEN: On-site hydrogen generation, Accessed: 08/2017 (2017).
URL http://hygear.com/technologies/hy-gen/

[20] N. A. Al-Mufachi, N. V. Rees, R. Steinberger-Wilkens, Hydrogen selective membranes: A review of palladium-based dense metal membranes 47 (2015) 540–551. doi:http://dx.doi.org/10.1016/j.rser.2015.03.026.

[21] T. Keller, PSA Technology: Beyond Hydrogen Purification, Accessed: 08/2017 (January 2016).
URL http://www.chemengonline.com/psa-technology-beyond-hydrogen-purification/?printmode=1

[22] UOP LLC, A Honeywell Company, UOP *Polybe*™ Pressure Swing Adsorption (PSA) Systems, Accessed: 08/2017 (2016).
URL https://www.uop.com/?document=polybed-psa-system-for-gas-extraction-purification&download=1

[23] International Energy Agency (IEA), Technology Roadmap - Carbon capture and storage 2013, Tech. rep. (2013).
URL http://www.iea.org/publications/freepublications/publication/TechnologyRoadmapCarbonCaptureandStorage.pdf

[24] International Energy Agency (IEA) Greenhouse Gas R&D Programme, Techno-Economic Evaluation of SMR Based Standalone (Merchant) Hydrogen Plant with CCS, Tech. rep. (2017).
URL http://ieaghg.org/exco_docs/2017-02.pdf

[25] S. A. Rackley, Carbon Capture and Storage, Elsevier, 2010.

[26] European Zero Emission Technology and Innovation Platform, Commercial Scale Feasibility of Clean Hydrogen, Tech. rep. (2017).
URL http://www.zeroemissionsplatform.eu/library/publication/272-cleanhydrogen.html

[27] A. Godula-Jopek (Ed.), Hydrogen Production by Electrolysis, Wiley-VCH, 2015.

[28] Development of Water Electrolysis in the European Union, Tech. rep., E4tech Sàrl with Element Energy Ltd, Accessed: 08/2017 (2014).
URL http://www.fch.europa.eu/sites/default/files/study%20electrolyser_0-Logos_0_0.pdf

[29] J. O. M. Bockris, The hydrogen economy: Its history, International Journal of Hydrogen Energy 38 (2013) 2579–2588. doi:https://doi.org/10.1016/j.ijhydene.2012.12.026.

[30] N. Z. Muradov, T. N. Veziroğlu, "Green" path from fossil-based to hydrogen economy: An overview of carbon-neutral technologies, International Journal of Hydrogen Energy 33 (2008) 6804–6839. doi:http://dx.doi.org/10.1016/j.ijhydene.2008.08.054.

[31] N. Z. Muradov, CO_2-free production of hydrogen by catalytic pyrolysis of hydrocarbon fuel, Energy & Fuels 12 (1998) 41–48. doi:http://dx.doi.org/10.1021/ef9701145.

[32] Kirk-Othmer (Ed.), Encyclopedia of Chemical Technology, John Wiley & Sons Inc, New Jersey, USA, 2007, Ch. Carbon Black.

[33] N. Z. Muradov, T. N. Veziroğlu, From hydrocarbon to hydrogen-carbon to hydrogen economy, International Journal of Hydrogen Energy 30 (2005) 225–237. doi:http://dx.doi.org/10.1016/j.ijhydene.2004.03.033.

[34] P. Risby, P. E. Stoknes, GasPlas, A Carbon Capture and Use Company, Presentation 8 June 2011, Accessed: 08/2017 (2011).
URL http://www.gasplas.com/resources/upload/news/160_110608_GasPlas_Presentation_UEA-email%201.pdf

[35] C. J. Cleveland, C. Morris, Handbook of Energy, Volume II: Chronologies, Top Ten Lists, and Word Clouds, Elsevier, 2014.

[36] Chemical & Engineering News, Plant De Triomphe: New polytrimethylene terephthalate plant is critical for the strategies of both Shell and its partner, Article on July 13, 2004, Accessed: 08/2017 (2004).
URL http://pubs.acs.org/cen/news/8228/8228earlybus2shell.html

[37] V. N. Kondratiev, Determination of the rate constant for thermal cracking of methane by means of adiabatic compression and expansion, in: Symposium (International) on Combustion, Vol. 10, 1965, pp. 319–322. doi:https://doi.org/10.1016/S0082-0784(65)80178-3.

[38] S. D. Robertson, Carbon formation from methane pyrolysis over some transition metal surfaces-II. Manner of carbon and graphite formation, Carbon 10 (1972) 221–222. doi:https://doi.org/10.1016/0008-6223(72)90045-0.

[39] L. S. Lobo, D. L. Trimm, Carbon formation from light hydrocarbons on nickel, Journal of Catalysis 29 (1973) 15–19. doi:https://doi.org/10.1016/0021-9517(73)90197-8.

[40] C.-J. Chen, M. H. Back, The thermal decomposition of methane. I. Kinetics of the primary decomposition to C2H6 + H2; rate constant for the homogeneous unimolecular dissociation of methane and its pressure dependence, Canadian Journal of Chemistry 53 (1975) 3580–3590. doi:https://doi.org/10.1139/v75-516.

[41] J. M. Roscoe, M. J. Thompson, Thermal decomposition of methane: Autocatalysis, International Journal of Chemical Kinetics 17 (1985) 967–990. doi:https://doi.org/10.1002/kin.550170905.

[42] S. Iijima, Helical microtubules of graphitic carbon, Nature 354 (1991) 56–58. doi:https://doi.org/10.1038/354056a0.

[43] S. Iijima, T. Ichihashi, Single-shell carbon nanotubes of 1-nm diameter, Nature 363 (1993) 603–605. doi:https://doi.org/10.1038/363603a0.

[44] N. M. Rodriguez, A review of catalytically grown carbon nanofibers, Journal of Materials Research 8 (1993) 3233–3250. doi:https://doi.org/10.1557/JMR.1993.3233.

[45] T. Zhang, M. D. Amiridis, Hydrogen production via the direct cracking of methane over silica-supported nickel catalysts, Applied Catalysis A: General 167 (1998) 161–172. doi:http://dx.doi.org/10.1016/S0926-860X(97)00143-9.

[46] P. Chen, X. Wu, J. Lin, K. L. Tan, High H_2 uptake by alkali-doped carbon nanotubes under ambient pressure and moderate temperatures, Science 285 (1999) 91–93. doi:https://doi.org/10.1126/science.285.5424.91.

[47] M. A. Ermakova, D. Y. Ermakov, G. G. Kuvshinov, Effective catalysts for direct cracking of methane to produce hydrogen and filamentous carbon: Part I. Nickel catalysts, Applied Catalysis A: General 201 (2000) 61–70. doi:https://doi.org/10.1016/S0926-860X(00)00433-6.

[48] B. C. Liu, S. C. Lyu, T. J. Lee, S. K. Choi, S. J. Eum, C. W. Yang, C. Y. Park, C. J. Lee, Synthesis of single- and double-walled carbon nanotubes by catalytic decomposition of methane, Chemical Physics Letters 373 (2003) 475–479. doi:https://doi.org/10.1016/S0009-2614(03)00636-5.

[49] S. Takenaka, S. Kobayashi, H. Ogihara, K. Otsuka, Ni/SiO_2 catalyst effective for methane decomposition into hydrogen and carbon nanofiber, Journal of Catalysis 217 (2003) 79–87. doi:http://dx.doi.org/10.1016/S0021-9517(02)00185-9.

[50] Q. Weizhong, L. Tang, W. Zhanwen, W. Fei, L. Zhifei, L. Guohua, L. Yongdan, Production of hydrogen and carbon nanotubes from methane decomposition in a two-stage fluidized bed reactor, Applied Catalysis A: General 260 (2004) 223–228. doi:https://doi.org/10.1016/j.apcata.2003.10.018.

[51] M. Pudukudy, Z. Yaakob, M. S. Takriff, Methane decomposition over Pd promoted $Ni/MgAl_2O_4$ catalysts for the production of COx free hydrogen and multiwalled carbon nanotubes, Applied Surface Science 356 (2015) 1320–1326. doi:http://dx.doi.org/10.1016/j.apsusc.2015.08.246.

[52] G. Allaedini, P. Aminayi, S. M. Tasirin, Methane decomposition for carbon nanotube production: Optimization of the reaction parameters using response surface methodology, Chemical Engineering Research and Design 112 (2016) 163–174. doi:https://doi.org/10.1016/j.cherd.2016.06.010.

[53] N. Muradov, Hydrogen from fossil fuel without CO_2 emissions, in: C. E. G. Padró, F. Lau (Eds.), Proceedings of an American Chemical Society Symposium on Hydrogen Production, Storage, and Utilization, August 22–26, 1999, New Orleans, Louisiana.

[54] U. P. M. Ashik, W. M. A. Wan Daud, J. Hayashi, A review on methane transformation to hydrogen and nanocarbon: Relevance of catalyst characteristics and experimental parameters on yield, Renewable and Sustainable Energy Reviews 76 (2017) 743–767. doi:https://doi.org/10.1016/j.rser.2017.03.088.

[55] N. Muradov, Catalysis of methane decomposition over elemental carbon, Catalysis Communications 2 (2001) 89–94. doi:https://doi.org/10.1016/S1566-7367(01)00013-9.

[56] E. K. Lee, S. Y. Lee, G. Y. Han, B. K. Lee, T.-J. Lee, J. H. Jun, K. J. Yoon, Catalytic decomposition of methane over carbon blacks for CO_2-free hydrogen production, Carbon 42 (2004) 2641–2648. doi:http://dx.doi.org/10.1016/j.carbon.2004.06.003.

[57] J. L. Pinilla, I. Suelves, M. J. Lázaro, R. Moliner, Kinetic study of the thermal decomposition of methane using carbonaceous catalysts, Chemical Engineering Journal 138 (2008) 301–306. doi:http://dx.doi.org/10.1016/j.cej.2007.05.056.

[58] N. Muradov, Hydrogen via methane decomposition: an application for decarbonization of fossil fuels, International Journal of Hydrogen Energy 26 (2001) 1165–1175. doi:http://dx.doi.org/10.1016/S0360-3199(01)00073-8.

[59] N. Shah, D. Panjala, G. P. Huffman, Hydrogen production by catalytic decomposition of methane, Energy & Fuels 15 (2001) 1528–1534. doi:http://dx.doi.org/10.1021/ef0101964.

[60] J. K. Dahl, K. J. Buechler, A. W. Weimer, A. Lewandowski, C. Bingham, Solar-thermal dissociation of methane in a fluid-wall aerosol flow reactor, International Journal of Hydrogen Energy 29 (2004) 725–736. doi:http://dx.doi.org/10.1016/j.ijhydene.2003.08.009.

[61] S. Rodat, S. Abanades, J. Coulié, G. Flamant, Kinetic modelling of methane decomposition in a tubular solar reactor, Chemical Engineering Journal 146 (2009) 120–127. doi:http://dx.doi.org/10.1016/j.cej.2008.09.008.

[62] N. Muradov, F. Smith, A. T-Raissi, Catalytic activity of carbons for methane decomposition reaction, Catalysis Today 102–103 (2005) 225–233. doi:http://dx.doi.org/10.1016/j.cattod.2005.02.018.

[63] I. Suelves, M. J. Lázaro, R. Moliner, J. L. Pinilla, H. Cubero, Hydrogen production by methane decarbonization: Carbonaceous catalysts, International Journal of Hydrogen Energy 32 (2007) 3320–3326, in: International Symposium on Solar-Hydrogen-Fuel Cells 2005. doi:http://dx.doi.org/10.1016/j.ijhydene.2007.05.028.

[64] D. P. Serrano, J. A. Botas, J. L. G. Fierro, R. Guil-López, P. Pizarro, G. Gómez, Hydrogen production by methane decomposition: Origin of the catalytic activity of carbon materials, Fuel 89 (2010) 1241–1248. doi:https://doi.org/10.1016/j.fuel.2009.11.030.

[65] J. Dufour, D. P. Serrano, J. L. Gálvez, J. Moreno, C. García, Life cycle assessment of processes for hydrogen production. Environmental feasibility and reduction of greenhouse gases emissions, International Journal of Hydrogen Energy 34 (2009) 1370–1376. doi:http://dx.doi.org/10.1016/j.ijhydene.2008.11.053.

[66] J. A. Botas, D. P. Serrano, R. Guil-López, P. Pizarro, G. Gómez, Methane catalytic decomposition over ordered mesoporous carbons: A promising route for hydrogen production, International Journal of Hydrogen Energy 35 (2010) 9788–9794. doi:https://doi.org/10.1016/j.ijhydene.2009.10.031.

[67] D. P. Serrano, J. Botas, P. Pizarro, G. Gómez, Kinetic and autocatalytic effects during the hydrogen production by methane decomposition over carbonaceous catalysts, International Journal of Hydrogen Energy 38 (2013) 5671–5683. doi:http://dx.doi.org/10.1016/j.ijhydene.2013.02.112.

[68] Cheap Tubes Inc, Cheap Tubes: Products, Accessed: 08/2017 (2017). URL https://www.cheaptubes.com/cheap-tubes-inc-online-shop/

[69] Asia Carbon Industries, Inc, Tech. rep., Accessed: 08/2017 (2012). [link]. URL http://edg1.precisionir.com/companyspotlight/NA019330/AsiaCarbonCorporateProfile.pdf

[70] Alibaba.com, Accessed: 08/2017 (2017). [link]. URL https://www.alibaba.com/showroom/carbon-black-prices.html

[71] Carbon Black Sales, Carbon Black - Description, Market Prospects, Industry History, Accessed: 08/2017. URL http://carbonblacksales.com/carbon-black-description-market-prospects-industry-history/

[72] Viet Delta Corp, Market analysis and price activated carbon coconut shell charcoal, activated carbon from December 2012 to November 2013, Accessed: 08/2017 (2014). URL http://vdeltafuel.com/news.html

[73] Steelonthenet.com, Met Coke Prices - Europe 2014-2017, Accessed: 08/2017 (2017). URL http://www.steelonthenet.com/files/blast-furnace-coke.html

[74] M. F. L. De Volder, S. H. Tawfick, R. H. Baughman, A. J. Hart, Carbon nanotubes: Present and future commercial applications, Science 339 (2013) 535–539. doi:http://dx.doi.org/10.1126/science.1222453.

[75] O. V. Kharissova, L. M. T. Martínez, B. I. Kharisov, Advances in Carbon Nanostructures, InTech, 2016, Ch. Chapter 7: Recent Trends of Reinforcement of Cement with Carbon Nanotubes and Fibers. doi:http://dx.doi.org/10.5772/61730.

[76] X. Liu, M. Wang, S. Zhang, B. Pan, Application potential of carbon nanotubes in water treatment: A review, Journal of Environmental Sciences 25 (2013) 1263–1280. doi:https://doi.org/10.1016/S1001-0742(12)60161-2.

[77] G. E. Froudakis, Hydrogen storage in nanotubes & nanostructures, Materials Today 14 (2011) 324–328. doi:https://doi.org/10.1016/S1369-7021(11)70162-6.

[78] H. Marsh, F. Rodríguez-Reinoso, Activated Carbon, Elsevier, 2006.

[79] B. H. R. Suryanto, C. Zhao, Surface-oxidized carbon black as a catalyst for the water oxidation and alcohol oxidation reactions, Chemical Communications 52 (2016) 6439–6442. doi:https://doi.org/10.1039/C6CC01319H.

[80] M. J. Forest, Rubber Analysis - Polymer, Compounds and Products, Tech. rep., Rapra Technology Ltd. (2001).

[81] G. Heinrich, M. Klüppel, A hypothetical mechanism of carbon black formation based on molecular ballistic deposition, Kautschuk, Gummi, Kunststoffe 54 (2001) 159–165.

[82] J. G. Speight, Handbook of Petroleum Product Analysis, John Wiley & Sons Inc, New Jersey, USA, 2015.

[83] A. Abánades, E. Ruiz, E. M. Ferruelo, F. Hernández, A. Cabanillas, J. M. Martínez-Val, J. A. Rubio, C. López, R. Gavela, G. Barrera, C. Rubbia, D. Salmieri, E. Rodilla, D.Gutiérrez, Experimental analysis of direct thermal methane cracking, International Journal of Hydrogen Energy 36 (2011) 12877–12886. doi:http://dx.doi.org/10.1016/j.ijhydene.2011.07.081.

[84] A. Abánades, C. Rubbia, D. Salmieri, Technological challenges for industrial development of hydrogen production based on methane cracking, Energy 46 (2012) 359–363. doi:http://dx.doi.org/10.1016/j.energy.2012.08.015.

[85] N. Triphob, S. Wongsakulphasatch, W. Kiatkittipong, T. Charinpanitkul, P. Praserthdam, S. Assabumrungrat, Integrated methane decomposition and solid oxide fuel cell for efficient electrical power generation and carbon capture, Chemical Engineering Research and Design 90 (2012) 2223–2234. doi:http://dx.doi.org/10.1016/j.cherd.2012.05.014.

[86] B. Parkinson, J. W. Matthews, T. B. McConnaughy, D. C. Upham, E. W. McFarland, Techno-economic analysis of methane pyrolysis in molten metals: Decarbonizing natural gas, Chemical Engineering & Technology 40 (2017) 1022–1030. doi:http://dx.doi.org/10.1002/ceat.201600414.

[87] M. Steinberg, Fossil fuel decarbonization technology for mitigating global warming, International Journal of Hydrogen Energy 24 (1999) 771–777. doi:http://dx.doi.org/10.1016/S0360-3199(98)00128-1.

[88] L. Weger, A. Abánades, T. Butler, Methane cracking as a bridge technology to the hydrogen economy, International Journal of Hydrogen Energy 42 (2017) 720–731. doi:http://dx.doi.org/10.1016/j.ijhydene.2016.11.029.

[89] O. V. Marchenko, S. Solomin, The future energy: Hydrogen versus electricity, International Journal of Hydrogen Energy 40 (2015) 3801–3805. doi:http://dx.doi.org/10.1016/j.ijhydene.2015.01.132.

[90] R. Raiko, T. Keipi, H. Tolvanen, J. Rajamäki, K. Tolvanen, Invention disclosure TTY/933/431/2014, Submitted to the Tampere University of Technology in 06/2014.

[91] S. R. Turns, An Introduction to Combustion: Concepts and Applications, McGraw-Hill Companies, Inc, 2012.

[92] J. I. Villacampa, C. Royo, E. Romeo, J. A. Montoya, P. D. Angel, A. Monzóna, Catalytic decomposition of methane over Ni-Al_2O_3 coprecipitated catalysts: Reaction and regeneration studies, Applied Catalysis A: General 252 (2003) 363–383. doi:http://dx.doi.org/10.1016/S0926-860X(03)00492-7.

[93] O. Olsvik, F. Billaud, Modelling of the decomposition of methane at 1273 K in a plug flow reactor at low conversion, Journal of Analytical and Applied Pyrolysis 25 (1993) 395–405, Proceedings of the 10th International Conference on Fundamental Aspects, Processes and Applications of Pyrolysis. doi:http://dx.doi.org/10.1016/0165-2370(93)80058-8.

[94] N. Ozalp, K. Ibrik, M. Al-Meer, Kinetics and heat transfer analysis of carbon catalyzed solar cracking process, Energy 55 (2013) 74–81. doi:http://dx.doi.org/10.1016/j.energy.2013.02.022.

[95] D. Trommer, D. Hirsch, A. Steinfield, Kinetic investigation of the thermal decomposition of CH_4 by direct irradiation of a vortex-flow laden with carbon particles, International Journal of Hydrogen Production 29 (2004) 627–633. doi:http://dx.doi.org/10.1016/j.ijhydene.2003.07.001.

[96] A. M. Dunker, J. P. Ortmann, Kinetic modeling of hydrogen production by thermal decomposition of methane, International Journal of Hydrogen Energy 31 (2006) 1989–1998. doi:http://dx.doi.org/10.1016/j.ijhydene.2006.01.013.

[97] M. Younessi-Sinaki, E. A. Matida, F. Hamdullahpur, Kinetic model of homogeneous thermal decomposition of methane and ethane, International Journal of Hydrogen Energy 34 (2009) 3710–3716. doi:http://dx.doi.org/10.1016/j.ijhydene.2009.03.014.

[98] A. F. Mills, Basic Heat and Mass Transfer, Prentice Hall, 1999.

[99] LOGE AB, Lund, LOGESOFT Manual, Book 1 (2016).

[100] LOGE AB, Lund, LOGESOFT Manual, Book 2 (2016).

[101] J. Rajamäki, Thermal decomposition and autothermal pyrolysis of methane, Master of Science Thesis, Tampere University of Technology, Finland (2014).

[102] Thermo Nicolet Corporation, Introduction to Fourier Transform Infrared Spectrometry, Accessed: 08/2017 (2001).
URL http://www.niu.edu/analyticallab/_pdf/ftir/FTIRintro.pdf

[103] Y. Leng, Materials Characterization: Introduction to Microscopic and Spectroscopic Methods, Wiley-VCH, 2013.

[104] C. Evans, R. Brundle, S. Wilson, Encyclopedia of Materials Characterization: Surfaces, Interfaces, Thin Films, Elsevier Inc, 1992.

[105] R. L. Busby, Hydrogen and Fuel Cells: A Comprehensive Guide, PennWell Corporation, 2005.

[106] Toyota, Long-distance driving with a hydrogen fuel cell car (2017).
URL https://www.toyota-europe.com/world-of-toyota/articles-news-events/long-distance-driving-with-toyota-mirai

[107] T. Ramsden, M. Ruth, V. Diakov, M. Laffen, T. A. Timbario, Hydrogen pathways: Updated cost, well-to-wheels energy use, and emissions for the current technology status of ten hydrogen production, delivery, and distribution scenarios, Tech. rep., National Renewable Energy Laboratory (NREL) (2013).

[108] Y. Zhang, J. Wang, X. Zhang, G. Sun, Experimental study of petroleum coke steam gasification catalyzed by black liquor in a fluidized bed, Energy Procedia 61 (2014) 472–475, in: The 6th International Conference on Applied Energy - ICAE2014. doi:http://dx.doi.org/10.1016/j.egypro.2014.11.1151.

[109] J. C. Molburg, R. D. Doctor, Hydrogen from Steam-Methane Reforming with CO_2 Capture, in: 20th Annual International Pittsburgh Coal Conference, September 15-19, 2003, Pittsburgh, PA, 2003.

[110] European Technology Platform for Zero Emission Fossil Fuel Power Plants, The Costs of CO_2 Capture, Transport and Storage: Post-demonstration CCS in the EU, Tech. rep. (2011).

[111] G. Towler, R. Sinnott, Chemical Engineering Design: Principles, Practice and Economics of Plant and Process Design, Elsevier Science, 2013.

[112] National Renewable Energy Laboratory (NREL), Energy Analysis, Simple Levelized Cost of Energy (LCOE) Calculator Documentation, Accessed: 08/2017 (2017).
URL http://www.nrel.gov/analysis/tech_lcoe_documentation.html

[113] European Energy Exchange, Natural Gas Daily Reference Price, Accessed: 08/2017 (2017).
URL https://www.eex.com/en/market-data/natural-gas/spot-market

[114] Nord Pool, Historical market data, Accessed: 08/2017 (2017).
URL http://www.nordpoolspot.com/historical-market-data/

[115] European Energy Exchange, European Emission Allowances, Accessed: 08/2017 (2017).
URL https://www.eex.com/en/market-data/

[116] M. Saxe, P. Alvfors, Advantages of integration with industry for electrolytic hydrogen production, Energy 32 (2007) 42–50. doi:https://doi.org/10.1016/j.energy.2006.01.021.

[117] J. Vandewalle, K. Bruninx, W. D'haeseleer, Effects of large-scale power to gas conversion on the power, gas and carbon sectors and their interactions, Energy Conversion and Management 94 (2015) 28–39. doi:http://dx.doi.org/10.1016/j.enconman.2015.01.038.

[118] U.S. Energy Information Administration, Annual Energy Outlook 2014 with projections to 2040, Tech. rep. (2014).

[119] European Commission, Quarterly Report on European Gas Market, fourth quarter of 2015 and first quarter of 2016, Tech. rep., The Market Observatory for Energy of the European Commission (2016).

[120] M. Fager-Pintilä, Thermocatalytic decomposition of methane, Master of Science Thesis, Tampere University of Technology (2012).

[121] E. B. Sebok, R. L. Taylor, Encyclopedia of Materials: Science and Technology, Elsevier Ltd., 2011, Ch. Carbon Blacks. doi:https://doi.org/10.1016/B0-08-043152-6/00173-X.

[122] L. S. Kassel, The thermal decomposition of methane, Journal of the American Chemical Society 54 (1932) 3949–3961. doi:https://doi.org/10.1021/ja01349a019.

[123] G. B. Skinner, R. A. Ruehrwein, Shock tube studies on the pyrolysis and oxidation of methane, The Journal of Physical Chemistry 63 (1959) 1736–1742. doi:http://dx.doi.org/10.1021/j150580a040.

[124] V. Kevorkian, C. E. Heath, M. Boudart, The decomposition of methane in shock waves, The Journal of Physical Chemistry 64 (1960) 964–968. doi:http://dx.doi.org/10.1021/j100837a002.

[125] H. B. Palmer, T. J. Hirt, The activation energy for the pyrolysis of methane, The Journal of Physical Chemistry 67 (1963) 709–711. doi:http://dx.doi.org/10.1021/j100797a502.

[126] M. Steinberg, Production of hydrogen and methanol from natural gas with reduced CO_2 emission, International Journal of Hydrogen Energy 23 (1998) 419–425. doi:https://doi.org/10.1016/S0360-3199(97)00092-X.

[127] M. Plevan, T. Geißler, A. Abánades, K. Mehravaran, R. K. Rathnam, C. Rubbia, D. Salmieri, L. Stoppel, S. Stückrad, T. Wetzel, Thermal cracking of methane in a liquid metal bubble column reactor: Experiments and kinetic analysis, International Journal of Hydrogen Energy 40 (2015) 8020–8033. doi:http://dx.doi.org/10.1016/j.ijhydene.2015.04.062.

[128] S. Rodat, S. Abanades, G. Flamant, Co-production of hydrogen and carbon black from solar thermal methane splitting in a tubular reactor prototype, Solar Energy 85 (2011) 645–652. doi:http://dx.doi.org/10.1016/j.solener.2010.02.016.

[129] M. Götz, J. Lefebvre, F. Mörs, A. M. Koch, F. Graf, S. Bajohr, R. Reimert, T. Kolb, Renewable Power-to-Gas: A technological and economic review, Renewable Energy 85 (2016) 1371–1390. doi:https://doi.org/10.1016/j.renene.2015.07.066.

[130] C. Yang, J. Ogden, Determining the lowest-cost hydrogen delivery mode, International Journal of Hydrogen Energy 32 (2007) 268–286. doi:https://doi.org/10.1016/j.ijhydene.2006.05.009.

[131] M. Voldsund, K. Jordal, R. Anantharaman, Hydrogen production with CO_2 capture, International Journal of Hydrogen Energy 41 (2016) 4969–4992. doi:http://dx.doi.org/10.1016/j.ijhydene.2016.01.009.

[132] International Energy Agency (IEA), Energy Technology Network, Hydrogen Production & Distribution, Accessed: 08/2017 (2007).
URL https://www.iea.org/publications/freepublications/publication/essentials5.pdf

Appendix: Original publications

Publication I

Tiina Keipi, Ville Hankalin, Jaakko Nummelin, Risto Raiko

Techno-economic analysis of four concepts for thermal decomposition of methane: Reduction of CO_2 emissions in natural gas combustion

Energy Conversion and Management, 110 (2016) 1–12.

Energy Conversion and Management 110 (2016) 1–12

Contents lists available at ScienceDirect

Energy Conversion and Management

journal homepage: www.elsevier.com/locate/enconman

Techno-economic analysis of four concepts for thermal decomposition of methane: Reduction of CO_2 emissions in natural gas combustion

Tiina Keipi [a,*], Ville Hankalin [b], Jaakko Nummelin [b], Risto Raiko [a]

[a] Department of Chemistry and Bioengineering, Tampere University of Technology, P.O. Box 541, 33101 Tampere, Finland
[b] ÅF-Consult, Bertel Jungin aukio 9, 02600 Espoo, Finland

ARTICLE INFO

Article history:
Received 7 September 2015
Accepted 21 November 2015

Keywords:
Carbon capture
Natural gas
Carbon black
Methane decomposition
Techno-economic analysis
Carbon dioxide

ABSTRACT

This paper presents a techno-economic analysis of four concepts that apply the thermal decomposition of methane (TDM) with the aim of reducing carbon dioxide emissions in natural gas combustion. Different technical solutions are applied to convert methane in natural gas to gaseous hydrogen, which is combusted to produce electricity with a steam power cycle, and solid carbon, which is assumed to be sold as carbon black. The cost of electricity production and the potential to reduce CO_2 emissions in each concept were evaluated and compared to the reference case of direct methane combustion. With a moderate emission allowance price (20 €/t_{CO_2}) and product carbon price (500 €/t_{carbon}) the cost of electricity production in the concepts was 12–58% higher than in the reference case. However, the price of product carbon had a significant effect on the feasibility of the concepts. Thus, the methane burner, which showed the best performance, produced 17% less CO_2 emissions per MWh_e and had a smaller cost of electricity production than the reference case already with the carbon price of 600—700 €/t_{carbon}.

1. Introduction

According to the estimates given by the International Energy Agency, global gas demand will grow from 3.4 trillion m^3 in 2012 to 5.4 trillion m^3 in 2040 [1]. This is partly because replacing coal with natural gas in power production is seen as attractive due to the lower carbon dioxide (CO_2) emissions of the latter. However, the regulation of CO_2 emissions is becoming stricter as, for example, the European Union has set a target of a 40% reduction in greenhouse gas emissions by 2030 compared to the levels in 1990 [2]. Consequently, the CO_2 emissions has to be reduced also in the use of natural gas [3,4].

The thermal decomposition of methane (TDM) is an endothermic reaction where methane is thermally converted to solid carbon, gaseous hydrogen, and traces of higher hydrocarbons. Eq. (1) presents a simplified reaction equation of TDM [5].

$$CH_4 \rightarrow C + 2H_2 \quad \Delta H_r^0 = +76\ \mathrm{kJ/mol_{CH_4}} \tag{1}$$

The equilibrium curve of TDM reaction presented, for example, in [6] shows that the degree of methane conversion increases with temperature. However, temperatures above 1200 °C are required to achieve a nearly complete conversion when no catalyst is applied. Li et al. [7] have further presented that increasing pressure has a negative effect on the TDM reaction. Catalysts can be applied to reduce the reaction temperature. This is a process called catalytic decomposition of methane (CDM). The properties of catalysts applied and the results achieved in CDM have been extensively summarized in reviews [8,9].

Muradov [5] almost two decades ago presented a conceptual idea to utilize TDM for the on-site production of hydrogen/methane blends from natural gas. According to the presented analysis, the TDM process consumes 1.7 times more methane in hydrogen production than steam reforming. However, steam reforming produces 5 times more CO_2 emissions than TDM, and thus TDM was seen as the most potential process for fossil fuel-based production of hydrogen without CO_2 emissions. Later, Muradov and Veziroğlu [10] presented hydrogen production based on TDM as a transitional period solution before shifting to a renewable-based hydrogen economy in the future. The key challenge of TDM was stated to be the enormous amount of solid carbon produced. Three potential end uses for large amount of carbon were presented: material for building and construction, electricity production by direct carbon fuel cells, and soil amendment.

TDM concept can be considered as an alternative technology for carbon capture and storage (CCS) in natural gas combustion. Compared to the conventional pre-combustion CCS technology that requires several process steps TDM could be a simpler process, and furthermore solid carbon from TDM can be a valuable product

* Corresponding author. Tel.: +358 50 301 4280.
E-mail address: tiina.keipi@tut.fi (T. Keipi).

http://dx.doi.org/10.1016/j.enconman.2015.11.057
0196-8904/

instead of gaseous CO_2, which is in most cases an unwanted product [11,12]. Furthermore, carbon capture in solid form in TDM prevents many of the problems related to the transportation and storage of gaseous CO_2 such as risk of CO_2 leakage or migration in sediments, which could have serious consequences for the environment and human beings [13–16].

An extensive amount of studies [17–23] that include either or both technical and economic analyses related to the pre-combustion carbon capture from natural gas are found in the literature, and the most relevant results are briefly summarized. Kanniche et al. [17] conducted a techno-economic study for different CCS technologies that are applied to pulverized coal combustion, integrated gasification combined cycle, and natural gas combined cycle (NGCC). Kanniche et al. stated that pre-combustion capture by the reforming of natural gas is fairly expensive compared to other CCS methods and it should be used rather in the production of hydrogen than in energy production. Lozza and Chiesa [22,23] conducted an economic analysis of pre-combustion capture technology where partial oxidation (PO) is combined with a NGCC and these costs compared to those of post-combustion carbon capture from NGCC. According to the results, adding the PO process to NGCC increased the relative investment cost ($/kW) by 40–59%, increased the cost of electricity by 36–43%, and resulted in a cost of avoided CO_2 as 39–46$/$t_{CO_2}$. with 90% CO_2 capture. Manzolini et al. [24] studied the cost of pre-combustion CO_2 capture based on pressure swing adsorption (PSA) in a natural gas combined cycle. According to the results, the presented pre-combustion process based on PSA increased the specific electricity production costs by 33–36% compared to NGCC without CO_2 capture. With a conventional pre-combustion capture based on methyldiethanolamine (MDEA) the increase was stated to be 38%.

One of the rare economic analyses of TDM was presented in a study by Triphob et al. [25], in which the hydrogen produced by TDM was utilized in a fuel cell. They presented the costs of electricity production with a solid oxide fuel cell (SOFC) when the hydrogen was produced alternatively with methane steam reforming or with TDM. An important benefit of TDM is the absence of CO_x in the product hydrogen, which extends the lifetime of SOFC. However, the solid carbon particles from TDM can be harmful to SOFC. As a conclusion, Triphob et al. stated that TDM provides technical advantages over, and is an economically more feasible method than methane steam reforming when producing hydrogen for SOFC. This is partly because TDM produces carbon, which was assumed to be a valuable by-product, whereas methane steam reforming produces undesired CO_2 emissions.

There is a very limited amount of research presented in the literature that further discusses the conceptual idea of TDM as a pre-combustion capture technology. Therefore, the techno-economic analysis presented in this paper produces valuable information. TDM can be applied to produce hydrogen for purposes other than on direct power production, such as upgrading biofuels or for other chemical processes, but this option is not further evaluated in this study. The theoretical background of TDM reaction and carbon black as well as the technical descriptions of the four concepts are given in Section 2. The assumptions and the basis of the techno-economic analysis are presented in Section 3. The results of the technical analysis, including the mass and energy balances, and economic analysis, including the investment and operational costs, are presented and discussed in Section 4. The discussion focuses on the cost of electricity production and the cost of avoided CO_2 emissions in each concept. Furthermore, sensibility analysis has been conducted to better understand the effect of product carbon price, operation time, and degree of methane conversion on the feasibility of the concepts. Section 5 concludes the results of this study and presents recommendations for further research. The technical solutions chosen in this study represent the currently available technology. All assumptions and input values of the evaluations are based on literature data, product information, expert opinions, and analysis by the authors.

2. Theory and concepts

2.1. Carbon black

Carbon black is a generic term for materials that are mainly composed of elemental carbon and have extremely small particle size and high surface area. Currently, carbon black is mainly produced from heavy oil by the oil-furnace process. The reaction temperature is 1400–1800 °C and the heat is provided by the partial combustion of aromatic oils in the feedstock. A less frequently applied process is the thermal black process (temperature requirement around 1300 °C) in which thermal decomposition of natural gas is applied to produce so-called thermal black. Thermal black is used in various rubber and plastic applications [26].

The production cost of carbon black is dominated by the feedstock cost, whereas the value of carbon black is highly dependent on its morphology. Public data about the present prices of carbon black is not widely available, and therefore, rough estimations based on the expertise of the authors are utilized in this study. According to a commercial source [27], the price of carbon black with special quality may vary from 3300 to 4000 €/t_{carbon} and with standard quality from 2300 to 3000 €/t_{carbon}. The price of thermal black is estimated to vary between 500 and 1400 €/t_{carbon}. The price of the product carbon in this study was chosen to be equal with the smallest price of thermal black, 500 €/t_{carbon}, in the scale given in [27], The smallest price in the scale varying from 500 to 1400 €/t_{carbon} was chosen to avoid overestimating the value of the product carbon. The amount of produced carbon in the concepts is calculated from the reaction equations of TDM, which are presented in Eqs. (2) and (5).

2.1.1. Environmental and health effects of carbon black

The main idea of TDM concept is to decrease the CO_2 emissions to the atmosphere and produce valuable solid carbon instead. However, the product carbon may have negative effects on environment and humans. These effects are shortly summarized here and more detailed information can be found in the references.

Nanoparticles have a representative dimension such as diameter of a particle or diameter of a fiber is less than 100 nm. In carbon black, the aggregate dimensions vary from tens to a few hundred nanometers. The nanoparticles have a high tendency to agglomerate and the carbon black agglomerates typically have a diameter less than 2 mm. Thus, carbon black occur both as nanoparticles and as fine particles, which are defined as particles with a diameter less than 2.5 μm [28].

The International Agency for Research and Cancer has defined carbon black as "possibly carcinogenic to humans". The primary industrial exposure to carbon black occurs in the carbon black production industry. In atmosphere, the effects of carbon black particles are the same as fine particles in general. For humans, fine particles cause different lung and heart diseases. The fine particles may reduce the visibility of air. However, as carbon black is not soluble in water, it will eventually end up in sediments and soil. Carbon black is not degradable, and therefore it is persistent in the environment. However, carbon black does not bioaccumulate and the potential of being toxic to aquatic organisms is low [28–31].

2.2. Reaction equations

The overall one-step reaction equations of TDM in the concepts are presented in this section. The heat demand of TDM reaction and reaction products in each concept are calculated based on

the equations. The required heat demand of TDM reaction is produced by partial combustion or by an external heat source. The technological implementation and the process flow charts of the concepts are presented in Section 2.3.

2.2.1. Concept 1 – partial combustion

In Concept 1, a part of the input methane is combusted to produce the heat demand of TDM reaction of the remaining methane. The overall reaction equation combines the methane combustion and TDM as is shown in Eq. (2).

$$CH_4 + 2y(O_2 + 3.77N_2) \rightarrow a(C + 2H_2) + (1 - a - y)CH_4 + y(CO_2 + 2H_2O + 7.52N_2) \quad (2)$$

The degree of methane conversion, i.e., the molar fraction of decomposed methane, is denoted by a. The degree of methane conversion depends on the reaction conditions, such as temperature and reaction time. Thus, the achieved degree of methane conversion is dependent on the selection of reactor parameters such as dimensions, volumetric gas flow, and temperature. Eq. (2) represents the overall reaction equation that occurs in combustion and quench chamber shown in Fig. 1.

Heat of conversion (Q) is the total energy requirement of the conversion process in the concepts. In Concept 1 the heat of conversion is the sum of the required reaction enthalpy (ΔH_r) and the sensible heat of air and methane:

$$Q = \dot{N}_{CH_4} c_{p,CH_4} M_{CH_4} \Delta T_{CH_4} + a \cdot \dot{N}_{CH_4} \Delta H_r + \dot{N}_{air} c_{p,air} M_{air} \Delta T_{air}, \quad (3)$$

where $\dot{N}_{CH_4}$ is the molar flow rate of input methane, c_{p,CH_4} the specific heat capacity of methane, M_{CH_4} the molar mass of methane, and ΔT_{CH_4} the difference between the reaction temperature and the temperature of the preheated methane stream, $\dot{N}_{air}$ the molar flow rate of input air, $c_{p,air}$ the specific heat capacity of air, M_{air} the molar mass of air, and ΔT_{air} the difference between the reaction temperature and the temperature of the preheated air stream. The reaction enthalpy ΔH_r depends on the reaction temperature, and the values applied in this study are adapted from [32].

The mass flow rate of methane which is combusted to supply the energy demand in Concept 1 ($\dot{m}_{comb.,CH_4}$) is calculated according to the following equation:

$$\dot{m}_{comb.,CH_4} = \frac{Q}{LHV_{CH_4}}, \quad (4)$$

where LHV_{CH_4} is the lower heating value of methane. The overall air factor denoted by y in Eq. (2) is defined as the ratio of molar air flow rate ($\dot{N}_{air}$) to the molar air flow rate that would be needed to achieve the stoichiometric combustion of input methane. The air factor y is iteratively determined using Eqs. (3) and (4) so that the heat from the partial combustion of input methane equals the heat of conversion.

2.2.2. Concepts 2–4 – thermal decomposition

In Concepts 2–4, where no air or oxygen is introduced in the conversion reaction, methane reacts according to Eq. (5). This reaction equation is modified from Eq. (1) by defining the conversion degree a as the molar fraction of decomposed methane.

$$CH_4 \rightarrow a(C + 2H_2) + (1 - a)CH_4 \quad (5)$$

The methane conversion degree is denoted by a similarly as in Concept 1. The TDM reaction occurs according to Eq. (5) in TDM reactors in Figs. 2 and 4. Furthermore, the same reaction occurs in the CDM reactor shown in Fig. 3.

For Concepts 2–3 the heat of conversion (Q), is the sum of sensible heat and reaction enthalpy (ΔH_r):

$$Q = \dot{N}_{CH_4} c_{p,CH_4} M_{CH_4} \Delta T_{CH_4} + a \cdot \dot{N}_{CH_4} \Delta H_r, \quad (6)$$

where the terms are defined similarly as in Eq. (3). For Concept 4, the heat of conversion (Q) also includes the sensible heat of the bed material stream:

$$Q = \dot{N}_{CH_4} c_{p,CH_4} M_{CH_4} \Delta T_{CH_4} + \dot{N}_{bed} c_{p,bed} M_{bed} \Delta T_{bed} + a \cdot \dot{N}_{CH_4} \Delta H_r, \quad (7)$$

where $\dot{N}_{CH_4}$ is the molar flow rate of input methane, c_{p,CH_4} the specific heat capacity of methane, M_{CH_4} the molar mass of methane, and ΔT_{CH_4} the difference between the reaction temperature and the temperature of the preheated methane stream.

2.3. Concept descriptions

The four TDM concepts analyzed in this study are presented in more detailed in this section. In all the concepts methane and other fluids are internally preheated prior to the reactor in order to minimize the heat from additional sources. The internal heat transfer from the product gas and product carbon of TDM reaction to the input gas streams is conducted by a closed cooling water (CCW). The additional heating that is required after preheating is produced by partial oxidation (Concept 1) or electricity (Concept 2 and 4). Solid carriers are utilized for heating in Concepts 3 and 4.

2.3.1. Methane burner

Concept 1 is based on the partial oxidation of methane that provides the heat of conversion. Since adding a catalyst to a burner is extremely challenging, non-catalytic thermal decomposition is

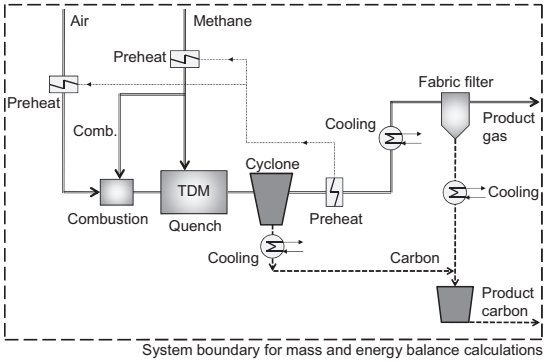

Fig. 1. Process diagram of Concept 1.

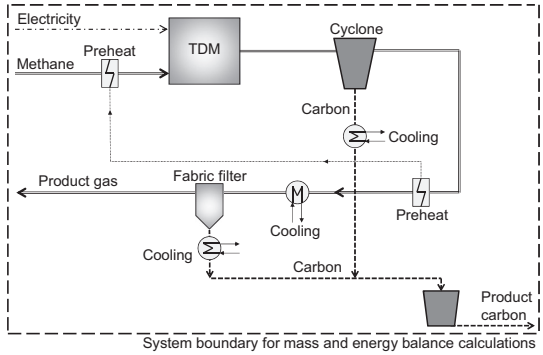

Fig. 2. Process diagram of Concept 2.

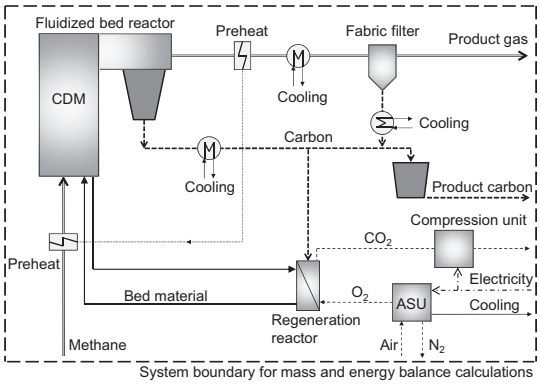

Fig. 3. Process diagram of Concept 3.

applied in this concept. The degree of methane conversion that can be achieved is highly dependent on the burner geometry. Increasing the reaction time by lengthening the reaction zone increases the reaction time and further enables higher methane conversion degrees.

The methane burner process may have two possible practical arrangements. In the first option, the partial oxidation and the TDM reaction occur at the same time in a burner. In the second option, part of the methane is combusted separately in a burner and the flue gas is introduced to an insulated quench chamber where the TDM reaction occurs. The latter configuration was chosen as the basis of Concept 1.

The total methane flow that is combusted was chosen to be divided into four parallel burners in order to achieve convenient burner dimensions. The dimensions of the reaction chambers and burners were chosen based on the gas velocity and the residence time in the reactor. The TDM reaction occurs at atmospheric pressure. A process flow diagram of Concept 1 is shown in Fig. 1. For simplicity the combustion and the quench are shown as two separate processes in the figure.

The product carbon is separated from the product gas with a cyclone and a filter. Besides the heat transfer from the product gas and carbon to the input streams, the products have to be further cooled down to achieve a suitable temperature for conventional fabric filters.

2.3.2. Power-to-carbon

In the power-to-carbon concept, electricity is used to provide the heat of conversion. The TDM reactor in Concept 2 can be powered with electrical heating elements or alternatively with a plasma torch. The heat of conversion can be provided by utilizing, for example, heating elements based on materials such as silicon-carbides (SiC) or molybdenum-disilicates ($MoSi_2$). These materials can typically handle temperature ranges up to 1300–1600 °C.

Applying a plasma torch enables the utilization of a high temperature range (1200–2200 °C) resulting in high degrees of methane conversion and high purity of product gas. The product carbon properties and quality can be modified by adjusting the temperature of the plasma torch. According to the computational model presented by [33] the temperature should be restricted below 2200 °C to prevent the production of a significant amount of harmful C_2H_2 and C_2H radicals.

Concept 2 is illustrated in Fig. 2. Electrical heating elements were chosen to provide the heat of conversion in Concept 2. The input methane is preheated by hot product gas before being fed to the reaction chamber. The reaction chamber is refractory-lined from inside and is operated at atmospheric pressure. The product carbon is separated from the product gas with a cyclone and a fabric filter. The product gas is cooled down to a temperature suitable for fabric filters. The product carbon is cooled to a temperature that is below its self-ignition temperature before being exposed to air.

2.3.3. Catalytic fluidized bed

The catalytic fluidized bed reactor concept is highly similar to existing technology applied in the petroleum refining industry [34]. Concept 3 applies the catalytic decomposition of methane (CDM), and therefore the process can be conducted at typical fluidized bed reaction temperatures (750–950 °C).

The fluidizing agent in Concept 3 is methane. The catalyst is mixed with bed material (sand) which also acts as a heat carrier to provide the heat needed in the TDM reaction. Adding the catalyst to the fluidized bed enables a large reactive surface area between the catalyst and methane. The drawback of this concept is that the product carbon contains catalyst particles as an impurity. Furthermore, regeneration of the catalyst is required. The catalyst regeneration is conducted by circulating bed material to the regeneration reactor. Additionally, a part of the product carbon is combusted is the regeneration reactor to heat up the bed material. In order to enable a more efficient capture of the resulting CO_2 stream, oxy-combustion is applied in the regeneration reactor. Oxygen is produced in an air separation unit (ASU). A part of the flue gas it is circulated back to the regeneration reactor in order to decrease the oxy-combustion temperature to a suitable level. The rest of the CO_2 is captured and compressed to a suitable pressure level (110 bar) for storage [35].

The process diagram of Concept 3 is illustrated in Fig. 3. The reactor type in Concept 3 is a cylinder shaped fluidized bed reactor with a cyclone for the separation of carbon from the product gas stream. The reactor is refractory-lined from inside. Methane is preheated with hot product gas before it enters the reaction chamber. The product gas is further cooled to a temperature that is suitable for fabric filtering.

2.3.4. Regenerative heat exchanger

The regenerative heat exchanger reactor (RHER) operates as a counter-flow heat exchanger between methane (flowing upwards) and bed material (flowing downwards). Therefore, the preheating of the input flow occurs inside the reactor. The reactor type is a refractory-lined cylinder and the bed material is chosen based on its capacity to transfer heat to and from the gases. The reactor tube is divided into three zones: the reaction zone in the middle, where the TDM reaction occurs; the upper zone, where the incoming bed material receives heat from the generated product gas; and lower zone, where the incoming methane stream receives heat from the bed material stream. Thus, the bed material acts both as a preheater for the methane and as a cooler for the product gas. An external heat source is introduced in the reaction zone to provide the heat of conversion. Heat to the reactor can be produced in several ways, e.g., natural gas combustion or electrical heating elements. In this study, electric heating was chosen and the heating elements were placed near the inner surface of the reactor. The heat transfer in the reactor is further analyzed in Section 3.2.

The process diagram of Concept 4 is shown in Fig. 4. Part of the product carbon accumulates on the surface of the bed material. The bed material is constantly flowing downwards, and thus the product carbon can be removed from the reactor. In a commercial scale reactor, after the carbon extraction the bed material is circulated back to the reactor by lifting the bed material up either mechanically or pneumatically. The particle size and the material of the bed material can be chosen so that the heat transfer in the reactor and carbon removal are optimized. Part of the solid carbon is extracted by filtering the product gas.

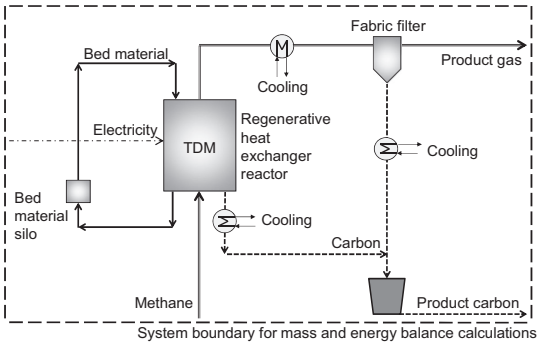

Fig. 4. Process diagram of Concept 4.

3. Techno-economic analysis

The calculation basis and the assumptions made in the analysis are presented in this section. The analysis presented in this paper is the preliminary evaluation of the feasibility of these concepts. Therefore, some input data is still uncertain as it is taken from the literature or is based on assumptions made by the authors. The methodology used in the techno-economic analysis is illustrated in Fig. 5.

3.1. Calculation basis

The technical solutions chosen in this study represent the currently available technology. In all the concepts, the product gas is combusted after TDM in order to produce electricity with a steam power cycle. It might also be possible to adjoin the TDM processes to an existing power or heat boiler. The possible end use of the product gas in a gas turbine is not considered in this paper since the amount of hydrogen that the current gas turbines can handle is limited and also the solid carbon in the product gas might cause special requirements for the gas turbine [11]. Since the focus in the study is to reduce CO_2 emissions, the purity in terms of hydrogen content in the resulting product gas was not of interest.

In this study, the produced carbon is assumed to be sold in the carbon black market with a price of 500 €/t_{carbon}. The effect of product carbon price on the feasibility of the concepts was studied with a sensibility analysis.

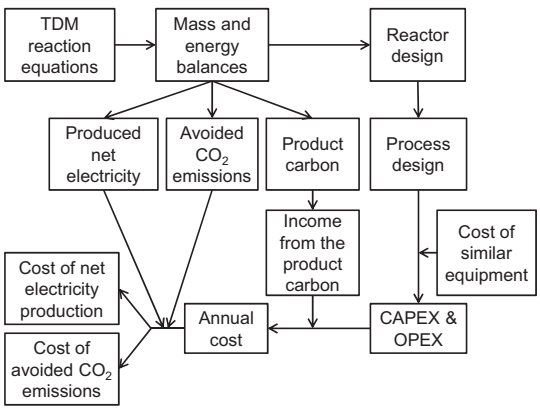

Fig. 5. Diagram of the methodology applied in the analysis.

The reference case in this study is the direct combustion of natural gas, which is for the sake of clarity replaced with methane in all calculations, to produce electricity with a steam power cycle. The reference plant is assumed to be an operating plant which still has operation time left and whose investment costs have been paid back already. The fuel input in the reference case is 150 MW, which is equal with the concepts. The efficiency of the electricity production in the reference case is 30%, the same as in all concepts, and no CCS is applied. Thus, the electricity production cost includes the cost of emission allowances (a moderate value of 20 €/t_{CO_2} assumed). It was decided that the product gas would be utilized to produce only electricity, and not, for example, additional heat. As the efficiency of the electricity production is rather low, the cost of electricity production in the reference case is 163 €/MWh_e which is considerably higher than the 10-year average Nord Pool system price (40 €/MWh_e) [36]. However, despite the high absolute costs of electricity production, it is possible to compare the concepts to the reference case in relative terms.

It is important to note that the results achieved in this study are not general as those highly depend on the assumptions made in the analysis. However, the results can be used to compare the four different TDM concepts with each other.

3.2. Technical assumptions

The main assumptions of the concepts are summarized in Table 1. All the concepts have a fuel input of 150 MW and for the sake of clarity, all the calculations are conducted for methane, as natural gas contains between 70% and 98% methane, depending on its origin [37,38]. The product gas is assumed to be a mixture of hydrogen and unreacted methane that contains solid carbon particles. In Concept 1, the combustion products (N_2, H_2O, and CO_2) are also present in the gas mixture due to the partial oxidation that is used to provide the heat of conversion. It is assumed that in this case the combustion produces CO_2, and thus no CO is present.

The reactor temperatures were selected based on the literature values summarized in [10]. The degree of methane conversion and reaction time in each concept were selected based on experimental research and calculations conducted at Tampere University of Technology. The degree of methane conversion as a function of temperature and residence time has been experimentally studied and the results have been used to determine the reactor dimensions in each concept. Heat losses for the concepts were assumed according to typical levels in similar thermal conversion chambers with an emphasis on reaction temperature and reactor surface area. The heat losses in all the concepts were assumed to be 1.0–2.0% of the fuel input.

Methane and air are assumed to enter the system at a temperature of 25 °C. Due to the poor heat transfer coefficient factors in gas-to-gas heat transfer, the chosen temperature differences between heating streams are kept at a moderate level (logarithmic temperature differences of 400–750 °C) in order to decrease the cost of heat exchangers. Therefore, the temperature of methane and air after preheating was chosen to be in the range of 600–700 °C. The lower temperature of 600 °C in Concept 3 is based on the lower temperature of the product gas. The in situ preheating in Concept 4 was calculated with a chosen terminal temperature difference (TTD) between bed material and methane stream (500 °C). Since the temperature of the bed material was 1200 °C when it leaves the reaction zone, the temperature of the preheated methane was 700 °C. Thus, it is assumed that heat is effectively

Table 1
Input values and assumptions made in analysis.

Assumption	Concept 1	Concept 2	Concept 3	Concept 4
Fuel input	150 MW	150 MW	150 MW	150 MW
Annual operation time	4500 h	4500 h	4500 h	4500 h
Degree of conversion	0.40	0.35	0.40	0.30
Reaction temp.	1350 °C	1350 °C	900 °C	1200 °C
Residence time	3.2 s	3.1 s	4.0 s	3.4 s
Heat of conversion	93 MJ/kmol	93 MJ/kmol	91 MJ/kmol	92 MJ/kmol
Heat losses	2.0%	2.0%	1.5%	1.0%
Temp. (air in)	25 °C	N/A	N/A	N/A
Temp. (methane in)	25 °C	25 °C	25 °C	25 °C
Temp. of methane after preheating	700 °C	700 °C	600 °C	700 °C
Temp. of air after preheating	700 °C	N/A	N/A	N/A
Temp. of product gas in filtering	250 °C	250 °C	250 °C	250 °C
Carbon separation eff. in cyclone	60%	60%	60%	N/A
Carbon separation eff. in reactor	N/A	N/A	N/A	50%
Carbon separation eff. of filter	100%	100%	100%	100%
TTD on carbon cooling	5 °C	5 °C	5 °C	5 °C
Temp. of CW in	25 °C	25 °C	25 °C	25 °C
Temp. of CW out	35 °C	35 °C	35 °C	35 °C
Pressure drop in CW cycle	4 bar	4 bar	4 bar	4 bar
CW pump eff.	78%	78%	78%	78%
Air factor (overall reaction)	0.20	N/A	N/A	N/A
Catalyst	No	No	Yes	No
Catalyst charge in reactor	N/A	N/A	0.1 kg/($m^3_{CH_4}$ h)	N/A
Catalyst lifetime	N/A	N/A	50 h	N/A
Regeneration temp.	N/A	N/A	1200 °C	N/A
Power of oxygen production	N/A	N/A	160 kWh/t_{O_2}	N/A
CO_2 compression work	N/A	N/A	0.4 GJ/t_{CO_2}	N/A
Heat capacity of bed material	N/A	N/A	N/A	0.42 kJ/(kg K)
Heat duty of preheaters	N/A	N/A	N/A	Equal to each other
Mass flow of bed material	N/A	N/A	N/A	20 kg/s

transferred from the bed material to methane, justifying the relatively high temperature of methane after the preheating zone.

Due to the small particle size of the product carbon, the cyclones in Concepts 1–3 are assumed to have a carbon separation efficiency of 60%. However, the following filters are assumed to extract all the remaining carbon from the product gas. As a whole, it is assumed that all the product carbon is collected and can be further utilized. The product gas temperature after cooling is assumed to be 250 °C, which is a typical temperature that conventional fabric filters can handle.

The cooling of the product carbon is assumed to have TTD of 5 °C compared to cooling water (CW), which means that the temperature of the product carbon is 30 °C when it leaves the system. The closed cooling water system in each concept is dimensioned based on the following initial values: inlet temperature, mass flow, pressure drop, and pump efficiency for cooling water.

Nickel is a widely studied and generally found as suitable catalyst for methane decomposition [6,8,9]. Therefore, a nickel based mixture (80% Ni with a support material based on aluminum), was chosen as a catalyst material in Concept 3. The required catalyst charge of 0.1 $kg_{cat}/(nm^3_{CH_4}\ h)$ was chosen based on study [39], and the lifetime of 50 h for a Ni-based catalyst based on the study in [9]. The minimum fluidization velocity was one parameter determining the reactor dimensions. The bed sand was heated by oxy-combustion in the regeneration chamber to a temperature of 1200 °C to maintain the reaction temperature of 900 °C in the reactor. Also the auxiliary electricity consumption of the ASU was taken into account with the best practice value for cryogenic air separation process (160 kWh/t_{oxygen}) [40]. CO_2 was captured from the ASU and its compression to 110 bar was assumed to require a work amount of 0.4 GJ/t_{CO_2} [41].

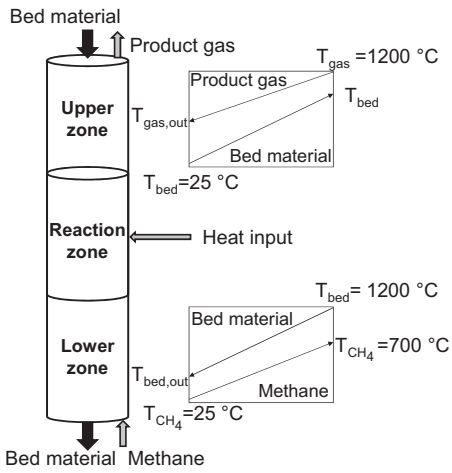

Fig. 6. Heat transfer in Concept 4. The numeric values in figure are based on expert opinions and are not experimentally verified.

In Concept 4, the bed material was assumed to have an input temperature of 25 °C and mass flow of 20 kg/s. The bed material was assumed to be steel and the material properties were chosen accordingly. The heat transfer in Concept 4 is presented in more detail in Fig. 6.

The amount of heat transferred from the bed material to methane in the lower zone and from product gas to bed material in the upper zone are assumed to be equal, as is presented in the following equation:

$$Q_{preheat} = \dot{m}_{CH_4} c_{p,CH_4} \Delta T_{CH_4,lower\ zone} = \dot{m}_{bed} c_{p,bed} \Delta T_{bed,lower\ zone} = \dot{m}_{bed} c_{p,bed} \Delta T_{bed,upper\ zone} = \dot{m}_{gas} c_{p,gas} \Delta T_{gas,upper\ zone} \quad (8)$$

Heat transfer in the reactor is based on expert opinions and is still to be experimentally verified.

3.3. Evaluation of investment costs

The investment costs for the process equipment were based on nominal price approximations in existing similar devices found in the power industry, such as natural gas burners, thermal conversion reactors, CFB reactors, air-to-air heat exchangers, flue gas cleaning components, and flue gas ducts. For simplicity the cost of the preheaters is approximated according to the price data from non-pressurized air-to-air shell and tube heat exchangers. The price of the steel bed material in Concept 4 was assumed to be 600 €/t. The erosion rate of the bed material is assumed to be slow, and therefore the cost of the bed material is allocated to the investment costs.

Cost distribution for total capital expenditure (CAPEX) was assumed to be similar to a typical power plant EPC-delivery, which includes equipment costs, process costs, automation and electrification costs, civil costs, and project costs (e.g. project management, engineering, and start-up). Costs for the initial supply material loads (catalyst in Concept 3 and bed material in Concept 4) were included in the project costs. Contingency for the cost estimate was assumed to be 30% of the equipment costs.

3.4. Evaluation of operating costs

The operational expenditure (OPEX) consisted of operating and maintenance (O&M) costs (2% of CAPEX), fuel costs (45 €/MWh_e), and other input material costs. The other materials were nickel based catalyst (10 €/kg) and the sand of the fluidized bed (4 €/t) in Concept 3. The costs of supply materials were based on the price level of nickel, aluminum, and sand. The costs of CO_2 emissions were calculated based on the emissions in each concept with a moderate cost of emission allowances (20 €/t_{CO_2}). The product carbon was assumed to have a price of 500 €/t_{carbon}, which has been presented as a moderate value for low quality carbon black named as thermal black. Selling the product carbon was the only source of income in the concepts.

In this study CAPEX was evenly divided in the chosen investment period of 10 years. The annual cost of electricity production was calculated as follows:

$$\text{Annual cost of electricity production} = \text{OPEX}_{annual} + \text{CAPEX}_{annual} - \text{INCOME}_{annual} \quad (9)$$

The annual cost of electricity production was divided by the annual electricity production to find out the specific costs (€/MWh_e). With certain input parameters, the annual cost becomes negative, which indicates a positive income with the assumptions in question. The owner's costs (e.g. taxes, permits and insurances), site specific costs (e.g. land use), and costs related to the existing power plant (e.g. modifications in the power cycle) were not included in the analysis.

For simplicity, the interest rate and inflation were assumed to be zero. In all concepts, CAPEX is small in comparison with OPEX, and therefore the interest rate and inflation have a minor influence on the annual cost of electricity production. However, CAPEX and OPEX in each concept are detailed in Table 5, and thus the effect of the investment rate and inflation can be calculated afterwards.

4. Results and discussion

4.1. Mass and energy balance results

The mass and energy balance calculations were conducted with the aforementioned calculation assumptions. The system boundaries for the mass and energy balance calculations are shown in the process diagrams in Section 2.3. The results of the mass balance calculations are summarized in Table 2. All the concepts have a methane mass flow of 3 kg/s, which is equal to the fuel power input of 150 MW based on the lower heating value of methane. Concept 1 has also an additional incoming stream of air (8 kg/s), which considerably increases the total mass flow in this concept. The outcoming mass flows of product carbon correlate well with the degree of methane conversion in each concept. In Concept 3, 0.4 kg/s of the primarily produced carbon (0.9 kg/s) is combusted to provide the heat of conversion (see Table 2).

Results from the energy balance calculations (Table 3) show the division between chemical (fuel) energy and sensible heat in product streams. Around 11–20% of the outcoming energy is bound to the solid carbon. The rest can be accounted for the product gas as a chemical energy or sensible heat part of which is removed by cooling.

In Concept 3 a part of the carbon stream is combusted to provide the heat of conversion, and the energy content of the product carbon is thus smaller than in the other concepts. Applying the catalyst in Concept 3 decreases the temperature that is required to achieve the TDM reaction, and consequently the heat of conversion. The reaction enthalpy is 91 MJ/kmol in Concept 3 compared to the 93 MJ/kmol required in Concepts 1 and 2 where the temperature is 1350 °C. However, the differences in the sensible enthalpy

Table 2
Results from the mass balance calculations.

	Concept 1 (kg/s)	Concept 2 (kg/s)	Concept 3 (kg/s)	Concept 4 (kg/s)
Mass balance, input				
Methane	3.0	3.0	3.0	3.0
Air	8.1	0	5.0	0
	11.1	3.0	8.0	3.0
Mass balance, output				
Product gas	10.2	2.2	2.1	2.3
Product carbon	0.9	0.8	0.5	0.7
CO_2 (regeneration)	0	0	1.6	0
N_2 (ASU)	0	0	3.8	0
Reaction products	11.1	3.0	8.0	3.0

Table 3
Results from the energy balance calculations.

	Concept 1 (MW)	Concept 2 (MW)	Concept 3 (MW)	Concept 4 (MW)
Energy balance, input				
Methane, fuel energy	126	150	150	150
Methane, combustion	23.6	0	0	0
Electricity	0	16.3	1.3	16.0
Total	150	166	151	166
Energy balance, output				
Carbon, fuel energy	29.5	25.8	16.3	22.1
Carbon, sensible heat	0	0	0	0
Cooling	9.5	6.0	2.6	7.3
N_2, sensible heat	0	0	0	0
CO_2, sensible heat	0	0	2.4	0
Product gas, sensible heat	4.4	2.1	2.5	2.5
Product gas, fuel energy	107	132	127	134
Total	150	166	151	166

of methane has a greater impact. The sensible enthalpy of methane is 89.2 MJ/kmol at 1350 °C, but only 51.4 MJ/kmol at 900 °C [32]. Consequently, due to the implementation of the catalyst, the heat of conversion in Concept 3 is 22% less than that in Concept 1 and 2.

The resulting product gas molar compositions and lower heating values (LHV) after carbon extraction are shown in Table 4. According to the results, the volumetric hydrogen content in the product gas was in the range of 24–57%. The highest content of hydrogen occurred in Concept 3 and the lowest in Concept 1, which is due to the presence of combustion products in Concept 1. Partial combustion in Concept 1 resulted also in lower hydrogen and methane fractions due to the presence of the combustion products in the product gas. Consequently, the calculated LHV was also lower in Concept 1.

4.2. Investment and operational costs

The annual cash flow estimate for each concept including CAPEX, OPEX, and operational incomes are shown in Table 5. The net electricity production in each concept was calculated by subtracting the internal electricity consumption of the process from the total electricity production. The specific cost of net electricity production is calculated by dividing the annual cost of electricity production by the annual net electricity production.

Fuel is the most significant cost in all the concepts. CAPEX is a minor cost compared to OPEX in all concepts except Concept 3. Concept 3 is the most expensive both in terms of CAPEX and OPEX, which correlates well with the complexity of this process. However, due to the low internal electricity consumption of the process, the net electricity production in Concept 3 is relatively high, resulting in moderate cost of electricity production. In Concept 1 the low internal electricity consumption and high amount of product carbon results in the lowest cost of electricity production among all the concepts. The cost of electricity production in the reference case is 163 €/MWh_e which includes both the fuel cost and the cost of CO_2 emission allowances. Thus, with the current assumptions, the cost of electricity production is 12–58% higher in the concepts than in the reference case. The effect of the product carbon price to the feasibility of the concepts is further analyzed in Section 4.4.

Table 4
Product gas molar composition and LHV in each concept after extraction of solid carbon.

Molar composition	Concept 1 (%)	Concept 2 (%)	Concept 3 (%)	Concept 4 (%)
H_2 (g)	28.0	51.9	57.1	46.2
CH_4 (g)	15.2	48.1	42.9	53.8
H_2O (g)	10.8	0	0	0
CO_2 (g)	5.4	0	0	0
N_2 (g)	41.1	0	0	0
LHV (MJ/kg)	10.4	59.8	60.6	57.7

4.3. CO_2 emissions

The CO_2 emissions of the concepts originate from the combustion of the product gas and in Concept 3 additionally from the regeneration reactor. In the reference case, which is the direct combustion of methane, the CO_2 emissions originate from the methane combustion. The CO_2 emissions from the concepts were compared with those from the reference case, as summarized in Table 6. The reduction of the CO_2 emissions in the concepts is

Table 5
Annual cash flow analysis for each concept. The arrows next to the values in the bottom row indicate whether the cost of electricity production is slightly higher (an upward pointing arrow) or notably higher (two arrows pointing upward) compared to the reference.

	Concept 1 (k€)	Concept 2 (k€)	Concept 3 (k€)	Concept 4 (k€)
CAPEX				
Equipment and project costs	11 110	7 226	24 916	9 029
Contingency (30%)	1 536	999	3 438	1 110
Total	12 646	8 225	28 354	10 139
OPEX				
Fuel costs	30 375	30 375	30 375	30 375
CO_2 emission costs	1 601	1 734	1 601	1 868
Other supply material costs	0	0	4 341	0
O&M costs (2%)	253	165	567	203
Total	32 229	32 274	36 884	32 445
Annual income				
Product carbon sales	7 282	6 371	4 036	5 461
Annual cost of electricity production (k€)	26 211	26 726	35 683	27 998
Cost of net electricity production (€/MWh_e)	↑183	↑↑255	↑216	↑↑257

Table 6
Net efficiency of electricity production and absolute and specific CO_2 emissions from the concepts. The arrows next to the values in the bottom row indicate whether the concept produce less (a downward pointing arrow) or more (an upward pointing arrow) CO_2 emissions per produced electricity compared to the reference case.

		Ref. case	Concept 1	Concept 2	Concept 3	Concept 4
Fuel input	MW	150	150	150	150	150
Operational hours	h	4500	4500	4500	4500	4500
Annual net electricity production	GWh	203	144	105	165	109
Electricity production net efficiency	%	30.0	21.4	15.5	24.5	16.1
CO_2 stored as carbon	kt_{CO_2}/a		54	47	30	40
CO_2 capture in gaseous form	kt_{CO_2}/a		0	0	24	0
CO_2 stored, total	kt_{CO_2}/a		54	47	54	40
CO_2 emissions	kt_{CO_2}/a	134	80	87	80	93
Specific CO_2emissions	t_{CO_2}/MWh_e	0.66	↓0.55	↑0.83	↓0.48	↑0.85

mainly due to the production of solid carbon. Thus, in Table 6 the product carbon is presented as 'CO_2 stored as carbon' which represents the amount of CO_2 emissions avoided when the product carbon is not combusted. As the fuel input was fixed in all concepts, the absolute amount of CO_2 emissions in the reference case represents the total annual amount of CO_2 from the concepts, which is either stored or released to the atmosphere. Hence, the CO_2 emissions from each concept are the total amount of stored CO_2 subtracted from the CO_2 emissions in the reference case. The absolute CO_2 emissions in each case are divided by the corresponding electricity production to achieve the specific CO_2 emissions (t_{CO_2}/MWh_e).

As the annual net electricity production in the concepts is less than in the reference case, the concepts actually produce more CO_2 per MWh than the reference case, but part of the emissions are captured. Therefore, the amount of captured CO_2 is more than is actually avoided by applying the concepts, as has been presented in [17]. The actually avoided CO_2 emissions are the difference between the quantity of CO_2 emissions from the reference case and the quantity of CO_2 emitted by a concept. This is the difference between the specific CO_2 emissions in the reference case and in a concept in Table 6.

The amount of electricity produced in the concepts is less than in the reference case. If the electricity production is wanted to remain as a constant, the fuel consumption has to increase. This may lead to the increase of the CO_2 emissions in the fuel transporting. However, this has not been considered in this study. Furthermore, utilizing the product carbon may cause additional CO_2 emissions, but those have been left out from this study.

It is shown in Table 6 that the specific CO_2 emissions of only Concepts 1 and 3 are lower than in the reference case. Therefore, with the assumptions in question only Concepts 1 and 3 provide an actual CO_2 reduction compared to the reference case. When Concepts 1 and 3 are applied, the avoided CO_2 emissions are respectively 0.11 t_{CO_2}/MWh_e and 0.18 t_{CO_2}/MWh_e compared to the reference case.

For Concepts 1 and 3 it is possible to calculate the cost of avoided CO_2 by dividing the difference between the electricity production costs in a concept and in the reference case by the amount of avoided CO_2 in a concept. With the current assumptions, the cost of avoided CO_2 emissions was 182 $€/t_{CO_2}$ in Concept 1 and 294 $€/t_{CO_2}$ in Concept 3. The effect of product carbon price on the cost of avoided CO_2 emissions is further analyzed in Section 4.5.

In all the concepts, the efficiency of net electricity production is lower compared to the reference case due to the reduced electricity production in the concepts. The relatively high initial electricity consumption in Concepts 2 and 4 further decreases the efficiency of electricity production. Due to both the high net efficiency of electricity production among the concepts and low specific CO_2 emissions in Concepts 1 and 3, these two concepts will be further evaluated.

4.4. Analysis of the cost of electricity production

The assumption that the internal electricity consumption of the concepts is covered by the electricity production in concepts is unfavorable, as the cost of electricity production in the concepts is significantly higher than the average market price of electricity. By contrast, an assumption that the electricity consumed in the concepts would be bought from the market at the market price would increase the net electricity production and decrease the cost of electricity production ($€/MWh_e$) in Concepts 2–4. The decrease in the cost of electricity production would be most significant in Concepts 2 and 4 which have the highest internal electricity consumption among the concepts.

Fig. 7 summarizes the costs of electricity production in each concept when the price of product carbon was varied. According to the results, in Concept 1 the cost of electricity production was the lowest among the concepts. With the aforementioned assumptions related to the operational parameters, the price of product carbon should be at least 700 $€/t_{carbon}$ so that the cost of electricity production in Concept 1 would be equal or less than in the reference case. The price of thermal black can be up to 1400 $€/t_{carbon}$, as stated in Section 2.1. Assuming the price of product carbon of

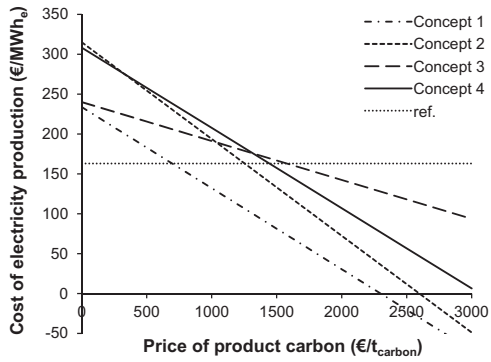

Fig. 7. Cost of electricity production in concepts with the variable prices of product carbon.

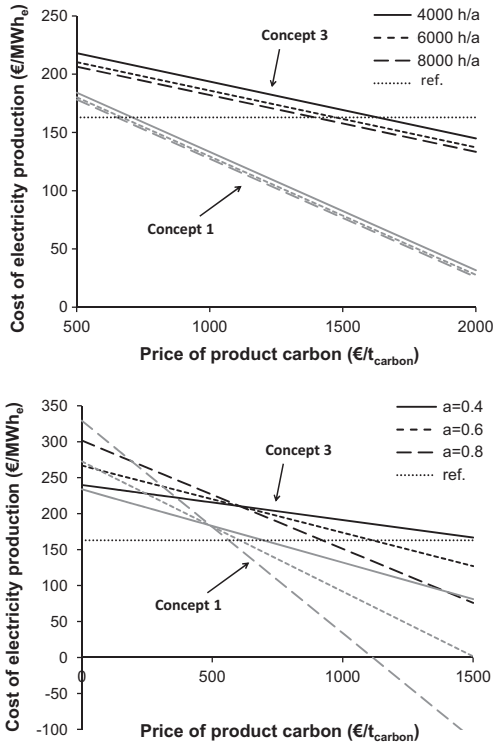

Fig. 8. Electricity production costs in Concept 1 (gray) and Concept 3 (black) as a function of product carbon price when the operation time (upper chart) and the degree of methane conversion (lower chart) are varied.

1400 €/t_{carbon}, applying Concepts 2–4 results in cost of electricity production that is almost equal with the reference case. Therefore, all the concepts could provide a feasible option to reduce CO_2 emissions in natural gas combustion.

Sensitivity analysis was conducted to find out the effect of several parameters (the product carbon price, annual operational time, and degree of methane conversion) on the feasibility of the concepts. Concepts 1 and 3 have shown the best performance among all the concepts, and therefore those were chosen for the sensibility analysis. Fig. 8 shows the effect of the annual operation time and the degree of methane conversion on the cost of electricity production in Concept 1 and 3. When the degree of methane conversion is varied, it is assumed that CAPEX remains the same, meaning that the reactor or auxiliary components do not require any modifications.

According to the analysis, in both concepts increasing the operational time from 4000 h/a to 8000 h/a decreased the cost of electricity production by 6—12 €/MWh_e when the investment period is 10 years. Hence, the effect of the annual operation time on feasibility is almost insignificant. By contrast, the influence of the degree of methane conversion on the cost of electricity production is much more significant. Increasing the conversion degree increases the income from the product carbon and results in decreased annual cost of electricity production according to Eq. (9). The product carbon prices 500 and 600 €/t_{carbon} are found as limiting values in Concepts 1 and 3, respectively, above which it is economically more feasible to produce more carbon and less electricity. By contrast, below these limiting values it is economically more feasible to produce less carbon and more electricity. However, the price of the product carbon has to be at least 600 €/t_{carbon} so that the cost of electricity production would be less than in the reference case.

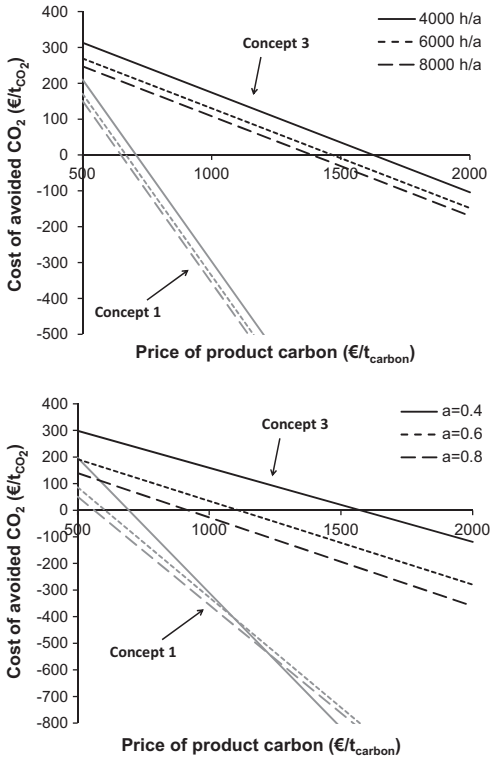

Fig. 9. Cost of avoided CO_2 emissions in Concept 1 (gray) and Concept 3 (black) as a function of product carbon price when the operation time (upper chart) and the degree of methane conversion (lower chart) are varied.

4.5. Analysis of the cost of avoided CO_2

The effect of the product carbon price, annual operational time, and degree of methane conversion on the cost of avoided CO_2 emissions in Concepts 1 and 3 was analyzed and the results are shown in Fig. 9. Increasing the annual operation time from 4000 h/a to 8000 h/a decreased the cost of avoided CO_2 emissions by 59—66 €/t_{CO_2}. Thus, the annual operation time has a remarkable effect on the cost of avoided CO_2 emissions in the concepts.

In Concept 3, the effect of conversion degree on the cost of avoided CO_2 was remarkable. Increasing the degree of methane conversion from 0.4 to 0.8 decreased the cost of avoided CO_2 in Concept 3 by 159—242 €/t_{CO_2} with product carbon prices of 500—2000 €/t_{carbon}, respectively. In Concept 1, a moderate price of product carbon (500 €/t_{carbon}) and high conversion degree (0.8) resulted in a moderate cost of avoided CO_2, 51 €/t_{CO_2}.

Especially in Concept 1, increasing the product carbon price rapidly decreases the cost of avoided CO_2. At product carbon prices of 650—700 €/t_{carbon} the cost of avoided CO_2 emissions becomes negative, indicating that the costs were smaller than in the reference case. Typically, the cost of CCS (including the capture, transport, and geological storage of CO_2) in current technology for a new natural gas combined cycle power plant is in the range of 40—90 $/$t_{CO_2}$ avoided. [42] This cost level was achieved with product carbon price of 500 €/t_{carbon} in Concept 1 and 800 €/t_{carbon} in Concept 3 when the degree of methane conversion was in both cases above 0.6.

Increasing the price of CO_2 emission allowances does not directly improve the feasibility of the concepts due to the produced CO_2 in the concepts. If a complete conversion were achieved, that is the degree of methane conversion of 1, Concepts 2 and 4 would not emit any CO_2. In Concept 3, there would be CO_2 emissions also with complete conversion, but they would be fully captured as gaseous CO_2 and stored.

5. Conclusion

This study presents and analyses four concepts that utilize thermal decomposition of methane to reduce CO_2 emissions in natural gas combustion. Based on the results of the techno-economic analysis with the current assumptions, applying TDM reduces the CO_2 emissions in electricity production (t_{CO_2}/MWh_e) in two concepts. The CO_2 emissions decrease when a part of the carbon is taken out from the feedstock in a solid form. Furthermore, the cost of avoided CO_2 decreases rapidly when more solid carbon is taken out from the feedstock.

Concept 1, a methane burner, had a high performance in terms of the cost of net electricity production and the CO_2 emissions per MWh of produced electricity. With the price of product carbon of 600—700 €/t_{carbon} the price of electricity production in Concept 1 was lower than in the reference case. With the assumptions in question, applying Concept 1 decreased the specific CO_2 emissions (t_{CO_2}/MWh_e) compared to the reference. At the same time, the cost of avoided CO_2 emissions became negative indicating smaller costs in Concept 1 compared to the reference. The high internal electricity consumption is the main drawback in Concept 2. Replacing electricity with plasma in Concept 2 could improve the quality of product carbon, and thus result in better feasibility. In Concept 3, the complexity of the process results in high CAPEX. However, the annual net electricity production is high, which results in low

CO_2 emissions per MWh of produced electricity. The cost of CO_2 capture and compression are taken into account, but the transportation and storage of CO_2 will cause additional costs. In Concept 4, the low degree of methane conversion and high internal electricity consumption results in the highest cost of net electricity production and CO_2 emissions per MWh of produced electricity among all the concepts. The technical solution to remove product carbon from the reactor is an advantage in Concept 4. One potential option to improve the feasibility of Concept 4 could be an autothermal heat production.

The price of product carbon was found to have a highly significant effect on the economy of the concepts. With the current assumptions, at the lowest a carbon price of 600—700 €/t_{carbon} was required to obtain an equal cost of electricity production with the reference case. In contrast to conventional CO_2 capture technologies, in which unwanted CO_2 is the end product, the value of the product carbon from TDM could make the process profitable. Increasing the price of product carbon to the level of 700—1500 €/t_{carbon} rapidly decreased both the cost of electricity production and the cost of avoided CO_2 emissions. TDM could be an especially suitable technology for peak load power plants. In these plants, it is not cost-efficient to apply conventional CCS technologies that require large investments in the infrastructure. More research and optimization is required in order to achieve high conversion rates and product carbon with suitable quality in TDM process. The price of the product carbon has a crucial effect on the feasibility, and therefore more research on the utilization of thermal black is required.

Acknowledgments

This work was carried out in the Carbon Capture and Storage Program (CCSP) research program coordinated by CLIC Innovation Ltd. with funding from the Finnish Funding Agency for Technology and Innovation, Tekes. Furthermore, the financial support received from ÅF-Consult Ltd., Fortum Plc, Gasum Ltd., Helen Ltd., Neste Plc, and Gasum Gas Fund is gratefully acknowledged. John Shepherd is acknowledged for proof reading this article.

References

[1] International Energy Agency (IEA). World Energy Outlook 2014, 2014. <http://www.worldenergyoutlook.org/publications/weo-2014/>.
[2] European Commission. 2030 Energy strategy. <http://ec.europa.eu/energy/en/topics/energy-strategy/2030-energy-strategy>; 2015 [accessed 11.05.15].
[3] International Energy Agency (IEA). Technology Roadmap – Carbon Capture and Storage, 2013. <http://www.iea.org/publications/free-publications/publication/technology-roadmap-carbon-capture-and-storage-2013.html>.
[4] Rokach J. Should we pursue carbon capture for natural gas? Electr J 2012;25:64–7. http://dx.doi.org/10.1016/j.tej.2012.06.001.
[5] Muradov N. CO_2-free production of hydrogen by catalytic pyrolysis of hydrocarbon fuel. Energy Fuels 1998;12:41–8. http://dx.doi.org/10.1021/ef9701145.
[6] Amin A, Croiset E, Epling W. Review of methane catalytic cracking for hydrogen production. Int J Hydrogen Energy 2011;36:2904–35. http://dx.doi.org/10.1016/j.ijhydene.2010.11.035.
[7] Li Y, Li D, Wang G. Methane decomposition to COx-free hydrogen and nano-carbon material on group 8–10 base metal catalysts: a review. Catal Today 2011;162:1–48. http://dx.doi.org/10.1016/j.cattod.2010.12.042.
[8] Abbas H, Wan Daud W. Hydrogen production by methane decomposition: a review. Int J Hydrogen Energy 2010;35:1160–90. http://dx.doi.org/10.1016/j.ijhydene.2009.11.036.
[9] Ashik U, Wan Daud W, Abbas H. Production of greenhouse gas free hydrogen by thermocatalytic decomposition of methane – a review. Renew Sustain Energy Rev 2015;44:221–56. http://dx.doi.org/10.1016/j.rser.2014.12.025.
[10] Muradov N, Veziroğlu T. From hydrocarbon to hydrogen–carbon to hydrogen economy. Int J Hydrogen Energy 2005;30:225–37. http://dx.doi.org/10.1016/j.ijhydene.2004.03.033.
[11] Rackley S. Carbon capture and storage. USA: Elsevier; 2010.
[12] Herzog H, Smekens K. IPCC special report on carbon dioxide capture and storage. Cambridge University Press; 2005. p. 105–78. [chapter Capture of CO_2].
[13] Blackford J, Hattam C, Widdicombe S. CO_2 leakage from geological storage facilities: environmental, societal, and economic impacts, monitoring and research strategies. UK: Woodhead Publishing; 2013. p. 149–78. [chapter Geological storage of carbon dioxide (CO_2) – Geoscience, technologies, environmental aspects and legal frameworks].
[14] Blackford J, Widdicombe S, Lowe D. Environmental risks and performance assessment of carbon dioxide (CO_2) leakage in marine ecosystems. UK: Woodhead Publishing; 2010. p. 344–73 [chapter Developments and innovation in carbon dioxide (CO_2) capture and storage technology, Volume 2: Carbon dioxide (CO_2) storage and utilization].
[15] Ardelan M, Steinnes E, Lierhagen S, Linde S. Effects of experimental CO_2 leakage on solubility and transport of seven trace metals in seawater and sediment. Sci Total Environ 2009;407:6255–66. http://dx.doi.org/10.1016/j.scitotenv.2009.09.004.
[16] Lewicki J, Birkholzer J, Tsang C-F. Natural and industrial analogues for leakage of CO_2 from storage reservoirs: identification of features, events, and processes and lessons learned. Environ Geol 2007;52:457–67. http://dx.doi.org/10.1007/s00254-006-0479-7.
[17] Kanniche M, Gros-Bonnivard R, Jaud P, Valle-Marcos J, Amann J-M, Bouallou C. Pre-combustion, post-combustion and oxy-combustion in thermal power plant for CO_2 capture. Appl Therm Eng 2010;30:53–62. http://dx.doi.org/10.1016/j.applthermaleng.2009.05.005 [Selected Papers from the 11th Conference on Process Integration, Modelling and Optimisation for Energy Saving and Pollution Reduction].
[18] Petrakopoulou F, Tsatsaronis G. Production of hydrogen-rich fuels for pre-combustion carbon capture in power plants: a thermodynamic assessment. Int J Hydrogen Energy 2012;37:7554–64. http://dx.doi.org/10.1016/j.ijhydene.2012.01.147 [7th Petite Workshop on the Defect Chemical Nature of Energy Materials, 14–17 March 2011, Storaas, Kongsberg, Norway].
[19] Ertesvåg I, Kvamsdal H, Bolland O. Exergy analysis of a gas–turbine combined-cycle power plant with precombustion CO_2 capture. Energy 2005;30:5–39. http://dx.doi.org/10.1016/j.energy.2004.05.029.
[20] Corradetti A, Desideri U. Analysis of gas–steam combined cycles with natural gas reforming and CO_2 capture. J Eng Gas Turb Power 2005;127:545–52. http://dx.doi.org/10.1115/1.1850941.
[21] Bolland O, Undrum H. A novel methodology for comparing CO_2 capture options for natural gas–fired combined cycle plants. Adv Environ Res 2003;7:901–11. http://dx.doi.org/10.1016/S1093-0191(02)00085-0.
[22] Lozza G, Chiesa P. Natural gas decarbonization to reduce CO_2 emissions from combined cycles – Part I: Partial oxidation. J Eng Gas Turb Power 2000;124:82–8. http://dx.doi.org/10.1115/1.1395581.
[23] Lozza G, Chiesa P. Natural gas decarbonization to reduce CO_2 emissions from combined cycles – Part II: Steam–methane reforming. J Eng Gas Turb Power 2000;124:89–95. http://dx.doi.org/10.1115/1.1395582.
[24] Manzolini G, Macchi E, Gazzani M. CO_2 capture in natural gas combined cycle with SEWGS. Part B: Economic assessment. Int J Greenhouse Gas Control 2013;12:502–9. http://dx.doi.org/10.1016/j.ijggc.2012.06.021.
[25] Triphob N, Wongsakulphasatch S, Kiatkittipong W, Charinpanitkul T, Praserthdam P, Assabumrungrat S. Integrated methane decomposition and solid oxide fuel cell for efficient electrical power generation and carbon capture. Chem Eng Res Des 2012;90:2223–34. http://dx.doi.org/10.1016/j.cherd.2012.05.014.
[26] Kirk-Othmer, editor. Encyclopedia of Chemical Technology. New Jersey, USA: John Wiley & Sons Inc; 2007 [chapter Carbon Black].
[27] Sid Richardson Carbon and Energy Co. Carbon black pricing. <http://www.sidrich.com/products-and-pricing/pricing/carbon-black-pricing/>; 2014 [accessed 03-07-15].
[28] Hosokawa M, Nogi K, Naito M, Yokoyama T, editors. Nanoparticle technology handbook. Elsevier; 2008.
[29] International Agency for Research on Cancer. IARC monographs on the evaluation of carcinogenic risks to humans, Volume 93: carbon black, titanium dioxide, and talc. Tech. rep., International Agency for Research on Cancer; 2010.
[30] International Carbon Black Association. Carbon black user's guide: safety, health, & environmental information. 2004.
[31] Environment Canada. Screening assessment for the challenge: carbon black; 2013. <https://www.ec.gc.ca/ese-ees/default.asp?lang=En&n=2CF>.
[32] National Institute of Standards and Technology. NIST-JANAF, Thermochemical tables. <http://kinetics.nist.gov/janaf/> [accessed 19-12-14].
[33] Kim K, Hong S, Lee S, Ju W. Continuous synthesis of nanostructured sheetlike carbons by thermal plasma decomposition of methane. IEEE Trans Plasma Sci 2007;35:434–43. http://dx.doi.org/10.1109/TPS.2007.892556.
[34] Winter F, Schratzer B. Applications of fluidized bed technology in processes other than combustion and gasification. UK: Woodhead Publishing; 2013. http://dx.doi.org/10.1533/9780857098801.5.1005. p. 1005–33. [chapter: Fluidized bed technologies for near-zero emission combustion and gasification].
[35] International Energy Agency (IEA). Improvement in power generation with post combustion capture of CO_2. Tech. rep., Report PH4/33, International Energy Agency; 2004.
[36] Stavseth E. The Nordic/Baltic power market. <http://www.nasdaqomx.com/digitalAssets/86/86050_npspotjune112013.pdf>; June 11th 2013 [accessed 31-08-15].
[37] International Energy Agency (IEA), Natural gas. <http://www.iea.org/aboutus/faqs/gas/>; 2014 [accessed 29-12-14].
[38] Finnish Gas Association. Maakaasukäsikirja (Handbook of Natural Gas); 2014. [in Finnish].

[39] Pinilla J, Suelves I, Lázaro M, Moliner R, Palacios J. Parametric study of the decomposition of methane using a $NiCu/Al_2O_3$ catalyst in a fluidized bed reactor. Int J Hydrogen Energy 2010;35:9801–9. http://dx.doi.org/10.1016/j.ijhydene.2009.10.008.

[40] Tranier J-P, Dubettier R, Perrin N. Air separation unit for oxy-coal combustion systems. In: IEAGHG 1st international oxyfuel combustion conference, Cottbus; 2009.

[41] International Energy Agency (IEA). IEA Greenhouse gas R&D programme, improvement in power generation with post-combustion capture of CO_2. Tech. rep., Report PH4/33, International Energy Agency; 2004.

[42] Herzog H, Smekens K. IPCC special report on carbon dioxide capture and storage. Cambridge University Press; 2005. p. 339–62. [chapter: Cost and economic potential].

Publication II

Tiina Keipi, Katariina E. S. Tolvanen, Henrik Tolvanen, Jukka Konttinen

Thermo-catalytic decomposition of methane: The effect of reaction parameters on process design and the utilization possibilities of the produced carbon

Energy Conversion and Management, 126 (2016) 923–934.

Energy Conversion and Management 126 (2016) 923–934

Contents lists available at ScienceDirect

Energy Conversion and Management

journal homepage: www.elsevier.com/locate/enconman

Thermo-catalytic decomposition of methane: The effect of reaction parameters on process design and the utilization possibilities of the produced carbon

Tiina Keipi *, Katariina E.S. Tolvanen, Henrik Tolvanen, Jukka Konttinen

Department of Chemistry and Bioengineering, Tampere University of Technology, P.O. Box 541, 33101 Tampere, Finland

ARTICLE INFO

Article history:
Received 6 July 2016
Received in revised form 19 August 2016
Accepted 20 August 2016
Available online 31 August 2016

Keywords:
Carbon capture
Hydrogen production
Methane decomposition
Natural gas
Process design

ABSTRACT

The study presents a path for selecting the reaction and reactor parameters of a process applying thermo-catalytic decomposition of methane (TDM). Temperature and catalyst are the main reaction parameters affecting the type of TDM carbon and defining the reaction's theoretical heat requirement. Secondly, the reaction parameters affect the reactor design including the selection of reactor type and heating source as well as the reactor dimensioning. The reactor dimensioning is discussed by highlighting the methane residence time requirement at different reaction conditions. Finally, the economic value of the TDM products is analyzed. According to the analyses, the reaction temperature and catalyst have a significant effect on reactor design and on the value and utilization possibilities of the TDM carbon. The prices of carbon products vary greatly as does the global demand of those. The utilization possibilities of carbon highly affect the overall viability of the TDM process and therefore should be carefully considered during process design.

1. Introduction

Tackling the global climate change requires the reduction of CO_2 emissions into the atmosphere. The International Energy Agency (IEA) has created several climate scenarios and analyzed which technologies could be utilized to achieve the CO_2 emission reductions required in each scenario. In the most ambitious scenario of IEA, the 2 °C scenario, the increase in the average global temperature will be limited to 2 °C [1]. The most recent target is to limit the increase in the average global temperature to 1.5 °C, which was the outcome of the Paris Climate Change Conference in 2015 [2]. The means to reduce CO_2 emissions include switching fossil fuels to carbon neutral fuels and energy efficiency improvements. Besides those, IEA has stated that carbon capture and storage (CCS) has a critical role in the reduction of CO_2 emissions [3]. IEA presumes in the 2 °C scenario that CCS technologies will to be implemented gradually from 2020 onward. The CCS technologies are based on the capture of CO_2 in a gaseous form and transportation to a storage site. However, the capture, transportation and storage of CO_2 requires considerable investments on infrastructure, and therefore the implementation of this technology is a time-consuming process. Thus, new solutions for the near-future CO_2 emission mitigation are urgently needed.

Thermo-catalytic decomposition of methane (TDM) could be applied to natural gas utilization with a benefit that it produces less CO_2 emissions than the conventional technologies. TDM is an endothermic reaction in which methane, which is the main component of natural gas, is thermally converted to solid carbon, gaseous hydrogen, and traces of higher hydrocarbons. Thus, instead of capturing gaseous CO_2, the carbon could be captured in a solid form. Dufour et al. have conducted several life cycle analyses [4–6] for processes where TDM has been applied to hydrogen production. They have compared the TDM process with the currently most common technology for hydrogen production, steam methane reforming (SMR), both with and without coupling CCS to the SMR process. The result of their analyses was that TDM was more environmentally-friendly process than SMR even when the SMR process was coupled to CO_2 capture and storage. Dufour et al. have also analyzed a theoretical case of autocatalytic TDM process where the product carbon would catalyze the TDM reaction and consequently the reaction temperature would be lower than in the non-catalytic thermal process. Consequently, this would result in a further reduction in environmental impact. However, so far the experimental observations of autocatalysis are limited to short periods at the beginning of the reaction [7].

* Corresponding author.
E-mail address: tiina.keipi@tut.fi (T. Keipi).

http://dx.doi.org/10.1016/j.enconman.2016.08.060
0196-8904/

Currently, natural gas is considered the cleanest fuel among the fossil fuels, but if the limits on CO_2 emissions become tighter, emission reductions are needed also in the utilization of natural gas [8]. The current global hydrogen production is approximately 7.2 EJ and nearly half of that is produced from natural gas with SMR, as stated by IEA [9]. Moreover, IEA has stated in the same report that hydrogen, when produced with low CO_2 emissions, could significantly contribute to the CO_2 emission reduction targets in the energy sector. IEA also estimates an increase in natural gas demand from the current 3.4 trillion m^3 to 5.4 trillion m^3 until 2040 [10].

TDM has been proposed to be applied to hydrogen production (potentially without CO_2 emissions) [11] to fulfill the demand of chemical industry or to be further utilized to produce electricity either by a steam-power cycle [12] or fuel cells [13]. Muradov [14] has analyzed the potential of TDM in hydrogen production and presented the benefits of TDM over SMR. Muradov and Veziroğlu [15] have conducted an economic analysis for TDM by studying the effect of the product carbon price on the hydrogen production cost. They have also presented typical prices of different carbon products, and number of these carbon products are valuable enough to make the TDM process economically more feasible than SMR. Keipi et al. [12] have previously published a techno-economic analysis of a commercial-scale TDM application. In that study, the conclusion was that the market value of the product carbon, which depends on its quality, is the main factor affecting the economic feasibility of the TDM processes when assuming a moderate cost of CO_2 emission allowances.

Different TDM reactor concepts have been investigated and presented in the literature, such as plasma-assisted TDM process [16,17], implementing TDM in a molten metal reactor [18–24] and a cyclic reactor that consists of separate heating and decomposition units which is known as the thermal black process introduced already at the 1920s [25]. Furthermore, various heating sources have been proposed to conduct the TDM reaction: an electric arc, partial combustion of feedstock methane, regenerative heat supply with cyclic heating and decomposition steps, and heat supply with heating elements outside the reactor [12,26]. Despite the numerous technical alternatives presented in the literature to conduct the TDM reaction, there is a lack of comprehensive analysis on the selection of TDM reaction and reactor parameters. The focus in this article is to highlight the different aspects that need to be taken into account when designing a TDM reactor. The selection of the TDM reaction and reactor parameters and the effect of those to the overall process design are analyzed. Altogether, this article presents a path illustrated in Fig. 1 along which the TDM reactor design can be conducted as a part of the overall process design.

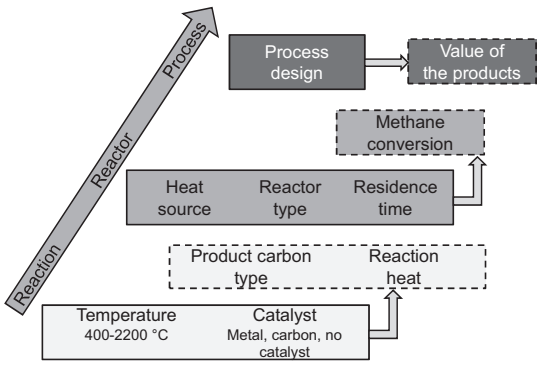

Fig. 1. The path for selecting the reaction, reactor and process parameters when applying TDM. The parameters that can be selected are inside the solid lines and inside the dashed lines are the consequent parameters.

2. Reaction parameters

The primary parameters in the TDM reaction are the reaction temperature and the catalyst. The selection of a catalyst and temperature are linked together and the mutual dependence of these two parameters is illustrated here by reviewing the experimental studies of TDM presented in the literature. Furthermore, these experimental studies can be applied to predict the type of product carbon even in a full-scale process.

2.1. Reaction equilibrium

In methane decomposition reaction, also known as methane decarburation, (direct) methane cracking or methane pyrolysis, methane is thermally decomposed to solid carbon, gaseous hydrogen, and traces of higher hydrocarbons. Eq. (1) presents the simplified reaction equation, that takes into account only the main products, carbon and hydrogen [11].

$$CH_4 \rightarrow C(s) + 2H_2 \quad \Delta H_r^0 = +74.9\ \text{kJ mol}^{-1} \tag{1}$$

The reaction enthalpy ΔH_r^0 is defined at a reference temperature of 298.15 K [27]. The maximum methane conversion in a certain temperature can be calculated by considering the equilibrium composition of the gas mixture containing methane and hydrogen in that temperature. Villacampa et al. [28] have presented the following equation for the Gibbs energy of TDM reaction as a function of temperature:

$$\Delta G^0(T) = 89658.88 - 102.27T - 0.00428T^2 - 2499358.99T^{-1} \tag{2}$$

Eq. (2) is calculated by assuming the formation of graphite in TDM, and therefore it is an approximation. Furthermore, the Gibbs energy can be expressed in the means of equilibrium constant K_p:

$$\Delta G_R(T) = \Delta G^0(T) + R_u T \cdot lnK_p \tag{3}$$

where R_u is the gas constant (8.314 J/mol K) and T is the reaction temperature (K). In the equilibrium state, the Gibbs energy is a minimum, i.e. $\Delta G_R(T)$ equals zero. For TDM reaction, the equilibrium constant depends on the partial pressures of methane ($P_{CH_4,eq.}$) and hydrogen ($P_{H_2,eq.}$) in the gas mixture as follows:

$$K_p(T) = \frac{(P_{H_2,eq.})^2}{P_{CH_4,eq.}} = \frac{(2 \cdot (P_{CH_4,0} - P_{CH_4,eq.}))^2}{P_{CH_4,eq.}} = \frac{4 \cdot P_{CH_4,0} \cdot a^2}{1 - a} \tag{4}$$

where $P_{CH_4,0}$ is the partial pressure of methane (atm) in the initial state and a is methane conversion (–). The methane conversion a is the proportion of the feedstock methane that dissociates according to Eq. (1) and its value varies from zero (no methane dissociation) to one (complete methane dissociation). Moreover, it is assumed in Eq. (4) that methane and hydrogen are the only gaseous components in the TDM reaction and the formed carbon is in its solid state. However, if desired, for example Snoeck et al. [29] have presented the thermodynamics of carbon filament formation in TDM more detailed.

Finally, Eqs. (2)–(4) were combined to present the methane conversion as a function of temperature in the equilibrium state. This is graphically presented later as a part of Section 3.2. In practice, this equilibrium curve states the maximum methane conversion that can be achieved at a certain temperature when the reaction time approaches infinity.

2.2. Product carbon type

The main products of TDM are gaseous hydrogen and solid carbon. The morphology of the product carbon depends heavily on the reaction conditions. The results of a literature survey focusing on the relation between carbon product properties, reaction temperature and catalyst are presented in Table 1 and Fig. 2.

Metal catalysts in TDM have a tendency to produce filamentous carbon products whereas the carbon catalyzed or thermal decomposition of methane produce mainly graphite-like carbon or carbon black. Compared to the graph presented by Muradov and Vesiroğlu [55] a decade ago, wider temperature ranges have been utilized in the experimental studies of TDM recently. Furthermore, the properties of carbon products (such as quality, purity and morphology) arising from TDM have been studied in more depth during recent years. Especially studies reporting nanotubes and their formation mechanisms have been presented more during the last ten years than before. Muradov and Vesiroğlu previously stated that at temperatures above 1200 °C the product is amorphous carbon, but later it has been defined more accurately as carbon black as shown in Fig. 2.

The temperature ranges suitable for non-catalytic, carbon catalyzed and metal catalyzed reactions are partially overlapping. However, the approximate temperature ranges suitable for each reaction type are as follows: below 800 °C metal catalyzed reaction, 800–1100 °C carbon catalyzed reaction and above 1100 °C non-catalytic TDM. The differences of carbon and metal catalysts in TDM are not limited to the different temperature ranges or different product carbons. The carbon catalysts have the following advantages over metal catalysts: lower cost, ability to tolerate harmful components and higher temperatures (which enables higher methane conversions to be achieved), and the possibly better marketability of the product carbon as the catalyst may not need to be separated from the product [55]. By contrast, the nanofibers and nanotubes that can be produced by metal catalysts have a higher value if the metal residues in the carbon product can be separated. These factors have to be taken into account when the TDM process is designed.

Although the main component in the catalyst (metal/carbon) defines the morphology of the product carbon, the other catalyst properties (such as the catalyst pretreatment, support material, particle size and phase of the catalyst) are also important. However, presenting the catalyst properties in detail is not the key focus in this article. More detailed information about the properties of catalysts employed in TDM can be found in the references of Tables 1 and 2 and for example in review articles [56,57].

2.3. Reaction heat demand

When the reaction temperature is selected, the amount of external heating needed in TDM can be determined. The external heat, denoted as reaction heat $Q_r(T_r, a)$ in this study, takes into account both the reaction enthalpy of TDM and the sensible enthalpy of the feedstock methane. The reaction heat depends on the reaction temperature and methane conversion as follows:

$$Q_r(T_r, a) = \Delta H_r(T_r) \cdot a + \Delta H_{s,feedstock}(T_r) \quad (5)$$

where $\Delta H_r(T_r)$ is the reaction enthalpy (kJ/mol) at the reaction temperature T_r, a is the methane conversion (–) and $\Delta H_{s,feedstock}(T_r)$ is the sensible enthalpy of feedstock methane (kJ/mol) at the reaction temperature. It is assumed that all the feedstock methane is heated to the reaction temperature, and therefore $\Delta H_{s,feedstock}(T_r)$ does not depend on the methane conversion. The reaction heat as a function of methane conversion at selected reaction temperatures is graphically presented in Fig. 3a. It shows that the required reaction heat increases with the reaction temperature and methane conversion. The reaction heat at 25 °C is the base line that illustrates the reaction enthalpy as a function of methane conversion, but the TDM reaction has not been observed at that low temperature.

An energy balance was created in order to investigate how the energy in the feedstock methane is bound to the TDM reaction products. The energy balance of TDM is:

$$LHV_{CH_4} + Q_r(T_r, a) = 2a \cdot LHV_{H_2} + a \cdot LHV_C(1-a) \cdot LHV_{CH_4} + \Delta H_{s,products}(T_r) \quad (6)$$

where LHV_{CH_4}, LHV_{H_2} and LHV_C are the lower heating values (LHV) of methane, hydrogen and carbon (kJ/mol); and $\Delta H_{s,products}(T_r)$ is the sensible enthalpy of the reaction products (kJ/mol). The lower heating value equals the reaction enthalpy of stoichiometric combustion which in practice means that the LHV represents the energy that can be released by combustion. In contrast, the sensible enthalpy represents the energy that can be utilized by applying heat exchangers. Here, both values presented are theoretical values, which do not take into account the heat losses in a real process. The energy balance of TDM for one mole of methane based on Eq. (6) is shown in Fig. 3b as a function of methane conversion.

In Fig. 3b, the energy balance of TDM is divided to input (LHV of the feedstock methane and the reaction heat) and output (LHV of the hydrogen, carbon and unreacted methane as well as the sensible enthalpy of those). The solid columns and the lowest patterned columns present the energy balance at the reaction temperature of 500 °C. The two highest patterns represent the additional reaction heat/sensible enthalpy when the reaction heat is increased from 500 °C first to 1000 °C and then to 1500 °C.

For example, in the case when the methane conversion is 1 and the reaction temperature 500 °C, the bound energy in methane and part of the reaction heat transfers to the products. A minor part of the reaction heat transfers as sensible enthalpy of the products. Increasing the reaction temperature to 1000 °C, increases the reaction heat which then transfers to the sensible enthalpy of the products.

As can be seen in Fig. 3b, the reaction heat is a minor component compared to the LHV of the reactants or reaction products. The reaction heat equals up to 20% of the total input energy or up to 40% of the LHV of product hydrogen, which is the case at temperature 1500 °C and with the methane conversion of 1. However, the main part of the reaction heat is transferred to the sensible heat of the reaction products, which can be utilized for example to preheat the feedstock methane, and thus, improving the overall energy balance of TDM. The part of the reaction heat that cannot be covered by internal heat transfer, has to be provided externally.

3. Reactor parameters

After determining the reaction parameters, the reactor type and the heating source can be selected. Furthermore, the residence time of methane in the reactor is an important parameter in the TDM reactor design.

3.1. Reactor types and heating sources

A literature survey on the experimental studies of TDM was conducted in order to determine the reactor types and heating sources that have been utilized to conduct the TDM reaction in a laboratory scale (Table 2 and Fig. 4).

The reactor types applied in the experimental research of TDM have been flow reactors, fluidized bed reactors and fixed bed reactors. Non-catalytic TDM reaction has been studied in flow reactors whereas the fluidized bed reactors and fixed bed reactors have been applied for tests conducted with catalysts. Moreover,

Table 1
Catalysts, temperature ranges, and product carbon types and qualities in methane decomposition.

Catalyst	Temp (°C)	Carbon product	Quality	Ref.
Activated carbon	1100	Carbon black		[30]
Carbon black	1100	Amorphous turbostratic carbon		[30]
Carbon black	900	Protrusions of stacked graphene layers	Knotty, branched, and bent protrusions of graphene layers	[31]
Carbon black	900	Graphite-like carbon	Conical and pillar shaped protrusions of layered carbon sheets	[32]
Carbon black	850	Uniform carbon coating		[33]
Carbon black	800	Graphite-like carbon		[34]
Carbon black	750–1050	Carbon protrusions and pillars		[35]
Co-based	900	Filamentous carbon		[36]
Co-based	800	Coiled nanotubes, bamboo tubes	Helically coiled carbon nanotubes and bamboo like nanotubes, some multi-walled carbon nanotubes (MWCNTs)	[37]
Co-based	800	Irregular carbon particles, particles with fruit-like morphology		[38]
Co-based	700	MWCNTs	Outer diameter 15–30 nm, inner diameter larger than at 600 °C, some helically coiled nanotubes and bamboo like structures	[37]
Co-based	700	MWCNTs	Curved and tangled hollow core MWCNTs, no defects on outer walls, outer diameter 6–14 nm (50% Co/MgO) 3–11 nm (25% Mo 25% Co/MgO)	[39]
Co-based	600	MWCNTs	Outer diameter 15–30 nm, inner diameter 5–15 nm, some bamboo-like structures with knots in the nanotubes	[37]
Co-based	500	Carbon nanofibers	diameter 10–30 nm	[37]
Fe-based	800	Carbon plates and fibers	Smooth elliptical shapes 610 nm–1 μm, carbon fibers with diameters 110–300 nm	[40]
Fe-based	800	Multilayer graphene sheets	Large amount of aggregated graphene sheets containing wrinkles and ripples, minor nanofibers contamination, iron particles enclosed in graphene sheets	[38]
Fe-based	700–800	MWCNTs	Over 90% deposited carbon MWCNTs, 10–15 graphene cylinders with a hollow center, some carbon fibers	[41]
Fe–Mo	750	Nanofilaments	Bamboo nanotubes with internal nodes disrupting a hollow core, MWCNTs with few layers 10–20 nm in diameter	[42]
Fe–Co	700	MWCNTs	No amorphous carbon, high crystallinity (ID/IG = 0,41), outer and hollow diameters 12–75 nm, about 50 graphene layers	[43]
Ni-based	1100	Nanofibers	Low quality	[30]
Ni-based	800	MWCNTs	XRD: thin, uniform, long, outer diameter 25–35 nm, high graphitization degree, good crystalline quality; TEM: outer diameter 18–20 nm, inner space of tube 8.5 nm, presence of metallic Ni	[38]
Ni–Pd	700	MWCNTs	Highly interwoven, uniform, thin, and long multiwalled nanotubes, outer diameter 30–35 nm, internal channel space 4–5 nm, wall thickness 16 nm, no amorphous carbon detected, high crystalline quality and graphitization degree	[44]
Ni-based	700	MWCNTs	ca. 20 nm in diameter, higher graphitic order	[45]
Ni-based	700	MWCNTs	Filaments 15–20 nm in diameter, hollow core	[46]
Ni-based	700–800	MWCNTs	Extremely thin nanotubes, 5–20 nm in diameter, hollow channels 2–5 nm	[47]
Ni-based	625–675	Filamentous carbon		[48]
Ni-based	600	Carbon nanofibers	15% Ni: outer diameter 50.54 nm; 30% Ni: 46.20 nm; fishbone-type structure with a hollow core	[49]
Ni-based	550	Filamentous carbon		[50]
Ni-based	550	Filamentous carbon	Hollow, cylindrical filaments, graphitic carbon with different degrees of defect of distortion	[51]
Ni-based	500–600	Carbon filaments	50–100 nm in diameter with hollow channels in the middle, 50–70 nm in diameter containing 2 branches 100–300 nm long	[47]
Ni–Cu–Co	500–850	Carbon nanofibers		[52]
Ni-based	400	Carbon filaments	20–30 nm in diameter,50–70 nm in diameter 100–300 nm long containing 2 branches, equal amounts of thin and thick filaments, thin filaments are strongly curved, defected fish-bone type graphite structure, no hollow interior	[47]
No catalyst	1550–1850	Carbon black	Powered by concentrated sunlight, ash free amorphous carbon, particle size 20–40 nm	[53]
No catalyst	1335–1655	Carbon black	Powered by concentrated sunlight, particle size 10–70 nm	[54]
No catalyst	1000–1200	Graphitic film	Smooth, shiny, graphitic film in the reaction area	[41]
No catalyst	850	Graphite-like carbon		[14]

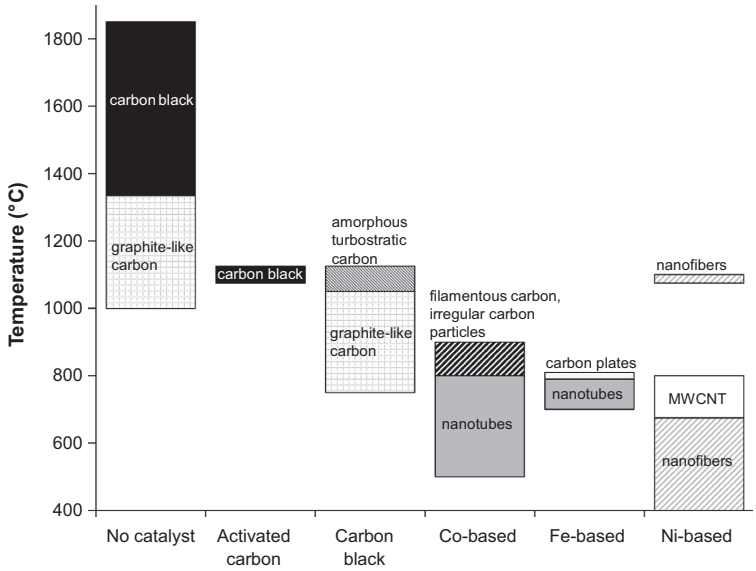

Fig. 2. Main carbon products obtained as a function of temperature and catalyst employed in the TDM reaction.

electrical furnaces and microwave ovens have been chosen as heating sources for tests with a catalyst whereas concentrated solar and plasma have been utilized to provide higher temperatures required in non-catalytic TDM reaction.

Structured catalytic reactors, especially honeycomb monoliths, and liquid metal reactors have been recently studied as an alternative to the typical fixed and fluidized bed reactors. The main advantage of monoliths is the large open frontal area, which results in a lower pressure drop than in packed bed reactors. However, the disadvantages of monoliths are related to the difficulties in the temperature control. [77] The liquid metal reactor enables efficient heat transfer properties between the liquid metal and methane gas [23].

Abánades et al. [78] have presented the technological challenges of TDM. Regarding direct thermal decomposition at temperatures well over 1000 °C, the main issue is the carbon clogging the reactor. Furthermore, at higher temperatures the residence times can be shorter, but the hardness of carbon deposition increases with temperature, which may complicate the carbon removal from the reactor. High temperatures can be achieved with concentrated solar power or with plasma. However, the plasma process requires electricity and then the CO_2 emissions from the electricity production have to be considered. With a catalyst, the methane decomposition occurs below 1000 °C, but the main issue is the carbon deposition on the catalyst surface that results in catalyst deactivation. Metal catalysts can be regenerated to remove the carbon deposition, but the drawback of the regeneration is again the formation of carbon dioxide. Capturing the gaseous CO_2 requires an additional process step and consumes more energy.

3.2. Reactor design

The reaction equilibrium presented in Section 2.1 is seldom reached in practice. In this study, the kinetic parameters found in the literature are utilized to determine the effect of methane residence time on the TDM reaction. A global one-step reaction model for TDM was chosen (Eq. (1)). The reaction rate equation

$$r = kP_{CH_4}^{m} \tag{7}$$

where P_{CH_4} is the partial pressure of methane (atm), m is the reaction order (–) and k is the rate constant, is commonly applied to study the kinetics of TDM [72,79–82]. The rate constant k is calculated from the Arrhenius law:

$$k = A \cdot exp^{-E_a/R_u T} \tag{8}$$

where A is the frequency factor, E_a is the activation energy (kJ/mol), R_u is the gas constant (8.314 J/mol K) and T is temperature (K).

In this study, the reaction rate was determined by taking into account the reactions both forward and backward:

$$r = \frac{dN}{dt} = k_{forward} \cdot P_{CH_4}^{m} - k_{backward} \cdot P_{H_2}^{n} \tag{9}$$

where N is the reacting amount (mol), t is time (s), rate constant $k_{forward}$ is calculated from Eq. (8) and n is the reaction order for the backward reaction, which was assumed to have a value of 1. The rate constant for the backward reaction, $k_{backward}$, was calculated in equilibrium state, i.e., when the reaction rate in Eq. (9) equals zero. Moreover, the partial pressures of methane and hydrogen in this calculation were determined from Eq. (1).

In order to exemplify the effect of residence time on the TDM reaction, calculations were done by exploiting the experimental data and kinetic parameters presented in the literature. The data for these examples were taken from [79] for an unsupported nickel catalyst and [72] for an activated carbon catalyst. These studies were chosen as the experimental and kinetic data were well presented in those and the catalysts (nickel and activated carbon) are widely studied in the literature and stated as suitable catalysts for TDM. Furthermore, in these studies a one-step reaction model was chosen to describe the TDM reaction similarly as in this study. The kinetic parameters adopted from [79,72] and utilized in calculations are shown in Table 3.

The kinetic parameters in Table 3 are calculated from the initial reaction rates that have been experimentally defined. Thus, in this study, the effect of residence time was calculated by assuming

Table 2
Literature survey on reactor types utilized in the experimental research of TDM.

Temp (°C)	Catalyst	Heat source	Reactor	Ref.
1130–1680	No catalyst	Concentrated solar energy	Fluid-wall aerosol flow reactor with graphite tube	[53]
1400–1500	No catalyst	Concentrated solar energy	Flow reactor with graphite tube	[54]
1400–1500	No catalyst	Concentrated solar energy	Flow reactor with graphite tube	[54]
1227–1427	No catalyst	Concentrated solar energy	Fluid-wall reactor made of stainless steel with internal graphite tube	[58]
1027–1327	No catalyst	Concentrated solar energy	Vortex-flow reactor made of steel allow	[59]
727–1327	No catalyst	Concentrated solar energy	Vortex-flow reactor made of steel allow	[60]
1227–1800	No catalyst	Plasma	DC plasma torch flow reactor made of stainless steel	[17]
820–980	Carbon black	Electrical furnace	Fluidized bed reactor with quartz tube	[61]
700–900	Activated carbon	Electrical furnace	Fluidized bed reactor with quartz tube	[62]
700–850	$CuAl_2O_4$	Electrical oven	Fluidized bed reactor with ceramic tube	[63]
500–850	$Ni/Cu/Al_2O_3$	Electrical furnace	Fluidized bed reactor with stainless steel tube	[64]
700	$NiCu/Al_2O_3$	Electrical furnace	Fluidized bed reactor with Kanthal tube	[65]
700	Ni–Cu–Al	Electrical furnace	Fluidized bed reactor with Kanthal tube	[66]
650–700	$Fe–Mo/Al_2O_3$	Electrical furnace	Fluidized bed reactor with quartz tube	[67]
650	Ni/SiO_2	Electrical furnace	Fluidized bed reactor with quartz tube	[68]
550–650	Ni-catalyst	Electrical furnace	Fluidized bed reactor with quartz tube	[69]
550	Ni-based	Electrical furnace	Vibrofluidized reactor with quartz tube	[50]
550	Ni, Ni–Cu	Electrical furnace	Vibrofluidized reactor with quartz tube	[70]
740–960	Carbon black	Electrical furnace	Fixed bed reactor with quartz tube	[34]
850–950	Carbon black	Electrical furnace	Fixed bed reactor with quartz tube	[31]
820–940	Activated carbon	Electrical furnace	Fixed bed reactor with quartz tube	[71]
800–900	Fe-based	Electrical furnace	Fixed bed reactor with quartz tube	[40]
750–900	Activated carbon	Electrical furnace	Fixed bed reactor with quartz tube	[72]
700–900	Activated carbon	Electrical furnace	Fixed bed reactor with quartz tube	[73]
500–900	Co–MgO	Electrical furnace	Fixed bed reactor with quartz tube	[36]
850	Carbon black	Electrical furnace	Fixed bed reactor with quartz tube	[33]
800	Activated carbon	Electrical furnace	Fixed bed reactor with quartz tube	[74]
800	Ni/SiO_2, Co/SiO_2, Fe/SiO_2	Electrical furnace	Fixed bed reactor with stainless steel tube	[38]
700	Co/MgO	Electrical furnace	Fixed bed reactor with quartz tube, horizontal	[39]
700	Pd promoted $Ni/MgAl_2O_4$ catalyst	Electrical furnace	Fixed bed reactor with stainless steel tube	[44]
700	Ni–Fe/MgO, Ni–Co/MgO, Fe–Co/MgO	Electrical furnace	Fixed bed reactor with quartz tube	[43]
550–700	Ni	Electrical furnace	Fixed bed reactor with quartz tube	[46]
550	Ni-based	Electrical furnace	Fixed-bed quartz reactor, plug-flow	[51]
700–900	Activated carbon	Microwave oven	Fixed bed reactor with quartz tube	[73]
800	Activated carbon	Microwave oven	Fixed bed reactor with quartz tube	[74]
750–900	Carbon monolith	Electrical furnace	Honeycomb monolith inside of a quartz tube	[75,76]
1100	No catalyst	Electrical oven	Liquid tin bubble column reactor with alumina tube	[21]
750–1100	No catalyst	Electrical furnace	Liquid tin bubble column reactor with alumina tube	[22]
930–1175	No catalyst	Electrical furnace	Liquid tin bubble column reactor with quartz tube	[19,20]
750–900	No catalyst	Electrical wire heaters	Liquid tin bubble column reactor with stainless steel tube	[23]
600–900	No catalyst	Electrical furnace	Molten metal bubble column reactor with stainless steel tube	[24]

constant reaction rates that equal with the initial reaction rates presented in reference studies [79,72]. This assumption does not take into account the gradual deactivation of the catalyst. In practice, this means an assumption that the catalyst is regenerated or renewed periodically to retain the high catalytic activity and the reactor clogging is under control. The gradual catalyst deactivation decreases the methane conversion, which has to be taken into account when dimensioning the reactor. However, each catalyst has a specific deactivation behavior, and thus, the influence of catalyst deactivation has to be calculated separately in each case.

The following parameters were applied when calculating the residence times: the partial pressure of input methane is 1 and the total pressure is 1 atm. The catalyst amounts were: 5.3 g_{cat}/mol_{CH_4} for the metal catalyst and 71.3 g_{cat}/mol_{CH_4} for the carbon catalyst. For the sake of consistency, the catalyst masses were chosen by assuming the same ratio of catalyst mass to the studied gas volume as was the ratio of the catalyst mass to the reactor volume in the experiments in [79]. The temperature ranges shown in Fig. 5 are chosen based on the suitable temperature ranges for different catalysts previously presented in Fig. 2. The calculated reaction rates were consistent with those presented in the reference studies [79,72]. The results of the two example cases shown in Fig. 5 are valid only with the assumptions presented previously and with the chosen catalysts. However, the effect of residence time in TDM reaction can be illustrated similarly when the reaction conditions and kinetic parameters are known. More detailed reaction mechanisms can be taken into account by utilizing commercial software [83,84].

Besides the residence time of methane in the reactor, there are other factors to be considered, such as the heat and mass transfer efficiencies.

4. Initial process design

As the product carbon is extracted from the process in a solid form and its heating value is not utilized, the lost heating value has to be compensated for. There are two options for this: the economic benefit due to the reduced requirement to buy carbon dioxide emission allowances and the possibility to sell the product carbon.

4.1. Value of the products

The utilization possibilities of the product carbon are in many studies [12,13,15] stated as a crucial factor when considering the viability and economic feasibility of TDM. In these analyses, the economic feasibility of TDM is based on the assumption is that the TDM product carbon can be further utilized, and therefore, has a certain market value. Even though the possible applications

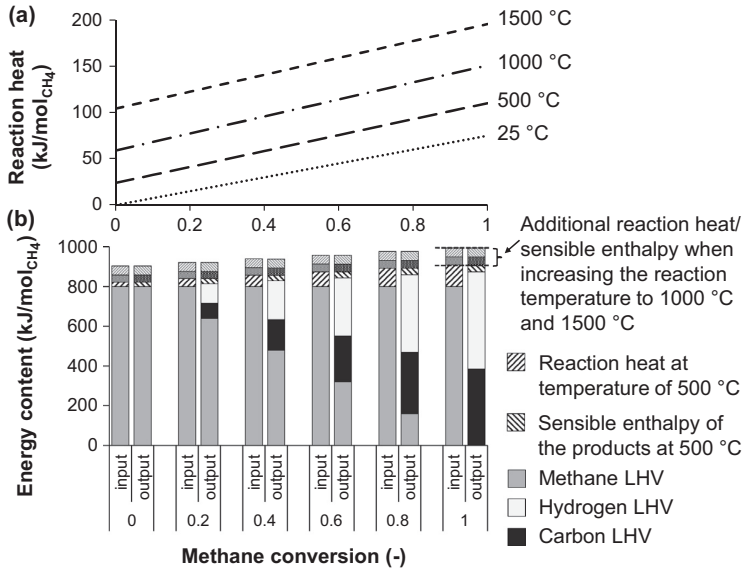

Fig. 3. (a) The reaction heat in TDM as a function of reaction temperature and methane conversion and (b) the energy balance for TDM. In graph b, the input energy consists of the LHV of methane and the reaction heat, whereas the output consists of the LHV of products (hydrogen, carbon and unreacted methane) and the sensible enthalpy of the products. Solid filled columns represent the LHV of feedstock/products and the lowest patterned columns represent the reaction heat/sensible enthalpy of the feedstock/products at reaction temperature of 500 °C. The two highest patterns represent the additional reaction heat/sensible enthalpy when the reaction heat is increased to 1000 °C and 1500 °C.

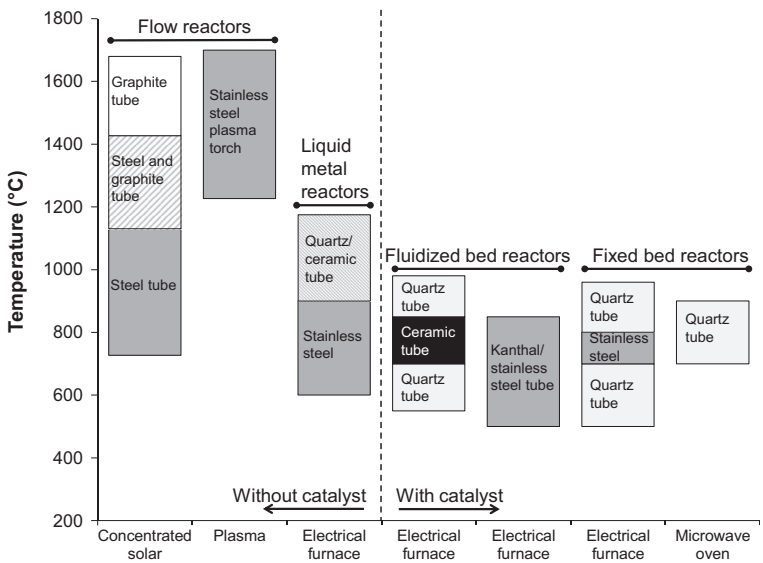

Fig. 4. A graphical presentation of the reactor types and heat source utilized in the experimental research of TDM reaction.

Table 3
The kinetic parameters presented in the literature and utilized in this study.

Catalyst	A	E_a	m	Ref.
Metal	1047.3 mol_{H2}/g_{cat} min $atm^{0.5}$	65.4 kJ/mol	0.63	[79]
Carbon	12,800 mol_{CH4}/g_{cat} s $atm^{0.5}$	194 kJ/mol	0.5	[72]

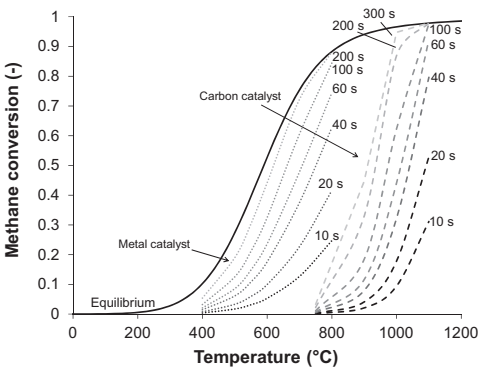

Fig. 5. Two examples of methane conversion dependence on temperature and residence time with metal (left set of curves) and carbon catalyst (right set of curves). Based on kinetic studies in [79,72].

of the product carbon are frequently highlighted in the TDM studies, the yearly consumption of these carbon products is seldom analyzed. Thus, the fact that the yearly consumption of different carbon products can be the factor limiting the utilization possibilities of TDM is not taken into account.

Therefore, a market analysis was conducted in order to demonstrate the potential of TDM in the current market situation. The current production volume of different carbon products was determined as follows: 8.1–9.4 million tonnes of carbon black [85,86], 1.9 million tonnes of activated carbon [87] and 500 million tonnes of metallurgical coke [88]. Furthermore, the yearly production of carbon nanotubes was 2.5 thousand tonnes in 2010 and back then it was estimated to reach 12 thousand tonnes in 2016 [89].

The current production volumes define the upper limit for the carbon produced by TDM, if TDM process is supposed to replace the current production methods. However, if alternative utilization possibilities for the product carbon are developed, the yearly carbon demand will increase providing more possibilities for the utilization of TDM carbon.

Calculations were done to estimate the amount of hydrogen and carbon that could be produced by the TDM process, in order to understand the potential of TDM better. Globally, the annual natural gas consumption was 3.4 trillion cubic meters in 2014 [10]. The global annual hydrogen production volume was 60 million tonnes in 2013 [9]. Thus, we calculated the situation where TDM would be applied to replace the current hydrogen production methods. First, the following assumptions were made: natural gas contains 100% of methane and the TDM process only produces hydrogen and carbon as presented in Eq. (1). Thus, the current global hydrogen demand would be fulfilled when 11% of global natural gas consumption is treated with TDM assuming a relatively high value for methane conversion, 0.9. At the same time, approximately 200 million tonnes of carbon would be produced annually. This amount is plenty more than the annual production volume of most of the carbon products, except metallurgical coke.

If the carbon production is taken as the starting point of the calculations, treating 0.6% of the global natural gas consumption with TDM (assuming a methane conversion of 0.9), would result in producing an amount of carbon that is equal with the current carbon black demand. At the same time, the TDM process would produce 3.3 million tonnes of hydrogen, which equals 6% of the annual global hydrogen production. This analysis, even though it is oversimplified, shows how the application possibilities of the product carbon limit TDM applications.

Therefore, new applications for the product carbon are needed. The following applications are frequently mentioned when a large-scale utilization of the TDM product carbon is concerned: building or construction material, direct carbon fuel cells to produce electricity, and soil amendment [55]. Metallurgical coke, which is used in steel production for the reduction of iron oxides, could possibly be replaced by TDM carbon. The main chemical property requirements for the metallurgical coke are the moisture content and the amount of volatile matter, ash, sulfur, phosphorus and alkalies. The important physical properties are particle size and size distribution, reactivity and strength [90]. If the properties of TDM carbon are suitable, replacing metallurgical coke could provide a large-scale application for TDM carbon.

Some carbon prices were also determined as a part of the market analysis to be utilized when estimating the value of the product carbon. The price of carbon black is 500–4000 €/tonne [91], activated carbon 1500 $/tonne [92] and metallurgical coke 150 €/tonne [93]. The price of multiwalled carbon nanotubes (MWCNT) depends on the diameter of the tubes and the purity level [94]. MWCNTs with a research grade quality have a price of 0.6–10 $/g. The price of industrial grade MWCNTs is 380 $/tonne (diameter 10–30 nm) and 200–400 $/tonne (diameter 20–40 nm). The industrial grade MWCNT products have lower purity than the research grade products [94]. In practice this means that the product contains higher amounts of amorphous carbon and residues from the production. The typical purity of industrial grade MWCNTs is 90% and those are suitable for applications such as conductive plastics and polymers, paints and epoxies [94].

The carbon prices presented here are collected from data that are available free of charge. Numerous extensive market analyses regarding the carbon products are available at various prices produced by for example Ceresana, Freedonia Group, IDTechEx, Innovative Research and Products Inc, Research and Markets, and Transparency Market Research. It is important to bear in mind, that the carbon prices presented here are valid with the current production methods and volumes. However, if a substantial amount of carbon will be produced by TDM, the carbon prices will most probably decrease.

Hydrogen is the other marketable product of TDM. Currently, depending on the technology, the production cost of hydrogen is in range of 0.05–0.1 €/N m^3 (natural gas steam reforming or coal gasification) and 0.16–0.3 €/N m^3 (electrolysis) [95]. However, the conventional hydrogen production methods utilize fossil fuels, produce CO_2 emissions, and consequently require additional CCS-technologies in the future. The presented hydrogen production costs can be used as a starting point when comparing the economic feasibility of TDM process to the conventional technologies.

4.2. Profit of CO_2 reduction

The possibility to produce less CO_2 emissions than the conventional technologies applied in natural gas utilization, is one of the main benefits of TDM. Besides the possibility that TDM product carbon may have a market value, producing solid carbon as such could be beneficial over producing gaseous CO_2. Storing the solid carbon can be an easier process and have a smaller environmental impact than storing gaseous CO_2. Furthermore, storing solid carbon could be an appealing alternative in countries where the legislation prevents CCS by injecting the gaseous CO_2 underground.

In this study, the CO_2 emissions from TDM were compared with those produced in the direct combustion of methane (Fig. 6a). The emissions of the TDM process were assumed to originate from the production of the reaction heat for the TDM reaction and combustion of the unconverted methane in the product gas. The reaction heat $Q_r(T_r, a)$ (see Section 2.3) is assumed to be produced by the

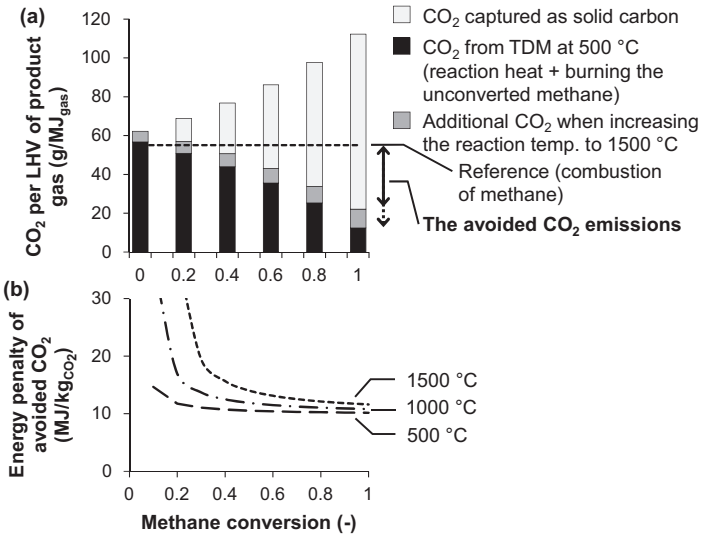

Fig. 6. (a) CO_2 emissions (g/MJ_{gas}) from TDM conducted at selected temperatures (500 °C and 1500 °C) compared to the emissions from the direct combustion of methane. (b) The energy bound to the product carbon in TDM proportioned to the avoided CO_2 emissions.

combustion of additional methane (with a theoretical efficiency of 100%), which causes CO_2 emissions. These emissions will decrease if the reaction heat is partly or completely provided from the CO_2-free sources (with renewable energy or internally with heat exchangers).

Thus, the black columns in Fig. 6a represent the CO_2 emissions from the production of reaction heat for TDM (at the reaction temperature of 500 °C) and the CO_2 emissions when the product gas from TDM (with different values of methane conversion) is burned. Furthermore, the gray columns represent the additional CO_2 emissions when the reaction temperature is increased from 500 °C to 1500 °C.

The CO_2 emissions were proportioned to the energy content of the product gas from TDM. Comparison was made to the reference case (methane combustion) that produces a constant amount of CO_2, 55 g per MJ of methane. Because the TDM reaction products consist of both solid and gaseous components, the energy content of the gaseous product decreases when the methane conversion is increased. Thus, more feedstock methane is needed when the gaseous product is supposed to fulfill a certain energy requirement, and consequently, more carbon is produced. Basically, one mole of solid carbon stored is equivalent to storing one mole of CO_2. However, due to the increased requirement of the feedstock, the reduction of the CO_2 emissions with TDM is not as much as the CO_2 equivalent of the extracted carbon in TDM. The actual avoided CO_2 emissions in TDM are the difference between the emissions from direct combustion and the emissions in TDM, as denoted by the arrow in Fig. 6a.

Up to 60–77% of the CO_2 emissions are avoided by TDM at the temperatures of 500–1500 °C compared to direct methane combustion when assuming that thereaction heat is produced by methane combustion. If the required reaction heat were to be produced without CO_2 emissions, e.g., from renewable sources or internally with heat exchangers, the complete TDM reaction would not produce any CO_2 emissions.

Fig. 6a also illustrates the effect of catalyst in TDM on the CO_2 emissions from the TDM process. The CO_2 emissions at reaction temperature 500 °C (suitable for metal catalysts) are marked with black columns and the additional CO_2 emissions caused by an increase of the temperature to 1500 °C (suitable for non-catalytic TDM) are marked with gray columns. Thus, with non-catalytic TDM, 60% of the CO_2 emissions can be avoided compared to the direct methane combustion (when methane conversion is 1). Decreasing the reaction temperature to 500 °C, results in avoiding 77% of the CO_2 emissions compared to the direct methane combustion. Thus, the increase of the avoided CO_2 emissions from 60% to 77% is the benefit of using a metal catalyst compared to the non-catalytic TDM.

Further calculations were conducted in order to find out the energy penalty of avoiding CO_2 emissions (MJ/kg_{CO_2}). The LHV of the product carbon shown in Fig. 3a was divided by the mass of the avoided CO_2 emissions (as marked with an arrow in Fig. 6a). The resulting graph of the energy penalty of avoiding CO_2 with TDM as a function of methane conversion is shown in Fig. 6b.

It is shown in Fig. 6a that when the methane conversion is low, the CO_2 emissions in TDM are more than in direct methane combustion, with the assumptions made at the beginning of this section. With a higher methane conversion than 0.1 at 500 °C and 0.3 at 1500 °C, TDM provides an actual reduction of CO_2 emissions compared to direct methane combustion. According to Fig. 6b, at temperatures 500 °C–1500 °C the energy penalty of TDM is 10–12 MJ/kg_{CO_2} at lowest. In contrast, the heat requirement of another carbon capture technology, chemical adsorption by amine solutions, is stated as 3–5 MJ/kg_{CO_2} [96,97]. Moreover, Bolland and Undrum [96] have presented an auxiliary heat of 0.33 MJ/kg_{CO_2} required to compress the captured CO_2 to the transportation pressure of 100 bar.

4.3. Auxiliary process components

This study focuses on introducing and analyzing the factors that affect the selection of reaction parameters in TDM and the design of TDM reactor. However, the auxiliary process parts have to be chosen and designed as well. The auxiliary process parts may include the following: separation of solid carbon from the product

gas (cyclone or filters), heat exchangers, auxiliary cooling, a catalyst regeneration system, CO_2 capture and flue gas cleaning. However, the design of these process parts is out of the scope of this article. Several examples of TDM process design in a commercial scale have been previously presented by Keipi et al. [12].

5. Conclusion

This article presented a path for selecting parameters for TDM reaction and the effect of those factors on the reactor design and further on the process design. The main reaction parameters, temperature and catalyst, affect the type of the TDM carbon and define the theoretical heat requirement of the reaction. The reactor design includes the selection of reactor type and heating source as well as reactor dimensioning. Temperature and catalyst are parameters that greatly affect the type of the TDM carbon as well as the reactor type and dimensions, thus having a significant effect on the economy of the TDM process.

The economic benefits of TDM are the reduction in CO_2 emissions compared to other hydrogen production methods and the possibility to sell the product carbon. In recent years the carbon product from TDM has attracted more attention and has led to more detailed analyses of the carbon product and its quality. With a moderate price of the CO_2 emission allowances, the economic feasibility of TDM is based on selling the product carbon. The current production volumes of different carbon products are limited, and therefore, new applications for the TDM carbon are needed in order to apply it in a larger scale. However, the increase in the carbon production volumes by TDM may decrease the value of these carbons. Therefore, the value and utilization possibilities of TDM carbon have to be considered carefully if TDM is to be applied in commercial scale.

With non-catalytic TDM, up to 60% of the CO_2 emissions can be avoided compared to direct methane combustion. When the reaction temperature would be decreased to 500 °C, for example by using a metal catalyst, the amount of avoided CO_2 emissions would increase up to 77%. Thus, the CO_2 emissions can be remarkably reduced by using a catalyst. Moreover, the selection of the catalyst has a crucial effect on the properties of the product carbon, and therefore on its price and utilization possibilities. As the catalyst and a suitable reaction temperature are linked together, those determine which reactor types and heating sources can be applied. In contrast, using a catalyst in the TDM process has only a minor effect on the energy balance of TDM. Additionally, the energy balance can be further improved by utilizing the internal heat transfer.

This article presents the factors that affect the design of a TDM process. This analysis can be utilized as a starting point when selecting the parameters for a TDM reactor or process whether it is a laboratory setup, a larger prototype or a conceptual study.

Acknowledgments

The study presented in this paper was carried out in the Carbon Capture and Storage Program (CCSP) research program coordinated by CLIC Innovation Ltd. with funding from the Finnish Funding Agency for Technology and Innovation, Tekes. The financial support received from Fortum, Gasum, Neste and Helen is gratefully acknowledged. Furthermore, the financial support given by the Tampere University of Technology (Finland) graduate school, the Gasum Gas Fund, the Walter Ahlström foundation (T.K.) and Tampere University of Technology (Finland) strategic funding (K.E.S.T.) is appreciated.

References

[1] International Energy Agency (IEA). Energy technology perspectives 2015. Tech rep; 2015.
[2] Framework Convention on Climate Change – Paris Agreement. <http://unfccc.int/paris_agreement/items/9485.php>; 2016 [accessed 23 May 2016].
[3] International Energy Agency (IEA). Technology roadmap – carbon capture and storage 2013. Tech rep. <http://www.iea.org/publications/free-publications/publication/technology-roadmap-carbon-capture-and-storage-2013.html>; 2013.
[4] Dufour J, Serrano DP, Gálvez JL, Moreno J, García C. Life cycle assessment of processes for hydrogen production. Environmental feasibility and reduction of greenhouse gases emissions. Int J Hydrogen Energy 2009;34:1370–6. http://dx.doi.org/10.1016/j.ijhydene.2008.11.053.
[5] Dufour J, Gálvez JL, Serrano DP, Moreno J, Martínez G. Life cycle assessment of hydrogen production by methane decomposition using carbonaceous catalysts. Int J Hydrogen Energy 2010;35:1205–12. http://dx.doi.org/10.1016/j.ijhydene.2009.11.093.
[6] Dufour J, Serrano DP, Gálvez JL, González A, Soria E, Fierro JLG. Life cycle assessment of alternatives for hydrogen production from renewable and fossil sources. Int J Hydrogen Energy 2012;37:1173–83. http://dx.doi.org/0.1016/j.ijhydene.2011.09.135.
[7] Serrano DP, Botas J, Pizarro P, Gómez G. Kinetic and autocatalytic effects during the hydrogen production by methane decomposition over carbonaceous catalysts. Int J Hydrogen Energy 2013;38:5671–83. http://dx.doi.org/10.1016/j.ijhydene.2013.02.112.
[8] Rokach JZ. Should we pursue carbon capture for natural gas? Electr J 2012;25:64–7. http://dx.doi.org/10.1016/j.tej.2012.06.001.
[9] International Energy Agency (IEA). Technology roadmap – hydrogen and fuel cells. Tech rep. <https://www.iea.org/publications/freepublications/publication/TechnologyRoadmapHydrogenandFuelCells.pdf>; 2015.
[10] International Energy Agency (IEA). World energy outlook 2014. Tech rep. <http://www.worldenergyoutlook.org/publications/weo-2014/>; 2014.
[11] Muradov NZ. CO_2-free production of hydrogen by catalytic pyrolysis of hydrocarbon fuel. Energy Fuels 1998;12:41–8. http://dx.doi.org/10.1021/ef9701145.
[12] Keipi T, Hankalin V, Nummelin J, Raiko R. Techno-economic analysis of four concepts for thermal decomposition of methane: Reduction of CO_2 emissions in natural gas combustion. Energy Convers Manage 2016;110:1–12. http://dx.doi.org/10.1016/j.enconman.2015.11.057.
[13] Triphob N, Wongsakulphasatch S, Kiatkittipong W, Charinpanitkul T, Praserthdam P, Assabumrungrat S. Integrated methane decomposition and solid oxide fuel cell for efficient electrical power generation and carbon capture. Chem Eng Res Des 2012;90:2223–34. http://dx.doi.org/10.1016/j.cherd.2012.05.014.
[14] Muradov N. Hydrogen via methane decomposition: an application for decarbonization of fossil fuels. Int J Hydrogen Energy 2001;26:1165–75. http://dx.doi.org/10.1016/S0360-3199(01)00073-8.
[15] Muradov NZ, Veziroğlu TN. Green path from fossil-based to hydrogen economy: An overview of carbon-neutral technologies. Int J Hydrogen Energy 2008;33:6804–39. http://dx.doi.org/10.1016/j.ijhydene.2008.08.054.
[16] Fulcheri L, Schwob Y. From methane to hydrogen, carbon and water. Int J Hydrogen Energy 1995;20:197–202. http://dx.doi.org/10.1016/0360-3199(94)E0022-Q.
[17] Kim KS, Hong SH, Lee SK, Ju WT. Continuous synthesis of nanostructured sheetlike carbons by thermal plasma decomposition of methane. IEEE Trans Plasma Sci 2007;35:434–43. http://dx.doi.org/10.1109/tps.2007.892556.
[18] Steinberg M. Fossil fuel decarbonization technology for mitigating global warming. Int J Hydrogen Energy 1999;24:771–7. http://dx.doi.org/10.1016/S0360-3199(98)00128-1.
[19] Geißler T, Plevan M, Abánades A, Heinzel A, Mehravaran K, Rathnam RK, et al. Experimental investigation and thermo-chemical modeling of methane pyrolysis in a liquid metal bubble column reactor with a packed bed. Int J Hydrogen Energy 2015;40:14134–46. http://dx.doi.org/10.1016/j.ijhydene.2015.08.102.
[20] Geißler T, Abánades A, Heinzel A, Mehravaran K, Müller G, Rathnam RK, et al. Hydrogen production via methane pyrolysis in a liquid metal bubble column reactor with a packed bed. Chem Eng J 2016;299:192–200. http://dx.doi.org/10.1016/j.cej.2016.04.066.
[21] Schultz I, Agar DW. Decarbonisation of fossil energy via methane pyrolysis using two reactor concepts: fluid wall flow reactor and molten metal capillary reactor. Int J Hydrogen Energy 2015;40:11422–7. http://dx.doi.org/10.1016/j.ijhydene.2015.03.126.
[22] Paxman D, Trottier S, Nikoo M, Secanell M, Ordorica-Garcia G. Initial experimental and theoretical investigation of solar molten media methane cracking for hydrogen production. Energy Proc 2014;49:2027–36. http://dx.doi.org/10.1016/j.egypro.2014.03.215.
[23] Plevan M, Geißler T, Abánades A, Mehravaran K, Rathnam RK, Rubbia C, et al. Thermal cracking of methane in a liquid metal bubble column reactor: experiments and kinetic analysis. Int J Hydrogen Energy 2015;40:8020–33. http://dx.doi.org/10.1016/j.ijhydene.2015.04.062.
[24] Serban M, Lewis MA, Marshall CL, Doctor RD. Hydrogen production by direct contact pyrolysis of natural gas. Energy Fuels 2003;17:705–13. http://dx.doi.org/10.1021/ef020271q.
[25] Kirk-Othmer, editor. Encyclopedia of chemical technology. New Jersey (USA): John Wiley & Sons Inc; 2007 [chapter Carbon Black].

[26] Holmen A, Olsvik O, Rokstad OA. Pyrolysis of natural gas: chemistry and process concepts. Fuel Process Technol 1995;42:249–67. http://dx.doi.org/10.1016/0378-3820(94)00109-7.

[27] National Institute of Standards and Technology. NIST-JANAF, thermochemical tables, www. <http://kinetics.nist.gov/janaf/>; 2016 [accessed 23 May 2016].

[28] Villacampa JI, Royo C, Romeo E, Montoya JA, Angel PD, Monzóna A. Catalytic decomposition of methane over Ni–Al_2O_3 coprecipitated catalysts: reaction and regeneration studies. Appl Catal A: Gen 2003;252:363–83. http://dx.doi.org/10.1016/S0926-860X(03)00492-7.

[29] Snoeck J-W, Froment GF, Fowles M. Filamentous carbon formation and gasification: Thermodynamics, driving force, nucleation, and steady-state growth. J Catal 1997;169:240–9. http://dx.doi.org/10.1006/jcat.1997.1634.

[30] Guil-Lopez R, Botas JA, Fierro JLG, Serrano DP. Comparison of metal and carbon catalysts for hydrogen production by methane decomposition. Appl Catal A: Gen 2011;396:40–51. http://dx.doi.org/10.1016/j.apcata.2011.01.036.

[31] Ryu BH, Lee SY, Lee DH, Han GY, Lee T-J, Yoon KJ. Catalytic characteristics of various rubber-reinforcing carbon blacks in decomposition of methane for hydrogen production. Catal Today 2007;123:303–9. http://dx.doi.org/10.1016/j.cattod.2007.02.001.

[32] Lee SY, Ryu BH, Han GY, Lee TJ, Yoon KJ. Catalytic characteristics of specialty carbon blacks in decomposition of methane for hydrogen production. Carbon 2008;46:1978–86. http://dx.doi.org/10.1016/j.carbon.2008.08.008.

[33] Suelves I, Lázaro MJ, Moliner R, Pinilla JL, Cubero H. Hydrogen production by methane decarbonization: Carbonaceous catalysts. Int J Hydrogen Energy 2007;32:3320–6. http://dx.doi.org/10.1016/j.ijhydene.2007.05.028 [International Symposium on Solar-Hydrogen-Fuel Cells 2005].

[34] Kameya Y, Hanamura K. Kinetic and Raman spectroscopic study on catalytic characteristics of carbon blacks in methane decomposition. Chem Eng J 2011;173:627–35. http://dx.doi.org/10.1016/j.cej.2011.08.017.

[35] Lee EK, Lee SY, Han GY, Lee BK, Lee T-J, Jun JH, et al. Catalytic decomposition of methane over carbon blacks for CO_2-free hydrogen production. Carbon 2004;42:2641–8. http://dx.doi.org/10.1016/j.carbon.2004.06.003.

[36] Wang HY, Ruckenstein E. Formation of filamentous carbon during methane decomposition over Co–MgO catalysts. Carbon 2002;40:1911–7. http://dx.doi.org/10.1016/S0008-6223(02)00032-5.

[37] Takenaka S, Ishida M, Serizawa M, Tanabe E, Otsuka K. Formation of carbon nanofibers and carbon nanotubes through methane decomposition over supported cobalt catalysts. J Phys Chem B 2004;108:11464–72. http://dx.doi.org/10.1021/jp048827t.

[38] Pudukudy M, Yaakob Z. Methane decomposition over Ni, Co and Fe based monometallic catalysts supported on sol gel derived SiO_2 microflakes. Chem Eng J 2015;262:1009–21. http://dx.doi.org/10.1016/j.cej.2014.10.077.

[39] Awadallah AE, Aboul-Enein AA, Aboul-Gheit AK. Impact of group VI metals addition to Co/MgO catalyst for non-oxidative decomposition of methane into CO_x-free hydrogen and carbon nanotubes. Fuel 2014;129:27–36. http://dx.doi.org/10.1016/j.fuel.2014.03.038.

[40] Konieczny A, Mondal K, Wiltowski T, Dydo P. Catalyst development for thermocatalytic decomposition of methane to hydrogen. Int J Hydrogen Energy 2008;33:264–72. http://dx.doi.org/10.1016/j.ijhydene.2007.07.054.

[41] Shah N, Panjala D, Huffman GP. Hydrogen production by catalytic decomposition of methane. Energy Fuels 2001;15:1528–34. http://dx.doi.org/10.1021/ef0101964.

[42] Torres D, Pinilla JL, Lázaro MJ, Moliner R, Suelves I. Hydrogen and multiwall carbon nanotubes production by catalytic decomposition of methane: Thermogravimetric analysis and scaling-up of Fe–Mo catalysts. Int J Hydrogen Energy 2014;39:3698–709. http://dx.doi.org/10.1016/j.ijhydene.2013.12.127.

[43] Awadallah AE, Aboul-Enein AA, El-Desouki DS, Aboul-Gheit AK. Catalytic thermal decomposition of methane to CO_x-free hydrogen and carbon nanotubes over MgO supported bimetallic group VIII catalysts. Appl Surf Sci 2014;296:100–7. http://dx.doi.org/10.1016/j.apsusc.2014.01.055.

[44] Pudukudy M, Yaakob Z, Takriff MS. Methane decomposition over Pd promoted Ni/$MgAl_2O_4$ catalysts for the production of COx free hydrogen and multiwalled carbon nanotubes. Appl Surf Sci 2015;356:1320–6. http://dx.doi.org/10.1016/j.apsusc.2015.08.246.

[45] Takenaka S, Kobayashi S, Ogihara H, Otsuka K. Ni/SiO_2 catalyst effective for methane decomposition into hydrogen and carbon nanofiber. J Catal 2003;217:79–87. http://dx.doi.org/10.1016/S0021-9517(02)00185-9.

[46] Suelves I, Lázaro MJ, Moliner R, Corbella BM, Palacios JM. Hydrogen production by thermo catalytic decomposition of methane on Ni-based catalysts: influence of operating conditions on catalyst deactivation and carbon characteristics. Int J Hydrogen Energy 2005;30:1555–67. http://dx.doi.org/10.1016/j.ijhydene.2004.10.006.

[47] Zaikovskii VI, Chesnokov VV, Buyanov RA. The relationship between the state of active species in a Ni/Al_2O_3 catalyst and the mechanism of growth of filamentous carbon. Kinet Catal 2001;42:813–20.

[48] Reshetenko TV, Avdeeva LB, Ismagilov ZR, Chuvilin AL, Ushakov VA. Carbon capacious Ni–Cu–Al_2O_3 catalysts for high-temperature methane decomposition. Appl Catal A: Gen 2003;247:51–63. http://dx.doi.org/10.1016/S0926-860X(03)00080-2.

[49] Uddin MN, Daud WMA Wan, Abbas HF. Co-production of hydrogen and carbon nanofibers from methane decomposition over zeolite Y supported Ni catalysts. Energy Convers Manage 2015;90:218–29. http://dx.doi.org/10.1016/j.enconman.2014.10.060.

[50] Ermakova MA, Ermakov DY, Kuvshinov GG, Plyasova LM. New nickel catalysts for the formation of filamentous carbon in the reaction of methane decomposition. J Catal 1999;187:77–84. http://dx.doi.org/10.1006/jcat.1999.2562.

[51] Zhang T, Amiridis MD. Hydrogen production via the direct cracking of methane over silica-supported nickel catalysts. Appl Catal A: Gen 1998;167:161–72. http://dx.doi.org/10.1016/S0926-860X(97)00143-9.

[52] Lua AC, Wang HY. Hydrogen production by catalytic decomposition of methane over Ni–Cu–Co alloy particles. Appl Catal B: Environ 2014;156–157:84–93. http://dx.doi.org/10.1016/j.apcatb.2014.02.046.

[53] Dahl JK, Buechler KJ, Weimer AW, Lewandowski A, Bingham C. Solar-thermal dissociation of methane in a fluid-wall aerosol flow reactor. Int J Hydrogen Energy 2004;29:725–36. http://dx.doi.org/10.1016/j.ijhydene.2003.08.009.

[54] Rodat S, Abanades S, Grivei E, Patrianakos G, Zygogianni A, Konstandopoulos AG, et al. Characterisation of carbon blacks produced by solar thermal dissociation of methane. Carbon 2011;49:3084–91. http://dx.doi.org/10.1016/j.carbon.2011.03.030.

[55] Muradov NZ, Veziroğlu TN. From hydrocarbon to hydrogen-carbon to hydrogen economy. Int J Hydrogen Energy 2005;30:225–37. http://dx.doi.org/10.1016/ j.ijhydene.2004.03.033.

[56] Abbas HF, Daud WMA Wan. Hydrogen production by methane decomposition: a review. Int J Hydrogen Energy 2010;35:1160–90. http://dx.doi.org/10.1016/j.ijhydene.2009.11.036.

[57] Ashik UPM, Daud WMA Wan, Abbas HF. Production of greenhouse gas free hydrogen by thermocatalytic decomposition of methane – A review. Renew Sustain Energy Rev 2015;44:221–56. http://dx.doi.org/10.1016/j.rser.2014.12.025.

[58] Abanades S, Flamant G. Hydrogen production from solar thermal dissociation of methane in a high-temperature fluid-wall chemical reactor. Chemical engineering and processing: process intensification, vol. 47. p. 490–8. http://dx.doi.org/10.1016/j.cep.2007.01.006 [in 10th French Congress on Chemical Engineering].

[59] Maag G, Zanganeh G, Steinfeld A. Solar thermal cracking of methane in a particle-flow reactor for the co-production of hydrogen and carbon. Int J Hydrogen Energy 2009;34:7676–85. http://dx.doi.org/10.1016/j.ijhydene.2009.07.037.

[60] Hirsch D, Steinfeld A. Solar hydrogen production by thermal decomposition of natural gas using a vortex-flow reactor. Int J Hydrogen Energy 2004;29:47–55. http://dx.doi.org/10.1016/S0360-3199(03)00048-X.

[61] Dunker AM, Kumar S, Mulawa PA. Production of hydrogen by thermal decomposition of methane in a fluidized-bed reactor – Effects of catalyst, temperature, and residence time. Int J Hydrogen Energy 2006;31:473–84. http://dx.doi.org/10.1016/j.ijhydene.2005.04.023.

[62] Lee KK, Han GY, Yoon KJ, Lee BK. Thermocatalytic hydrogen production from the methane in a fluidized bed with activated carbon catalyst. Catal Today 2004;93–95:81–6. http://dx.doi.org/10.1016/j.cattod.2004.06.080 [selections from the presentations of the 3rd Asia-Pacific Congress on Catalysis].

[63] Ammendola P, Chirone R, Ruoppolo G, Russo G. Production of hydrogen from thermo-catalytic decomposition of methane in a fluidized bed reactor. Chem Eng J 2009;154:287–94. http://dx.doi.org/10.1016/j.cej.2009.03.048 [in XVIII International Conference on Chemical Reactors – CHEMREACTOR -18 (September 29–October 3, 2008, Malta)].

[64] Weizhong Q, Tang L, Zhanwen W, Fei W, Zhifei L, Guohua L, et al. Production of hydrogen and carbon nanotubes from methane decomposition in a two-stage fluidized bed reactor. Appl Catal A: Gen 2004;260:223–8. http://dx.doi.org/10.1016/j.apcata.2003.10.018.

[65] Pinilla JL, Suelves I, Lázaro MJ, Moliner R, Palacios JM. Parametric study of the decomposition of methane using a NiCu/Al_2O_3 catalyst in a fluidized bed reactor. Int J Hydrogen Energy 2010;35:9801–9. http://dx.doi.org/10.1016/j.ijhydene.2009.10.008.

[66] Pinilla JL, Moliner R, Suelves I, Lázaro MJ, Echegoyen Y, Palacios JM. Production of hydrogen and carbon nanofibers by thermal decomposition of methane using metal catalysts in a fluidized bed reactor. Int J Hydrogen Energy 2007;32:4821–9. http://dx.doi.org/10.1016/j.ijhydene.2007.08.013.

[67] Shah N, Ma S, Wang Y, Huffman GP. Semi-continuous hydrogen production from catalytic methane decomposition using a fluidized-bed reactor. Int J Hydrogen Energy 2007;32:3315–9. http://dx.doi.org/10.1016/j.ijhydene.2007.04.040 [in International Symposium on Solar-Hydrogen-Fuel Cells 2005].

[68] Aiello R, Fiscus JE, zur Loye H-C, Amiridis MD. Hydrogen production via the direct cracking of methane over Ni/SiO_2: catalyst deactivation and regeneration. Appl Catal A: Gen 2000;192:227–34. http://dx.doi.org/10.1016/S0926-860X(99)00345-2.

[69] Amin AM, Croiset E, Malaibari Z, Epling W. Hydrogen production by methane cracking using Ni-supported catalysts in a fluidized bed. Int J Hydrogen Energy 2012;37:10690–701. http://dx.doi.org/10.1016/j.ijhydene.2012.04.082.

[70] Avdeeva LB, Goncharova OV, Kochubey DI, Zaikovskii VI, Plyasova LM, Novgorodov BN, et al. Coprecipitated Ni-alumina and Ni–Cu-alumina catalysts of methane decomposition and carbon deposition. II. Evolution of the catalysts in reaction. Appl Catal A: Gen 1996;141:117–29. http://dx.doi.org/10.1016/0926-860X(96)00026-9.

[71] Al-Hassani AA, Abbas HF, Daud WW. Hydrogen production via decomposition of methane over activated carbons as catalysts: Full factorial design. Int J Hydrogen Energy 2014;39:7004–14. http://dx.doi.org/10.1016/j.ijhydene.2014.02.075.

[72] Kim MH, Lee EK, Jun JH, Kong SJ, Han GY, Lee K, et al. Hydrogen production by catalytic decomposition of methane over activated carbon: kinetic study. Int J Hydrogen Energy 2004;29:187–93. http://dx.doi.org/10.1016/S0360-3199(03)00111-3.

[73] Domínguez A, Fidalgo B, Fernández Y, Pis JJ, Menéndez JA. Microwave-assisted catalytic decomposition of methane over activated carbon for CO_2-free hydrogen production. Int J Hydrogen Energy 2007;32:4792–9. http://dx.doi.org/10.1016/j.ijhydene.2007.07.041.
[74] Fidalgo B, Fernández Y, Domínguez A, Pis JJ, Menéndez JA. Microwave-assisted pyrolysis of CH_4/N_2 mixtures over activated carbon. J Anal Appl Pyrol 2008;82:158–62. http://dx.doi.org/10.1016/j.jaap.2008.03.004.
[75] Gatica JM, Gómez DM, Harti S, Vidal H. Monolithic honeycomb design applied to carbon materials for catalytic methane decomposition. Appl Catal A: Gen 2013;458:21–7. http://dx.doi.org/10.1016/j.apcata.2013.03.016.
[76] Gatica JM, Cifredo GA, Blanco G, Trasobares S, Vidal H. Unveiling the source of activity of carbon integral honeycomb monoliths in the catalytic methane decomposition reaction. Catal Today 2015;249:86–93. http://dx.doi.org/10.1016/j.cattod.2014.12.015.
[77] Heck RM, Gulati S, Farrauto RJ. The application of monoliths for gas phase catalytic reactions. Chem Eng J 2001;82:149–56. http://dx.doi.org/10.1016/S1385-8947(00)00365-X [Frontiers in Chemical Reaction Engineering].
[78] Abánades A, Rubbia C, Salmieri D. Technological challenges for industrial development of hydrogen production based on methane cracking. Energy 2012;46:359–63. http://dx.doi.org/10.1016/j.energy.2012.08.015.
[79] Wang HY, Lua AC. Deactivation and kinetic studies of unsupported Ni and Ni–Co–Cu alloy catalysts used for hydrogen production by methane decomposition. Chem Eng J 2014;243:79–91. http://dx.doi.org/10.1016/j.cej.2013.12.100.
[80] Abbas HF, Daud WMA Wan. Thermocatalytic decomposition of methane using palm shell based activated carbon: Kinetic and deactivation studies. Fuel Process Technol 2009;90:1167–74. http://dx.doi.org/10.1016/j.fuproc.2009.05.024.
[81] Pinilla JL, Suelves I, Lázaro MJ, Moliner R. Kinetic study of the thermal decomposition of methane using carbonaceous catalysts. Chem Eng J 2008;138:301–6. http://dx.doi.org/10.1016/j.cej.2007.05.056.
[82] Muradov N, Chen Z, Smith F. Fossil hydrogen with reduced CO_2 emission: modeling thermocatalytic decomposition of methane in a fluidized bed of carbon particles. Int J Hydrogen Energy 2005;30:1149–58. http://dx.doi.org/10.1016/j.ijhydene.2005.04.005.
[83] Borghei M, Karimzadeh R, Rashidi A, Izadi N. Kinetics of methane decomposition to CO_x-free hydrogen and carbon nanofiber over Ni–Cu/MgO catalyst. Int J Hydrogen Energy 2010;35:9479–88. http://dx.doi.org/10.1016/j.ijhydene.2010.05.072 [In The 1st Iranian Conference on Hydrogen & Fuel Cell].
[84] Ozalp N, Ibrik K, Al-Meer M. Kinetics and heat transfer analysis of carbon catalyzed solar cracking process. Energy 2013;55:74–81. http://dx.doi.org/10.1016/j.energy.2013.02.022.
[85] International Carbon Black Association (ICBA). What is carbon black?. <http://www.carbon-black.org/index.php/what-is-carbon-black>; 2016 [accessed 23 June 2016].
[86] The Freedonia Group. World carbon black. <http://www.freedoniagroup.com/DocumentDetails.aspx?ReferrerId=FG-01&studyid=2596>; 2010 [accessed 23 June 2016].
[87] Worldwide P. Activated carbon: US regulatory changes boost market for activated carbon. <http://www.process-worldwide.com/us-regulatory-changes-boost-market-for-activated-carbon-a-366700/>;2012 [accessed 23 June 2016].
[88] Noble Group. Supplying China: examining the role of China in global steel markets. <http://www.slideshare.net/ulziimyagmar/23032012-examing-the-role-of-china-in-global-steel-markets-neil-t-dhar>; 2012 [accessed 23 June 2016].
[89] Nanowerk. Global carbon nanotubes market – industry beckons. <http://www.nanowerk.com/spotlight/spotid=23118.php>;2011 [accessed 23 June 2016].
[90] Díez MA, Alvarez R, Barriocanal C. Coal for metallurgical coke production: predictions of coke quality and future requirements for cokemaking. Int J Coal Geol 2002;50:389–412. http://dx.doi.org/10.1016/S0166-5162(02)00123-4.
[91] Sid Richardson Carbon and Energy Co. Carbon black pricing. <http://www.sidrich.com/products-and-pricing/pricing/carbon-black-pricing/>; 2014 [accessed 7 March 2015].
[92] Viet Delta Corp. Market analysis and price activated carbon coconut shell charcoal, activated carbon from December 2012 to November 2013. <http://vdeltafuel.com/news.html>; 2014.
[93] Steelonthenet.com. Met coke prices – Europe 2010-2016. <http://www.steelonthenet.com/files/blast-furnace-coke.html>; 2016.
[94] Cheap Tubes Inc. Cheap tubes: products. <https://www.cheaptubes.com/cheap-tubes-inc-online-shop/>; 2016.
[95] International Energy Agency (IEA). Energy technology network, hydrogen production & distribution. <http://www.iea-etsap.org/Energy_Technologies/Energy_Supply/Hydrogen_Production_and_Distribution.asp>; 2014 [accessed 21 June 2016].
[96] Bolland O, Undrum H. A novel methodology for comparing CO_2 capture options for natural gas-fired combined cycle plants. Adv Environ Res 2003;7:901–11. http://dx.doi.org/10.1016/S1093-0191(02)00085-0.
[97] Gibbins JR, Crane RI, Lambropoulos D, Booth C, Roberts CA, Lord M. Maximizing the effectiveness of post combustion CO_2 capture systems. In: Proceedings of the 7th international conference on greenhouse gas control technologies. Vancouver (BC, Canada): Elsevier Science; 2005.

Publication III

Tiina Keipi, Tian Li, Terese Løvås, Henrik Tolvanen, Jukka Konttinen

Methane thermal decomposition in regenerative heat exchanger reactor: Experimental and modeling study

Energy, 135 (2017) 823–832.

Energy 135 (2017) 823–832

Contents lists available at ScienceDirect

Energy

journal homepage: www.elsevier.com/locate/energy

Methane thermal decomposition in regenerative heat exchanger reactor: Experimental and modeling study

Tiina Keipi [a, *], Tian Li [b], Terese Løvås [b], Henrik Tolvanen [a], Jukka Konttinen [a]

[a] Laboratory of Chemistry and Bioengineering, Tampere University of Technology, P.O. Box 541, 33101 Tampere, Finland
[b] Department of Energy and Process Engineering, Norwegian University of Science and Technology, Kolbjørn Hejes vei 1B, NO-7491 Trondheim, Norway

ARTICLE INFO

Article history:
Received 17 February 2017
Received in revised form
8 May 2017
Accepted 30 June 2017
Available online 4 July 2017

Keywords:
CCS
Hydrogen production
Kinetics
Methane cracking
Methane decomposition

ABSTRACT

In this work, thermal decomposition of methane (TDM) was experimentally studied at nominal gas temperatures of 1070 K–1450 K in a non-catalytic laboratory test reactor. The purpose was to use a simple kinetic mechanism to describe the TDM reaction, which could be applied in industrial reactor design. The experimental data was utilized to optimize global kinetic parameters describing the TDM reaction in the test reactor. For comparison, a 37-step reaction mechanism for TDM was adopted from the literature. When analyzing experimental datasets from the literature, the optimized global kinetics provided better agreement with the experimental data than the 37-step mechanism when the reactor temperature profiles were defined in detail. Since the 37-step mechanism was not able to predict the solid carbon formation well enough, the mechanism was slightly adjusted according to a reaction flow and sensitivity analysis. Additionally, it was suggested that the 37-step mechanism can be improved by optimizing the reaction mechanism by using a detailed experimental data of hydrocarbon formation in TDM achieved in an environment where the temperature profiles are fully defined.

1. Introduction

Nowadays, H_2 is widely utilized in the chemical industry, and furthermore, it has been proposed as a potential clean energy carrier in the future as it does not produce CO_2 when combusted [1]. Transition towards hydrogen economy requires the development of hydrogen production, storage, distribution and utilization technologies as well as regulatory changes [2–4]. Hydrogen production technologies that are both economically feasible and produce less CO_2 emissions are needed. Potential larger-scale low-CO_2 emission technologies for hydrogen production are water decomposition [5], water electrolysis by using renewable energy [6] and biomass gasification [7]. Additionally, CO_2 emissions of steam reforming of natural gas, which is the currently most applied hydrogen production technology [1], could be reduced when combined with CO_2 capture and storage (CCS) [8].

Decarbonization of fossil fuels, and especially treating natural gas by the thermal decomposition of methane (TDM), has been proposed as a potential technology in the transition towards H_2 economy [9]. The reaction equation for the endothermic TDM reaction ($\Delta H_r^0 = +76$ kJ/mol) is the following [10]:

$$CH_4 \rightarrow C(s) + 2H_2. \quad (1)$$

Instead of gaseous CO_2, TDM produces solid carbon, which in some cases can be considered as a value-added product. According to previous studies [11,12], TDM can be an economically feasible process only if the value of this product carbon is sufficiently high, i.e., 500–1000 EUR/tonne of carbon, which is comparable to the price of low-quality carbon black. When the CO_2 emissions are considered, TDM has been found as a more preferable technology for H_2 production than the currently most applied steam methane reforming (SMR), even if carbon capture and storage would be coupled with SMR [13–15].

A catalyst can be utilized to accelerate the TDM reaction, but the benefit of non-catalytic TDM over catalytic reaction is that it avoids impurities in the product carbon originating from the catalyst. Regarding non-catalytic TDM, many studies ([16–22]) have focused on concentrated solar power reactors, which could enable H_2 production with zero CO_2 emissions. However, a possible reactor concept for non-catalytic TDM is a regenerative heat exchanger reactor, which was first presented by part of the authors [11]. Previously, the carbon particle removal to avoid reactor clogging has been identified as the main challenge restraining the industrial

* Corresponding author.
E-mail address: tiina.keipi@tut.fi (T. Keipi).

http://dx.doi.org/10.1016/j.energy.2017.06.176
0360-5442/

development of TDM [23], which this new concept could avoid. The bed material in the reactor enables both effective heat transfer and conveys the product carbon out from the reactor.

Modeling the reaction kinetics involved is an important part of the TDM reactor design. Both the global kinetics [18,24] and more detailed kinetic mechanisms [18,19] have been presented for non-catalytic TDM modeling in the literature. However, the reaction temperatures in these studies have been from 1500 K to over 2000 K. Therefore, those mechanisms cannot be directly applied to the reaction conditions of a regenerative heat exchanger reactor, which operates at a temperature of 1000 K–1500 K and an approximate residence time of 1 s–10 s.

In this study, the objective was to find, for reactor design purposes, a relatively simple kinetic model to describe the non-catalytic TDM reaction below 1500 K. First, the simplest way to describe the reaction kinetics, a global mechanism, was studied in order to find out its applicability on modeling TDM. The experimental data, which was achieved with a laboratory test reactor that mimics the operation of a regenerative heat exchanger reactor, was applied to optimizing the kinetic parameters for the global TDM reaction by using a specifically written MATLAB-based plug flow reactor model. Second, the optimized global kinetics was compared with a rather simple 37-step reaction mechanism presented by Ozalp et al. [19]. The 37-step reaction mechanism was further developed based on a reaction flow and sensitivity analysis to improve its ability to predict solid carbon formation at temperatures 1000 K–2000 K. Thus, this article complements the previous knowledge in this field of study by providing (i) experimental data of non-catalytic TDM reaction at nominal gas temperatures of 1070 K–1450 K with specially defined temperature profiles, (ii) kinetic parameters for the global TDM reaction that were successfully applied to predict methane conversion in non-catalytic TDM and (iii) suggestions for improving the 37-step reaction mechanism for non-catalytic TDM presented in the literature.

2. Experimental section

2.1. Experimental setup

The experimental work presented and discussed in this paper was conducted with an experimental setup demonstrated in Fig. 1. The laboratory test reactor mimics the regenerative heat exchanger reactor previously presented by part of the authors [11]. The main

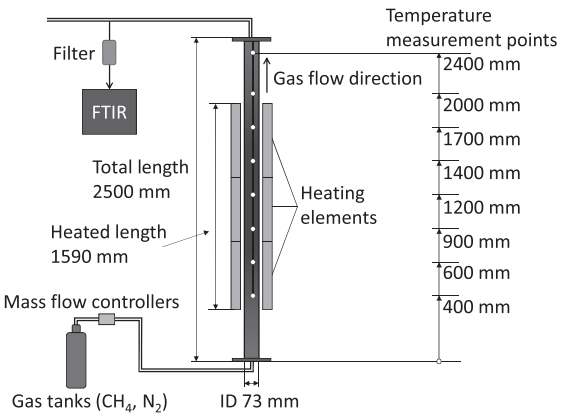

Fig. 1. A sketch of the laboratory scale test rector.

simplification in the test reactor is that there is no bed material circulation. The substantially high heat capacity of the solid bed material stabilizes the reactor temperature and makes the reactor appropriate for experimental kinetic studies.

The primary part of the experimental setup was the vertically mounted reactor tube made of Kanthal APM iron-chromium-aluminum (FeCrAl) alloy. The reactor tube had the following dimensions: the inner diameter of 73 mm, the outer diameter of 83 mm and the length of 2500 mm. In order to enable opening and closing of the reactor tube, there were flanges at both ends of the tube. During the operation, the joints of the flanges were sealed with copper seals.

The middle part of the reactor tube was electrically heated with three circular Fibrothal RAC 200/500 heating modules which were insulated with Fibrothal insulation modules. Each heating module had a heating power of 19.7 kW. The modules were separately controlled with an Eurotherm 7100 A thyristor unit combined with an Eurotherm 3204 temperature controller.

The reactor tube was filled with spherical ceramic beads with an approximate diameter of 10 mm. The ceramic beads served as a heat exchange material that stabilized the temperature and gas flow profiles in the reactor tube. Moreover, a part of the product carbon deposited on the surface of the beads. The void fraction, i.e., the proportion of empty space in the reactor, was separately defined to be 0.4. The determination was done experimentally by counting the number of beads that fit into a certain volume and estimating the void fraction mathematically.

The temperature profile inside the reactor tube was measured by using eight measuring points as shown in Fig. 1. Temperature was measured continuously with K-type thermocouples and recorded with a data logger in 2-s intervals. The experiments were conducted with reactor maximum temperatures between 1070 K and 1450 K. The gas mixture containing CH_4 (purity 99.995%) and N_2 (purity 99.95%) with different mixture ratios entered the reactor at room temperature. For modeling purposes, the product gas temperature at the reactor end was assumed to be 30 K less than that measured at the eighth measurement point, which was located 10 cm below the reactor outlet. The assumption is based on the extrapolation of the decreasing gas temperature at the reactor end. This assumption has a minor significance, since the gas temperature at the reactor end is well below the temperature where TDM reaction occurs.

To control the gas flow rates, mass flow controllers (Bronkhorst) in the range of 0–15 dm^3/min were used. The product gas flowed continuously out from the top end of the reactor tube. After exiting the reactor, part of the outcoming gas was extracted for analyzing purposes. The part of the product gas that was not analyzed was bubbled through water to remove the remaining carbon particles before discarding. The reactor was maintained inert during the periods of heating and quenching with a constant N_2 flow of 6 dm^3/min.

Prior to the gas analysis, the product gas flowed through an inline filter with stainless steel housing that sifted 93% of the carbon particles with a diameter more than 0.01 μm out. A continuous analysis of the product gas composition was conducted with a Fourier transform infrared spectroscopy (FTIR) in 30-s intervals. The examination procedure was as follows: the product gas was pumped into the sampling unit during the first 10 s and the composition of the sample gas was examined during the following 20 s. The FTIR analyzer has a limitation that it cannot detect biatomic homonuclear molecules, such as N_2 and H_2 in this case. Therefore, the methane conversion was calculated by comparing the measured methane concentration values to the initial concentration. The methane conversion a is defined in this article as follows:

$$a = \frac{n_{CH_4,inlet} - n_{CH_4,outlet}}{n_{CH_4,inlet}}, \quad (2)$$

where $n_{CH_4,inlet}$ and $n_{CH_4,outlet}$ are respectively the amount of CH_4 (mol) at the reactor inlet and outlet.

2.2. Experimental arrangement

A total of 48 separate cases were measured. The following parameters were recorded in each case: the volumetric flow of CH_4/N_2 mixture, the reactor temperature profile and the composition of the product gas. Before each measurement case, a stable temperature profile was achieved. Similarly, the reported methane conversion was calculated based on an average of 10 stabilized gas composition measurement points, which corresponds to a measurement period of 2.5 min. Experiments were conducted with total gas volumetric flows ranging from 5 dm^3/min to 16 dm^3/min measured at NTP conditions, which resulted in residence times between 6 s and 21 s. The inlet gas composition, temperature profiles and corresponding methane conversion values for each experimental case are presented in Appendix.

In order to ensure that the product carbon that deposited in the reactor did not affect the gas flow, the heat transfer, or the TDM reaction, an oxygen flow was fed to the reactor between each measurement to oxidize the product carbon that had formed during the previous measurement. Furthermore, the effect of deposited carbon during the experimental runs was minor since the mass of the ceramic beads in the reactor was thousand times the theoretical maximum carbon amount that could have been deposited during an average 15-min experimental run. The focus in this study was not on the product carbon quality, however, some qualitative analyses were conducted in order to verify (i) that carbon was formed during the tests and (ii) based on elementary analysis the carbon purity was high and it contained only a hint of impurities.

2.3. Measurement uncertainty evaluation

The uncertainty of the measurements originated mostly from two sources: measurement of the volumetric gas flow with the mass flow controllers and the gas analysis with FTIR. The numeric values for measurement uncertainties were given by the manufacturer of each measurement device. In the case of measuring the volumetric gas flow the uncertainty was 0.5% whereas in the gas composition analysis the measurement uncertainty had an absolute value of 0.2% points. The measurement uncertainties are shown in the experimental results in Section 4. The error bars for the measurement uncertainties were truncated when exceeding the natural limits, i.e., conversion beyond values from 0 to 1, according to the recommendation given by the Analytical Methods Committee of the Royal Society of Chemistry [25].

3. Modeling of the reaction kinetics

3.1. Chemical kinetics

For reactor design purposes was the chemical kinetics of the global methane decomposition reaction studied. The reaction rate r (mol/s) was defined as:

$$r = \frac{dn_{CH_4}}{dt} = k_{forward} \cdot {c_{CH_4}}^n - k_{backward} \cdot {c_{H_2}}^m, \quad (3)$$

following standard formulations where n_{CH_4} is the amount of CH_4 (mol), t is time (s), c_{CH_4} and c_{H_2} are the concentrations of CH_4 and H_2 (mol/cm^3), $k_{forward}$ and $k_{backward}$ are rate constants and n and m are the reaction orders (−) for forward and backward reactions, respectively [26]. The rate constants for forward and backward reactions were assumed to follow the Arrhenius law:

$$k = A \cdot \exp[-E_a/(R_u T)], \quad (4)$$

where A is the frequency factor, E_a is the activation energy (kJ/mol), R_u is the gas constant (8.314 J/molK) and T is temperature (K) [26]. The rate constants and frequency factors use units of cm^3, J, mol and s.

In this study, the experimental data was used to optimize the Arrhenius parameters for the forward reaction and the reaction orders for forward and backward reactions. Next, the kinetic parameters for the backward reaction were solved by using the following relationship [26]:

$$k_{backward} = \frac{k_{forward}}{K_c}. \quad (5)$$

The equilibrium constant K_c (−) values were taken from the literature [27] and modified into the following exponential form:

$$K_c = 941,272.1 \cdot \exp\,[-96,425.0/(R_u T)]. \quad (6)$$

The gas flow in the laboratory test reactor was modeled as a plug flow where the tracked element had a constant mass. The pressure drop dP (Pa) for a packed bed reactor was calculated as follows [28]:

$$\frac{dP}{dx} = \frac{150\mu V_c}{\mathscr{L}_c^2} + \frac{1.75\rho V_c^2}{\mathscr{L}_c}, \quad (7)$$

where μ is the dynamic viscosity (Ns/m^2), ρ is density (kg/m^3). The characteristic velocity V_c (m/s) and characteristic length $\mathscr{L}_c$ (m) were defined as follows:

$$V_c = \frac{\dot{m}}{\rho \varepsilon_v A_c} \quad (8)$$

and

$$\mathscr{L}_c = d_p\left(\frac{\varepsilon_v}{1-\varepsilon_v}\right), \quad (9)$$

where $\dot{m}$ is the gas mass flow (kg/s), A_c is the cross-sectional area of the bed (m^2), d_p is the diameter of the spherical bed particles (m) and ε_v is the void fraction (−), i.e., the proportion of the empty space in the packed bed [28].

3.2. Kinetic parameter optimization

The kinetic parameters were optimized by using a particularly written MATLAB-based function. Table 1 presents the optimized kinetic parameters and the derived Arrhenius parameters for the backward reaction. In the MATLAB-based reactor model, a plug flow element was tracked through the reactor length and the methane conversion at the reactor end was compared with the experimental values. The function minimized the square error

Table 1
The kinetic parameters defined in Eqs. (3) and (4) achieved by optimization of the global TDM reaction parameters to correspond the experimental data. The reaction rate uses the units cm^3, J, mol and s.

	A	E_a (kJ/mol)	n (−)	m (−)
Forward	$8.5708 \cdot 10^{12}$	337.12	1.123	–
Backward	$1.1190 \cdot 10^{7}$	243.16	–	0.9296

between the calculated methane conversion and the measured values in each case. The optimization was conducted by using the function 'fminsearch' in MATLAB.

In the literature, activation energies of 208 kJ/mol [24] and 370 kJ/mol [18] have been reported when the kinetic parameters for a global non-catalytic TDM reaction have been derived from experiments conducted at temperatures above 1500 K. For a high-temperature (above 2000 K) rapid decomposition the activation energies of 356 kJ/mol–402 kJ/mol have been reported for a first order global reaction in the literature [24]. Thus, the activation energy defined in this study for the global reaction, 337 kJ/mol for lower temperature, is in line with the activation energies for non-catalytic decomposition reaction reported by others. Significantly lower values for the activation energy (147 kJ/mol–162 kJ/mol) have been reported when carbon particles have been laden to a vortex-flow at temperatures above 900 K [29], or 31 kJ/mol–85 kJ/mol when a carbon catalyst has been added to the solar powered reactor at temperatures above 723 K [30]. Furthermore, the reaction order for the forward reaction defined in this study, 1.123, is close to value 1, which is generally presented for the global TDM reaction [18,24,29].

3.3. Constant pressure reactor model

The MATLAB-based model was suitable for studying the global TDM reaction. However, in order to simulate the reactor with detailed chemistry and enable the use of the pre-defined temperature profiles from experiments, the homogeneous 0D constant pressure reactor model in LOGESoft was found appropriate [31]. In this model, the reactor was assumed to be closed system, and hence the mass conservation equation was as follows:

$$\frac{\partial m}{\partial t} = 0. \tag{10}$$

The mass fraction of the ith species in the gas mixture, Y_i (−), was

$$\frac{\partial Y_i}{\partial t} = \frac{r_i M_i}{\rho}, \tag{11}$$

where ρ is the density (kg/m^3), r_i is the reaction rate (mol/(m^{3}s)) and M_i is the molecular mass (kg/mol) of the ith species in the gas mixture [32]. The thermodynamic properties of gases were calculated by utilizing the NASA polynomials [31].

Even though the constant pressure reactor model was applied, a pressure drop does in fact occur in the test reactor. This pressure drop was calculated during the kinetic parameter optimization and according to the results the pressure drop along the total reactor length was not more than 0.3%. Therefore, the constant pressure reactor model was considered suitable for simulating the test reactor.

Initially the temperature profiles in the test reactor were measured as a function of position, but those were converted to time-dependent profiles during the kinetic parameter optimization. The gas temperature in the constant pressure model was set to follow the time-dependent temperature profiles so that the modeling results were directly comparable with the experimental data. Furthermore, the gas temperature in the test reactor was assumed to be uniform in the radial direction. This assumption was considered valid since the gas velocity was rather low and the heat capacity of the beads in the reactor was large compared to that of the gas mixture. Additionally, the distances between the beads were small.

Furthermore, it was assumed that the gas and bed temperatures in the reactor were equal. In order to justify this assumption, a separate numerical analysis was conducted in which the heat transfer efficiency between the beads and gas was defined. In the analysis, the test reactor was modeled as a packed bed reactor and the gas temperature was calculated based on heat transfer between the gas and bed. As a simplification, the bed temperature was defined equal with the measured reactor temperature profile. The conclusion was that the gas temperature deviates from the bed temperature only at the beginning and at the end of the reactor where the reactor temperature changes steeply. However, the gas temperature is practically the same as the bed temperature in the part of the reactor where the temperature is above 1000 K. This is also the most remarkable area considering the kinetic parameter optimization. Thus, it is justified to neglect the heat transfer between the gas and the reactor from the reaction kinetics analysis.

4. Results

4.1. Experiments and global kinetics

The methane conversion values from the experiments and from the modeling of the test reactor using the optimized global kinetics are shown in Fig. 2. Each data point corresponds to one of the 48 experimental cases. The results achieved with the optimized global kinetics did not depend on the model selection but both the plug flow reactor model and the constant pressure reactor model predicted highly equal methane conversion values. The error bars indicate the uncertainty in the experiments. Since the measurement uncertainty in the gas composition analysis had an absolute value that depended on the selected measurement range, the measurement uncertainty was the highest in cases where the methane concentration in the input gas was the lowest. In order to clarify the graphical format in Fig. 2, the cases are presented in the order of increasing experimental methane conversion and the same order is used throughout the paper. Since the global kinetic parameters were optimized using the experimental data, the modeling values follow well the experimental ones. In most of the cases, the modeling values are within the limits of measurement uncertainties in Fig. 2.

Four experimental cases are presented in Fig. 3 to exemplify the temperature profiles in the test reactor and to compare the experimental methane conversion values to the modeling values

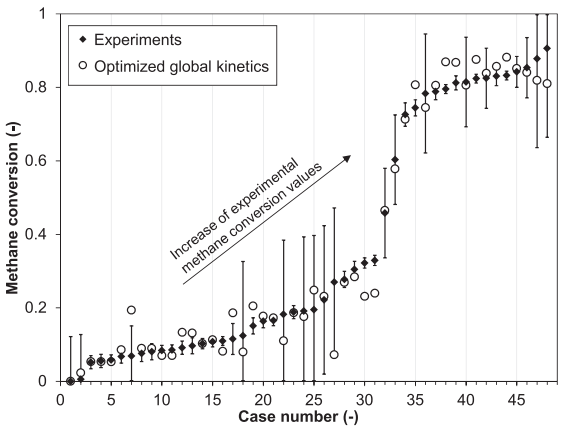

Fig. 2. Comparison of the experimental methane conversion with the values from the modeling using the optimized global kinetics. Each case represents a single measurement. Detailed data for each measurement is presented in Appendix.

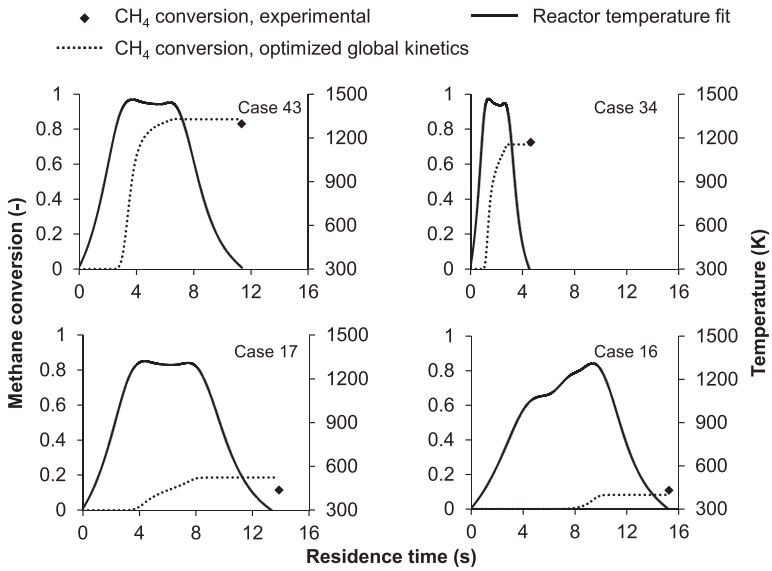

Fig. 3. Comparison of the experimental methane conversion values to the modeling values with the optimized global kinetics in four example cases. The reactor temperature fits were formed during the optimization process based on reactor temperature measurements.

with the optimized global kinetics. These cases were chosen as they represent the high (Case 43 and Case 34) and low (Case 17 and Case 16) nominal gas temperatures during the experiments. The deviation between the experimental and modeling methane conversion values was smaller in cases where the reactor maximum temperature was high, above 1300 K, and as a result, the methane conversion was high. This is mainly due to the global mechanism optimization procedure, where the function minimized the absolute difference between the model values and experiments, and thus, weighted the high methane conversion values.

4.2. 37-Step reaction mechanism

In order to evaluate the operation of the optimized global kinetics, comparison was done to other mechanisms presented in the literature. Detailed mechanisms for the TDM reaction have been presented previously for instance by Rodat et al. [18] and Ozalp et al. [19]. Among those, the mechanism by Ozalp et al. was chosen here since it was available with full kinetic parameter information. This kinetic mechanism was originally developed by Olsvik and Billaud [33] who conducted non-catalytic methane decomposition experiments in a plug flow reactor at reactor maximum temperature of 1273 K with methane conversion values below 0.01 and modeled the TDM reaction with homogenous gas phase chemical kinetics. The reaction kinetics model consisting of 36 reactions was used to explain the decomposition of methane to other hydrocarbons and the modeling results correlated well with the experiments.

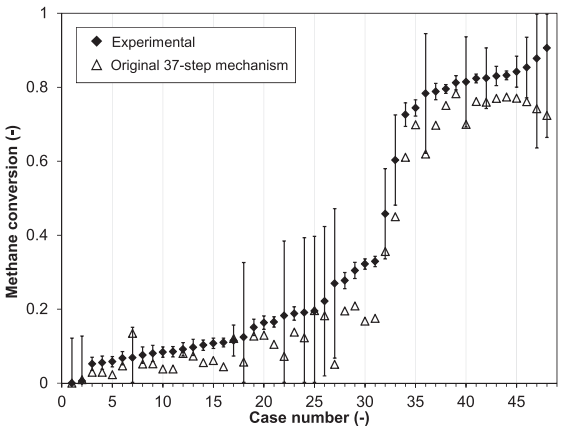

Fig. 4. Comparison of methane conversion values between the own experiments and modeling with the 37-step reaction mechanism of Ozalp et al. [19]. Each case represents a single measurement.

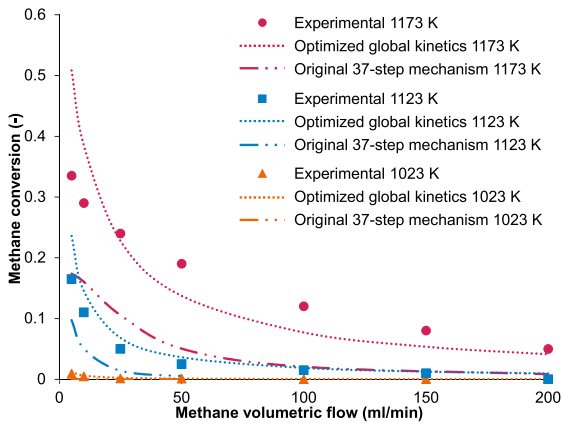

Fig. 5. Comparison of the methane conversion between Plevan's experimental results, modeling results with the optimized global kinetics and with the 37-step reaction mechanism of Ozalp et al. [19].

Later, Ozalp et al. [19] revised the reaction kinetics by adding an irreversible reaction that takes into account the solid carbon formation. Ozalp et al. used the 37-step reaction mechanism to simulate the non-catalytic methane decomposition at 1823 K–2300 K with short residence times (<0.1 s). Even though Ozalp et al. presented that solid carbon was formed during the experiments at 1823 K, their kinetic mechanism proposed negligible carbon formation at that temperature. Ozalp et al. [19] reported that the kinetic mechanism was able to predict solid carbon formation only at temperatures above 2100 K, which is well above the temperature range used in this study and also in industrial reactors other than solar or plasma reactors.

First, the 37-step mechanism was applied to model the TDM reaction in the test reactor. The experimental and modeling results are shown in Fig. 4. According to the results, the 37-step mechanism constantly predicted lower methane conversion values than the experiments. Furthermore, the 37-step mechanism predicted negligible solid carbon formation, even though the carbon formation was detected experimentally. This coincides with the conclusion stated by Ozalp et al. [19] that this kinetic model cannot predict solid carbon formation well at temperatures below 2000 K.

In order to test the optimized global kinetics and the 37-step mechanism for different reactor conditions and different temperature ranges, experiments from the literature [34] were chosen to be modeled with both kinetics. These experiments were conducted by Plevan et al. [34], who studied TDM in a bubble column reactor and conducted additional tests with a blank tube at the nominal gas temperatures of 1023 K, 1123 K and 1173 K. Furthermore, Plevan et al. conducted numerical studies of this setup and concluded that the global reaction mechanisms found in the literature were not sufficient to explain the TDM reaction, and proposed the utilization of a more detailed mechanism and reverse reactions.

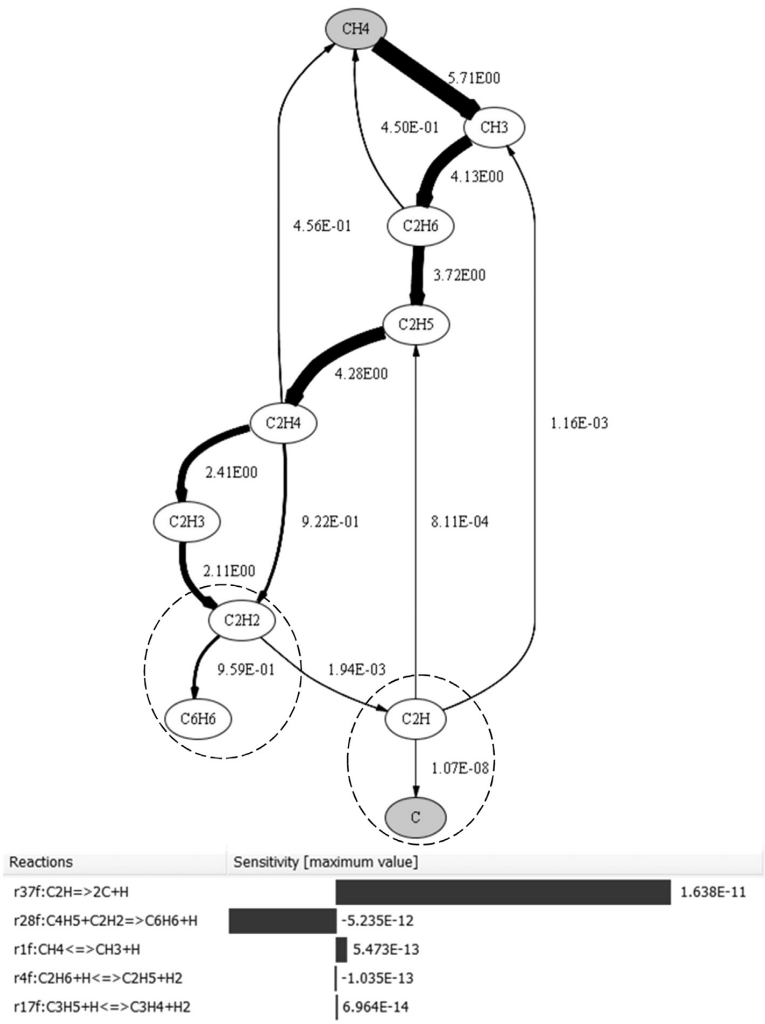

Fig. 6. The reaction flow analysis (mol/m^3) and sensitivity analysis for 100% CH_4 at 1500 K and at reaction time of 10 s by using the 37-step reaction mechanism of Ozalp et al. [19]. The two most essential reactions in this study are marked with dashed circles. The sensitivity analysis of carbon production presents the five most effective reactions in the 37-step reaction mechanism.

Here, the experimental conditions in the study of Plevan et al. [34] are modeled with the optimized global kinetics proposed in this study and with the 37-step mechanism adopted from the literature. The gas residence time in the reactor was calculated based on the gas volumetric flows, reactor dimensions and reactor temperature profiles presented in the study of Plevan et al. The experimental and modeling results are presented in Fig. 5. The optimized global kinetics shows especially good agreement with the experimental data at temperatures 1023 K and 1123 K. In all cases the 37-step mechanism predicts too low methane conversion similarly than is shown above in Fig. 4.

The global kinetic parameters were optimized in this study based on experimental data that contains measured temperature profiles, which due to the beads corresponded well with the gas temperature profiles, and a reasonable correspondence was achieved between the model values and the experiments of Plevan et al. [34]. In contrast, the 37-step mechanism, which was originally developed by Olsvik and Billaud [33], is based on experiments conducted at the reactor maximum temperature of 1273 K and simulations conducted at the constant temperature of 1243 K, which is 30 K below the reactor maximum temperature in the experiments. The inadequate temperature profile definition during the experiments and simulations might be the fundamental reason for the deviation between the modeling and experimental values in Figs. 4 and 5. Studying this further would require revising the 37-step mechanism by using experimental data of hydrocarbon formation in TDM produced in an environment where the temperature profiles are defined in detail. However, the experimental data in this study was not sufficient for this purpose. Therefore, this study focuses on another previously reported flaw of the 37-step mechanism, which is the inability to predict solid carbon formation below 2000 K [19]. This mechanism was chosen for further optimization since it is a rather simple mechanism and the full kinetic parameter information is publicly available. Therefore, this model could be utilized for prospective research and reactor design purposes.

4.3. Sensitivity analysis and mechanism improvement

In order to identify the most important reactions in the mechanism concerning the formation of solid carbon, a reaction flow and sensitivity analyses were performed according to the work of Soyhan et al. [35] (Fig. 6). The analyses were conducted at a reference temperature of 1500 K, considerably lower than the 2000 K previously studied.

According to the reaction flow analysis, a high amount of benzene was formed from acetylene whereas the route from acetylene to C_2H and finally to solid carbon was minor. Furthermore, the sensitivity analysis revealed how the benzene formation competed with the carbon formation. Therefore, the reaction of solid carbon formation from C_2H (Reaction 37) was adjusted in order to accelerate the solid carbon formation and, as a result, speed up the C_2H formation from acetylene. As a consequence, this modification reduced benzene formation from acetylene.

The activation energy of (Reaction 37) was decreased to speed up the carbon formation and the frequency factor was adjusted slightly by trial and error method. The resulting kinetic parameters are shown in Table 2. Finally, the adjusted mechanism was applied to model several TDM experiments presented in the literature.

First, the adjusted parameters were tested in an experimental case (10% CH_4 in Ar at 1823 K) presented by Rodat et al. [36], which was modeled by using the original 37-step mechanism and comparison was conducted to the modeling results with the adjusted 37-step mechanism (Fig. 7). Adjusting the kinetics improved the agreement between the model values and experiments. The adjusted 37-step mechanism predicted the H_2 production better than the original 37-step mechanism and was also able to predict the solid carbon formation at lower temperatures. Moreover, the adjusted 37-step mechanism predicted acetylene decomposition, even though the rate of this reaction was slightly too high in comparison with the experiments.

Table 2
The original and adjusted Arrhenius parameters (defined in Eq. (4)) for (Reaction 37) in the reaction mechanism developed by Ozalp et al. [19].

	A	E_a (kJ/mol)	n (−)	Ref.
$C_2H \rightarrow 2C + H$(37)	$4.68 \cdot 10^{16}$	124	0.0	[19]
$C_2H \rightarrow 2C + H$(37)	$4.68 \cdot 10^{15}$	62	0.0	This work

Second, the adjusted 37-step mechanism was applied to model the experiments of Billaud and Gueret [37], who studied methane decomposition to other hydrocarbons with an electrically heated flow reactor of which temperature was reported as 1263 K. The modeling values were mainly in a good agreement with the experiments as shown in Fig. 8. The modeling values deviated the most from the experiments in the case of acetylene and benzene. These deviations may be partly because the 37-step mechanism consists of a limited amount of hydrocarbon species, and therefore, the mechanism was not able to predict the formation and decomposition of all the species measured by Billaud and Gueret.

Both in Figs. 7 and 8 the models predict faster methane decomposition and formation of other components that has been detected during the experiments. The reason for this might be that the temperature profiles in the experiments in Refs. [36,37] were not constant even thought it was assumed in this study. Since only one temperature value was given for each experiment in these studies, modeling was conducted here in constant temperatures, which were equal to the given temperature levels. When analyzing Figs. 7 and 8, it appears that a temperature ramp might have occurred in the first part of the reactor during the experiments where the gas has warmed up from the inlet temperature to the given temperature level. An increasing temperature ramp in the measurements would cause a slower methane decomposition and product gas formation in the first part of the reactor than a constant temperature profile.

Finally, the adjusted 37-step mechanism was compared with the

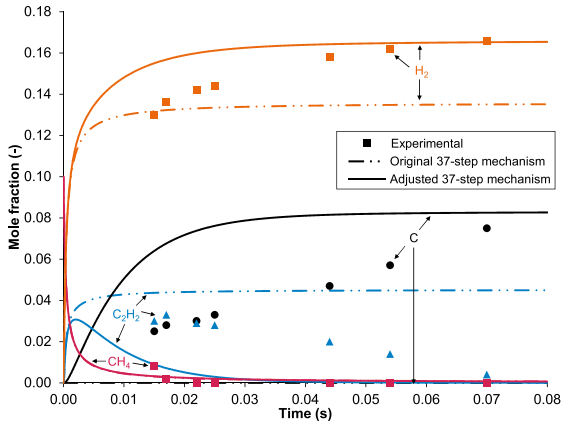

Fig. 7. Comparison of the experimental methane conversion data (10% CH_4 in Ar at 1823 K) from Rodat et al. [36] and the modeling results using the original and adjusted kinetic parameters for the 37-step reaction mechanism.

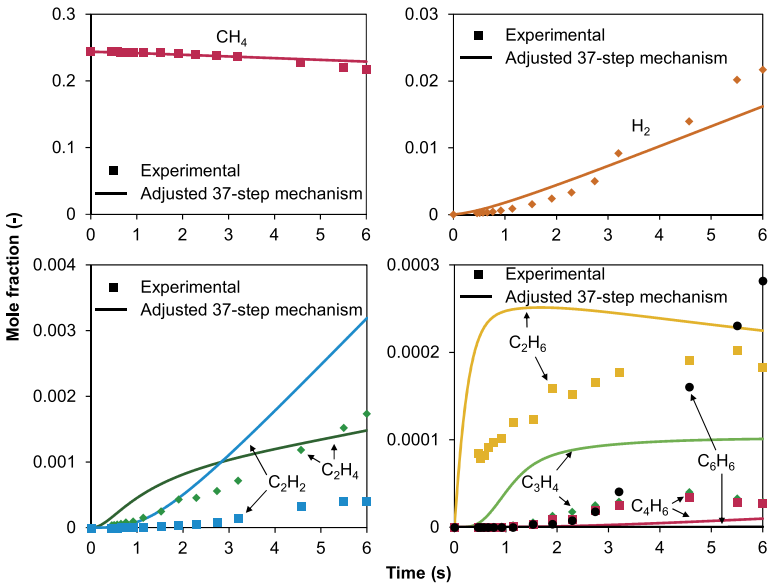

Fig. 8. Comparison of the product gas composition from methane decomposition experiments at 1263 K and 1 atm (marker symbols) [37] and from modeling with the adjusted 37-step reaction mechanism (solid lines).

simulation results of Rodat et al. [18], who studied methane decomposition with a highly detailed homogenous reaction mechanism (over 240 species and 14,000 reactions) and verified this kinetic model with their experimental data achieved at 1670 K–1770 K. Both the original 37-step mechanism and the adjusted 37-step mechanism are here studied in a case where the constant temperature is 1700 K and residence time is 1×10^{-6} s–100 s. The modeling results are compared with the simulation results of Rodat et al. [18] in Fig. 9. A total mass fraction less than 1 in Fig. 9 indicates that hydrocarbons other than selected here have been formed.

Similarly as observed previously in Fig. 7, the original 37-step mechanism predicted low H_2 and high acetylene formation as well as a slow decomposition of acetylene in comparison with the simulations of Rodat et al. [18]. The original 37-step mechanism was not able to predict the solid carbon formation at the selected

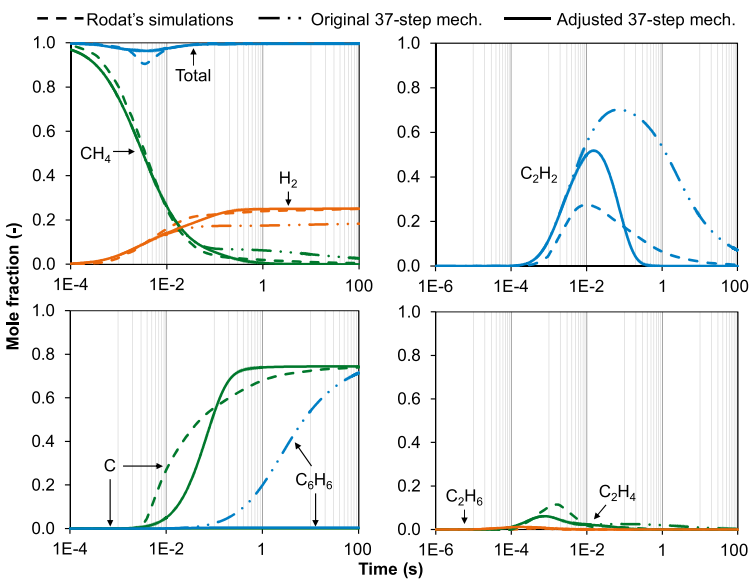

Fig. 9. Results of methane decomposition modeling at 1700 K by using the original 37-step reaction mechanism (dash-dot lines) and the adjusted 37-step reaction mechanism (solid lines) compared with the simulation results of Rodat et al. [18] (dashed lines).

temperature of 1700 K, but instead predicted formation of very high amounts of benzene, as was previously noticed in the reaction flow and sensitivity analyses in Fig. 6.

Adjusting the 37-step mechanism improved the agreement to the simulation results of Rodat et al. [18]. The major improvement of the adjusted kinetics was that it predicted carbon formation comparable to the Rodat's results and predicted a negligible amount of benzene. Furthermore, the adjusted 37-step mechanism predicted a more moderate formation and the faster decomposition of acetylene compared with the original 37-step mechanism.

In conclusion, it can be stated that the adjustment of the 37-step mechanism provided better correspondence with the experimental and simulation results at temperatures below 2000 K. The solid carbon formation in the 37-step mechanism followed a particularly simple reaction path, but in general, the solid carbon formation from hydrocarbon pyrolysis is stated to proceed via formation of PAHs, as presented in numerous experimental [38,39] and modeling studies [40–42]. Regarding the carbon formation, an option to improve the 37-step mechanism could be to take into account these more detailed models for carbon formation in TDM. However, rather than adding complex PAH and soot formation mechanisms to the 37-step mechanism, for example, the kinetic model of Rodat et al. [18], where the PAH and soot formation are included already, could be utilized.

5. Conclusion

In this paper, two simple kinetic mechanisms to describe the TDM reaction in a non-catalytic reactor were studied. The global kinetic mechanism, where the kinetic parameters were optimized based on experiments conducted in this study, was found to predict methane conversion accurately in non-catalytic TDM experiments where the temperature profiles were defined. Therefore, this mechanism will be chosen for future reactor design. The 37-step mechanism, which was adopted from the literature, has potential in a detailed modeling of hydrocarbon formation in TDM. However, two flaws were identified concerning this mechanism. First, the 37-step mechanism was unable to predict solid carbon formation, but that was successfully improved in this study. Second, the temperature profile determination during the 37-step mechanism development has been inadequate and that might be the reason for inaccuracies between the modeling and experimental results detected in this study. Improvement would require producing experimental data of formation of numerous hydrocarbons in TDM in an environment where the reactor temperature profiles are defined in detail, and finally, utilizing this data to optimize the kinetic parameters of the 37-step mechanism again.

Acknowledgments

The study presented in this paper was carried out in the Carbon Capture and Storage Program (CCSP) research program coordinated by CLIC Innovation Ltd. with funding from the Finnish Funding Agency for Technology and Innovation, Tekes. The financial support received from Fortum, Gasum, Helen, and Neste is gratefully acknowledged. Furthermore, the first author wishes to acknowledge the financial support of the Tampere University of Technology (Finland) graduate school, Fortum Foundation and Walter Ahlström Foundation. Last, the contribution of Juha Savolainen toward designing and installing the electrical installation and automation system of the experimental setup is acknowledged.

Appendix A. Supplementary data

Supplementary data related to this article can be found at http://dx.doi.org/10.1016/j.energy.2017.06.176.

References

[1] International Energy Agency (IEA). Technology roadmap - hydrogen and fuel cells. Tech. rep. 2015. https://www.iea.org/publications/freepublications/publication/TechnologyRoadmapHydrogenandFuelCells.pdf.
[2] Neef H-J. International overview of hydrogen and fuel cell research. Energy 2009;34:327–33. http://dx.doi.org/10.1016/j.energy.2008.08.014.
[3] Penner SS. Steps toward the hydrogen economy. Energy 2006;31:33–43. http://dx.doi.org/10.1016/j.energy.2004.04.060.
[4] da Silva Veras T, Mozer TS, da Costa Rubim Messeder dos Santos D, da Silva César A. Hydrogen: trends, production and characterization of the main process worldwide. Int J Hydrogen Energy 2017;42:2018–33. http://dx.doi.org/10.1016/j.ijhydene.2016.08.219.
[5] Orhan MF, Babu BS. Investigation of an integrated hydrogen production system based on nuclear and renewable energy sources: comparative evaluation of hydrogen production options with a regenerative fuel cell system. Energy 2015;88:801–20. http://dx.doi.org/10.1016/j.energy.2015.06.009.
[6] Nastasi B, Basso GL. Hydrogen to link heat and electricity in the transition towards future smart energy systems. Energy 2016;110:5–22. http://dx.doi.org/10.1016/j.energy.2016.03.097.
[7] Doranehgard MH, Samadyar H, Mesbah M, Haratipour P, Samiezade S. High-purity hydrogen production with in situ CO_2 capture based on biomass gasification. Fuel 2017;202:29–35. http://dx.doi.org/10.1016/j.fuel.2017.04.014.
[8] Blok K, Williams RH, Katofsky RE, Hendriks CA. Hydrogen production from natural gas, sequestration of recovered CO_2 in depleted gas wells and enhanced natural gas recovery. Energy 1997;22:161–8. http://dx.doi.org/10.1016/S0360-5442(96)00136-3.
[9] Weger L, Abánades A, Butler T. Methane cracking as a bridge technology to the hydrogen economy. Int J Hydrogen Energy 2017;42:720–31. http://dx.doi.org/10.1016/j.ijhydene.2016.11.029.
[10] Muradov NZ. CO_2-Free production of hydrogen by catalytic pyrolysis of hydrocarbon fuel. Energy & Fuels 1998;12:41–8. http://dx.doi.org/10.1021/ef9701145.
[11] Keipi T, Hankalin V, Nummelin J, Raiko R. Techno-economic analysis of four concepts for thermal decomposition of methane: reduction of CO_2 emissions in natural gas combustion. Energy Convers Manag 2016;110:1–12. http://dx.doi.org/10.1016/j.enconman.2015.11.057.
[12] Triphob N, Wongsakulphasatch S, Kiatkittipong W, Charinpanitkul T, Praserthdam P, Assabumrungrat S. Integrated methane decomposition and solid oxide fuel cell for efficient electrical power generation and carbon capture. Chem Eng Res Des 2012;90:2223–34. http://dx.doi.org/10.1016/j.cherd.2012.05.014.
[13] Dufour J, Serrano DP, Gálvez JL, Moreno J, García C. Life cycle assessment of processes for hydrogen production. Environmental feasibility and reduction of greenhouse gases emissions. Int J Hydrogen Energy 2009;34:1370–6. http://dx.doi.org/10.1016/j.ijhydene.2008.11.053.
[14] Dufour J, Gálvez JL, Serrano DP, Moreno J, Martínez G. Life cycle assessment of hydrogen production by methane decomposition using carbonaceous catalysts. Int J Hydrogen Energy 2010;35:1205–12. http://dx.doi.org/10.1016/j.ijhydene.2009.11.093.
[15] Dufour J, Serrano DP, Gálvez JL, González A, Soria E, Fierro JLG. Life cycle assessment of alternatives for hydrogen production from renewable and fossil sources. Int J Hydrogen Energy 2012;37:1173–83. http://dx.doi.org/10.1016/j.ijhydene.2011.09.135.
[16] Dahl JK, Buechler KJ, Weimer AW, Lewandowski A, Bingham C. Solar-thermal dissociation of methane in a fluid-wall aerosol flow reactor. Int J Hydrogen Energy 2004;29:725–36. http://dx.doi.org/10.1016/j.ijhydene.2003.08.009.
[17] Dahl JK, Buechler KJ, Finley R, Stanislaus T, Weimer AW, A L, et al. Rapid solar-thermal dissociation of natural gas in an aerosol flow reactor. Energy 2004;29:715–25. http://dx.doi.org/10.1016/S0360-5442(03)00179-8.
[18] Rodat S, Abanades S, Coulié J, Flamant G. Kinetic modelling of methane decomposition in a tubular solar reactor. Chem Eng J 2009;146:120–7. http://dx.doi.org/10.1016/j.cej.2008.09.008.
[19] Ozalp N, Ibrik K, Al-Meer M. Kinetics and heat transfer analysis of carbon catalyzed solar cracking process. Energy 2013;55:74–81. http://dx.doi.org/10.1016/j.energy.2013.02.022.
[20] Abanades S, Flamant G. Hydrogen production from solar thermal dissociation of methane in a high-temperature fluid-wall chemical reactor. In: Chemical engineering and processing: process intensification, vol. 47; 2008. p. 490–8. http://dx.doi.org/10.1016/j.cep.2007.01.006. 10th French Congress on Chemical Engineering.
[21] Maag G, Zanganeh G, Steinfeld A. Solar thermal cracking of methane in a particle-flow reactor for the co-production of hydrogen and carbon. Int J Hydrogen Energy 2009;34:7676–85. http://dx.doi.org/10.1016/j.ijhydene.2009.07.037.
[22] Hirsch D, Steinfeld A. Solar hydrogen production by thermal decomposition of natural gas using a vortex-flow reactor. Int J Hydrogen Energy 2004;29:47–55. http://dx.doi.org/10.1016/S0360-3199(03)00048-X.
[23] Abánades A, Rubbia C, Salmieri D. Technological challenges for industrial development of hydrogen production based on methane cracking. Energy 2012;46:359–63. http://dx.doi.org/10.1016/j.energy.2012.08.015.
[24] Dahl JK, Barocas VH, Clough DE, Weimer AW. Intrinsic kinetics for rapid

decomposition of methane in an aerosol flow reactor. Int J Hydrogen Energy 2002;27:377–86. http://dx.doi.org/10.1016/S0360-3199(01)00140-9.
[25] Measurement uncertainty and confidence intervals near natural limits, AMC Technical Briefs No. 26A (2008). URL www.rsc.org/amc.
[26] Turns SR. An introduction to combustion: concepts and applications. McGraw-Hill Companies, Inc; 2012.
[27] Villacampa JI, Royo C, Romeo E, Montoya JA, Angel PD, Monzóna A. Catalytic decomposition of methane over Ni-Al_2 O_3 coprecipitated catalysts. React Regen Stud Appl Catal A General 2003;252:363–83. http://dx.doi.org/10.1016/S0926-860X(03)00492-7.
[28] Mills AF. Basics of heat and mass transfer. Prentice Hall; 1999.
[29] Trommer D, Hirsch D, Steinfield A. Kinetic investigation of the thermal decomposition of CH_4 by direct irradiation of a vortex-flow laden with carbon particles. Int J Hydrogen Prod 2004;29:627–33. http://dx.doi.org/10.1016/j.ijhydene.2003.07.001.
[30] Abanades S, Kimura H, Otsuka H. Kinetic investigation of carbon-catalyzed methane decomposition in a thermogravimetric solar reactor. Int J Hydrogen Energy 2015;40:10744–55. http://dx.doi.org/10.1016/j.ijhydene.2015.07.023.
[31] LOGE AB. Lund, LOGESOFT manual, book 1. 2016.
[32] LOGE AB. Lund, LOGESOFT manual, book 2. 2016.
[33] Olsvik O, Billaud F. Modelling of the decomposition of methane at 1273 K in a plug flow reactor at low conversion. J Anal Appl Pyrolysis 1993;25:395–405. http://dx.doi.org/10.1016/0165-2370(93)80058-8. Proceedings of the 10th International Conference on Fundamental Aspects, Processes and Applications of Pyrolysis.
[34] Plevan M, Geißler T, Abánades A, Mehravaran K, Rathnam RK, Rubbia C, et al. Thermal cracking of methane in a liquid metal bubble column reactor: experiments and kinetic analysis. Int J Hydrogen Energy 2015;40:8020–33. http://dx.doi.org/10.1016/j.ijhydene.2015.04.062.
[35] H. Soyhan, P. Amnéus, F. Mauss, C. Sorusbay, A skeletal kinetic mechanism for the oxidation of iso-octane and N-Heptane validated under engine knock conditions, SAE Technical Paper1999-01-3484. http://dx.doi.org/10.4271/1999-01-3484.
[36] Rodat S, Abanades S, Flamant G. Co-production of hydrogen and carbon black from solar thermal methane splitting in a tubular reactor prototype. Sol Energy 2011;85:645–52. http://dx.doi.org/10.1016/j.solener.2010.02.016.
[37] Billaud F, Gueret C. Thermal decomposition of pure methane at 1263 K. Experiments and mechanistic modelling. Thermochim Acta 1992;211:303–22. http://dx.doi.org/10.1016/0040-6031(92)87029-A.
[38] Böhm H, Jander H, Tanke D. PAH growth and soot formation in the pyrolysis of acetylene and benzene at high temperatures and pressures: modeling and experiment 27. In: Twenty-seventh symposium (international) on combustion volume one; 1998. p. 1605–12. http://dx.doi.org/10.1016/S0082-0784(98)80570-5.
[39] Böhm H, Jander H. PAH formation in acetylene–benzene pyrolysis. Phys Chem Chem Phys 1999;1:3775–81. http://dx.doi.org/10.1039/A903306H.
[40] Lucas P, Marchand A. Pyrolytic carbon deposition from methane: an analytical approach to the chemical process. Carbon 1990;28:207–19. http://dx.doi.org/10.1016/0008-6223(90)90115-F.
[41] Vlasov PA, Warnatz J. Detailed kinetic modeling of soot formation in hydrocarbon pyrolysis behind shock waves. Proc Combust Inst 2002;29:2335–41. http://dx.doi.org/10.1016/S1540-7489(02)80284-X.
[42] Agafonov GL, Naydenova I, Vlasov PA, Warnatz J. Detailed kinetic modeling of soot formation in shock tube pyrolysis and oxidation of toluene and n-heptane. Proc Combust Inst 2007;31:575–83. http://dx.doi.org/10.1016/j.proci.2006.07.191.

Appendix A.

Case	Gas input flow (dm^3/min) CH_4	N_2	Temperature (°C) in measurement points (m) 0.4	0.6	0.9	1.2	1.4	1.7	2	2.4	Methane conversion (-)
1	0.1	6	226	390	593	738	744	801	666	90	0.000
2	0.1	6	783	942	941	949	925	940	710	84	0.006
3	1	8	660	800	798	977	956	1050	837	93	0.052
4	1	8	663	800	797	979	955	1050	837	94	0.055
5	1	6	684	828	935	995	967	998	811	102	0.058
6	1	8	796	920	982	1024	995	1026	825	103	0.068
7	0.15	6	905	1020	1050	1025	1006	1020	768	67	0.069
8	0.5	5	635	800	827	972	973	1049	813	89	0.076
9	0.5	5	656	800	806	976	966	1053	816	89	0.081
10	1	6	660	800	801	976	959	1050	824	90	0.084
11	1	6	664	800	798	978	957	1050	831	92	0.085
12	1	8	942	1024	1016	1023	989	1025	829	107	0.092
13	0.5	5	801	918	983	1025	995	1025	810	100	0.097
14	1	6	725	863	968	1025	995	1025	819	102	0.103
15	1	6	801	921	985	1026	995	1025	816	100	0.108
16	1	5	669	800	797	980	957	1050	825	92	0.110
17	0.3	6	899	1025	1025	1026	1013	1027	766	59	0.115
18	0.05	5	618	801	841	969	983	1050	801	86	0.124
19	0.5	5	945	1025	1020	1024	988	1025	813	105	0.151
20	1	8	270	560	904	1045	1053	1069	850	109	0.164
21	1	6	943	1025	1018	1024	988	1025	821	106	0.166
22	0.05	5	805	920	985	1025	994	1025	808	102	0.182
23	1	8	245	534	903	1045	1058	1070	852	107	0.188
24	0.05	5	942	1025	1023	1025	987	1026	810	107	0.191
25	0.05	5	227	527	916	1044	1066	1070	834	101	0.195
26	0.05	5	257	550	908	1045	1057	1070	837	106	0.222
27	0.05	5	649	801	814	973	968	1050	812	89	0.270
28	0.5	5	262	552	908	1045	1056	1070	838	105	0.277
29	0.5	5	233	529	909	1045	1063	1070	838	102	0.305
30	1	6	266	557	905	1045	1056	1070	847	107	0.322
31	1	6	239	531	905	1046	1060	1070	846	105	0.329
32	0.1	6	945	1081	1089	1093	1061	1082	837	92	0.458
33	0.1	6	970	1099	1108	1111	1078	1100	859	93	0.603
34	1	15	1138	1165	1159	1165	1128	1165	938	83	0.726
35	1	10	1137	1165	1163	1165	1133	1165	891	77	0.744
36	0.1	8	1032	1146	1155	1159	1124	1150	910	95	0.783
37	1	10	1142	1165	1161	1165	1130	1165	917	80	0.788
38	1	5	1130	1161	1163	1160	1126	1161	839	92	0.795
39	0.7	6	1176	1163	1163	1168	1138	1165	883	110	0.812
40	0.1	6	1036	1150	1159	1162	1128	1155	888	95	0.815
41	1	5	1140	1165	1164	1165	1133	1165	884	77	0.824
42	0.15	6	1123	1165	1165	1165	1138	1165	865	75	0.825
43	0.5	6	1071	1163	1163	1168	1139	1165	880	108	0.831
44	1	5	1136	1170	1167	1170	1145	1169	864	68	0.832
45	0.3	6	1064	1164	1165	1168	1142	1166	874	107	0.842
46	0.15	6	1062	1164	1168	1170	1146	1169	864	107	0.854
47	0.05	6	1124	1171	1169	1170	1148	1170	858	67	0.878
48	0.05	6	1134	1166	1165	1166	1135	1165	872	76	0.906

Publication IV

Tiina Keipi, Henrik Tolvanen, Jukka Konttinen

Economic analysis of hydrogen production by methane thermal decomposition: Comparison to competing technologies

Submitted to Energy Conversion and Management in August 2017

Tampereen teknillinen yliopisto
PL 527
33101 Tampere

Tampere University of Technology
P.O.B. 527
FI-33101 Tampere, Finland

ISBN 978-952-15-4057-8
ISSN 1459-2045